

https://dspace.org/

Upgrading Semi-Soft Coking Coal by Hydrothermal Treatment: Caking and structural properties

Ndumo, Jabulile

2024-02

University of the Witwatersrand, Johannesburg

https://hdl.handle.net/10539/38882

Ndumo, Jabulile. (2024). Upgrading Semi-Soft Coking Coal by Hydrothermal Treatment: Caking and structural properties. [Master's dissertation, University of the Witwatersrand, Johannesburg]. WIReDSpace. https://hdl.handle.net/10539/38882

Downloaded from a DSpace repository. https://dspace.org/



UNIVERSITY OF THE
WITWATERSRAND,
JOHANNESBURG

Upgrading Semi-Soft Coking Coal by Hydrothermal Treatment: Caking and structural properties

MSc RESEARCH DISSERTATION

Prepared by

Jabulile Ndumo

1108901

Submitted to

School of Chemical and Metallurgical Engineering, Faculty of Engineering and the Built Environment, University of the Witwatersrand, Johannesburg, South Africa

Supervisor(s):

Prof. Samson Bada

September, 2023

DECLARATION

I declare that this dissertation is my own, unaided work. It is being submitted for the degree of Master of Science in Engineering (Chemical Engineering) at the University of the Witwatersrand, Johannesburg. It has not been submitted before for any degree or examination in any other university.

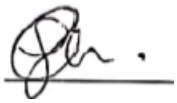

Jabulile Ndumo

September 2023

ABSTRACT

Based on the current challenges faced by the metallurgical industry in South Africa in importing quality reductants, there is an urgent need to investigate a new approach to enhance the semi-soft coal available in the country. Importing prime coking coal has increased the steel price, resulting in many downstream operations involving steel closing down in the country. With a surplus of semi-soft coking coal in South Africa, this research sought to look into this kind of abundant coal to enhance its property as a reductant for blast furnace applications. For this reason, a study was conducted on two Southern African coals, Grootegeluk (semi-soft coking coal) and Moatize (higher quality coal). Both coals were individually hydrothermally treated and then blended at different ratios to further upgrade their metallurgical properties.

The as-received Moatize coal showed properties that were more of prime coking coal with high total carbon content (76.50%), a crucible swelling index of nine, a maximum dilatation of 59% and volatile matter of 20.39%. It was a highly vitrinite coal with a vitrinite reflectance of 1.28%, a higher micropore volume than mesopore volume and a very low maximum fluidity of 24 dial divisions per minute (ddpm). According to the initial test, the Grootegeluk coal sample had a crucible swelling index of 5.5, a high volatile matter of 35.02% and a low vitrinite reflectance of 0.72%. In addition, the sample had a maximum dilatation of -10%, a maximum fluidity of 3ddpm and a higher mesopore volume than the Moatize coal.

Hydrothermal treatment was conducted on the coal samples at numerous temperatures (100ºC to 200ºC), at various residence times (30 to 90 minutes) and at different coal masses (300 to 600grams (g)). According to the results, the optimal hydrothermal conditions were 200ºC, 90 minutes and 600g. Another hydrothermal treatment was performed at a higher temperature and residence time of 280ºC and 180 minutes. The same sample mass of 600g was used and the result showed no further improvement. The coal samples were then blended at various Grootegeluk/Moatize ratios (15% to 50% Grootegeluk), and further hydrothermal treatment tests were carried out based on the optimum conditions achieved. Both the hydrothermal test and the blending of the coal led to a coal with volatile matter ranging from 21.46% to 23.79%, which is a required specification for metallurgical application. The total carbon of the enhanced coal blend also ranged from 68.8% to 82.10%, with total sulphur below 1%. The mesopore-micropore ratio of the treated blend was higher than the individual coal samples, which is what is expected of a metallurgical coal.

Based on these findings, coke was produced and analysed to identify a coke capable of withstanding blast furnace conditions. Using the particle reactivity index (PRI), proximate

analysis and the pore size distribution, 90-(50% Grootegeluk+50% Moatize)-C product was identified as the coke with the least PRI and high fixed carbon. Further investigation showed that the blending and hydrothermal treatment affected the coal's physiochemical, rheological and micro-molecular properties. The study has established that metallurgical properties of the locally mined semi-soft coking can be enhanced solely and when mixed with a hard coal.

Even though the 90-(50%GG+50%M)-C did not meet the overall specifications required for use in the blast furnace, it was identified as a suitable reductant for other metallurgical applications.

ACKNOWLEDGEMENTS

I would first and foremost appreciate and thank God. Without God I would never be anywhere near the end of this research. This was the hardest thing I have had to do to date. I have received grace upon grace and for that I am thankful.

To my supervisor Prof. Samson Bada, I profoundly thank all the guidance and support. I have been one of the most challenging and slowest students over the period but he never gave up on me. I know there are times that were difficult, but he was very patient with me. I thank you for that. I am glad I had such a great supervisor. I pray that God continues to bless and strengthen you. To Dr Jibril Abdulsalam, thank you every insight you shared.

To all my colleagues, especially the Clean Coal Technology Group, every conversation we held shaped me. To my parents, thank you for not giving up on me and supporting me without seeing the end goal.

I want to express my sincere gratitude to the (DSI/NRF) National Research Fund through the South Africa Research Chairs Initiative (SARChI) Clean Coal Technology Grant (Grant Number: 86421) for the financial support on the research. Opinions, findings and conclusions expressed are those of the author and are not necessarily to be attributed to the NRF.

Modimo a lehlonolofatse kamehla. Kea leboha.

DEDICATION

I would like to dedicate this thesis to my mother and father Lindiwe Ndumo-Masina and Amon Frank Masina.

CONTENTS

DECLARATION i
ABSTRACT ii
ACKNOWLEDGEMENTS iv
DEDICATION v
CONTENTS vi
LIST OF FIGURES ix
LIST OF TABLES xi
NOMENCLATURE xii
CHAPTER ONE: INTRODUCTION 1
1.1 RESEARCH BACKGROUND AND MOTIVATION 1
1.2 PROBLEM STATEMENT 2
1.3 HYPOTHESIS 3
1.4 RESEARCH QUESTIONS 3
1.5 RESEARCH AIMS AND OBJECTIVES 3
1.6 DISSERTATION OUTLINE 4
CHAPTER TWO: LITERATURE REVIEW 5
2.1 STEEL PRODUCTION 5
2.1.1 Direct Reduction Process 5
2.1.2 Indirect Reduction Process 10
2.2 COAL CHARACTERISATION 14
2.2.1 Proximate Analysis 15
2.2.2 Fourier-Transform Infrared Spectroscopy 15
2.2.3 Petrography 16
2.2.4 Coal Surface Area and Pore Volume 19
2.2.5 Rheological Properties of Coking Coal 20
2.2.6 Coal Reactivity Index and Strength After Reaction 25
2.2.7 Typical Characteristics of CokingCoal 27
2.3 TECHNIQUES FOR UPGRADING LOW-GRADE COAL AS A COKING COAL 28
2.3.1 Coal Briquetting and Tar Replacement 28
2.3.2 Microwave Drying 29
2.3.3 Carbonisation and Pyrolysis 29
2.3.4 Hydrothermal Treatment 30

2.4 ALTERNATIVE REDUCING AGENTS 32
2.4.1 Hydrogen 32
2.4.2 Shredder Residue Material 35
2.5 SUMMARY 35
CHAPTER THREE: RESEARCH METHODOLOGY 36
3.1 INTRODUCTION 36
3.2 EQUIPMENT 37
3.3 CHARACTERISATION 37
3.3.1 Proximate Analysis 37
3.3.2 Ultimate Analysis 38
3.3.3 Total Carbon and Sulphur 39
3.3.4 Fourier-Transform Infrared Spectroscopy 39
3.3.5 Gieseler Fluidity 39
3.3.6 Ruhr Dilatation Test 39
3.3.7 Free Swelling Index 39
3.3.8 Roga Index 40
3.3.9 Surface Area, Pore Volume and Pore Area 40
3.3.10 Petrographic Analysis 40
3.4 HYDROTHERMAL TREATMENT 41
3.4.1 Hydrothermal Treatment of Coal 41
3.4.2 Coal Blending for Further Hydrothermal Treatment 43
3.5 COKING TESTS 43
3.6 SUMMARY 44
CHAPTER FOUR: RESULTS AND DISCUSSIONS 45
4.1 INTRODUCTION 45
4.2 CHARACTERISATION OF THE RAW COAL SAMPLES 45
4.2.1 Physiochemical Characterisation of the Raw Coal Samples 45
4.2.2 The Rheological Characterisation of Grootegeluk and Moatize Coals 48
4.2.3 The Micro-Molecular Characterisation of Grootegeluk and Moatize Coal 49
4.3 CHARACTERISATION OF HYDROTHERMALLY TREATED SAMPLES 52
4.4 CHARACTERISATION OF HYDROTHERMALLY TREATED COAL BLENDS 57
4.5 THE EFFECT OF HYDROTHERMAL TREATMENT AND BLENDING OF GROTEGELUK AND MOATIZE COAL SAMPLES ON RHEOLOGICAL PROPERTIES OF 90-(50%GG+50%M) BLEND 60
4.6 FOURIER-TRANSFORM INFRARED SPECTROSCOPY ANALYSIS 61

4.7 COKE TESTS 63
CHAPTER FIVE: CONCLUSION AND RECOMMENDATIONS 71
5.1 CONCLUSION 71
5.2 RECOMMENDATIONS 72
REFERENCES 1
APPENDIX A 24

LIST OF FIGURES

Figure 2.1: Mindrex process flow diagram (Hamadeh *et al*., 2018, p.2).....7
Figure 2.2: The Corex process flow diagram (Liu *et al*., 2019, p.445) 8
Figure 2.3: A visual description of the Fastmet process (Michishita & Tanaka, 2010, p.71) ...9
Figure 2.4: Pulverised coal injection (Industrial Efficiency Technology Database, 2012, p.9) 11
Figure 2.5: A blast furnace (Babich & Senk, 2015, p.510) 12
Figure 2.6: The Gieseler Plastometer test temperature range (Eun, 2012).....21
Figure 2.7: The dilatation test of coal (UNT Digital Library, 2021, p.21) 23
Figure 2.8: The standard 'buttons' for the free Swelling Index (FitzGerald & Zambrowski, 2023, p.23). 24
Figure 2.9: The effect of rheological properties on coke strength properties (Eun *et al*., 2012, p.74) 25
Figure 2.10: The coke strength after reaction (CSR) evolution over the years at Arcelor Mittal (Todoshuk *et al*., 2004, p.16).....26
Figure 2.11: Hydrogen colour palette: the origin and production route (Panic', *et al*., 2022, p.5) 33
Figure 3.1: The process flow diagram 36
Figure 3.2: Berghof BR series reactor and accessories (DKSH Group, 2018, p.3).....41
Figure 4.1: The Fourier-Transform Infrared Spectroscopy spectra of Moatize and Grootegeluk (GG) coal samples.....47
Figure 4.2: Moatize coal sample with (a) inertinite (IN) and clay (CL), (b) fusinite (FUS) and (c) natural coke 49
Figure 4.3: Grootegeluk coal with (a) colledilite (COL) and inert semifusinite (ISF), (b) quartz (Qu) and (c) pyrite (P).....50
Figure 4.4: The Density functional theory pore size distribution of the raw Grootegeluk (GG) and raw Moatize coal 52
Figure 4.5: The pore size distribution of 100% Grootegeluk (GG), GG-HTC-600A, GG-HTC-600-B2 and GG-HTC-600C.....55
Figure 4.6: The Density functional theory pore size distribution of the 100% Moatize, M-HTC-30-9, M-HTC-90-9 and M-HTC-180-1 57
Figure 4.7: The Density functional theory pore size distribution of the Grootegeluk (GG)/Moatize (M) coal blends.....60
Figure 4.8: The FTIR spectra of the reacted coal blends vs the raw coal samples (Grootegeluk (GG) and Moatize (M)).....62
Figure 4.9: The mass loss versus time graph of 100% Grootegeluk (GG-C) and GG-HTC-B2-C.....63
Figure 4.10: The mass loss versus time graph for 100% Moatize-C and M-HTC-600-B2-C .64
Figure 4.11: The mass loss versus time graph of the carbonised hydrothermal coal blends of Grootegeluk (GG) and Moatize (M) coals.....65
Figure 4.12 The Density functional theory pore size distribution of 100% Grootegeluk (GG)-C and GG-HTC-600-B2-C.....67
Figure 4.13: The Density functional theory pore size distribution of 100% Moatize (M) and M-HTC-600-B2-C 68

Figure 4.14: The Density functional theory pore size distribution of the carbonised hydrothermal blend coal samples.....69

LIST OF TABLES

Table 2.1: The effect of rank and macerals on the volatile matter (Wagner, 2021) 18
Table 2.2: A summary of maceral group qualities (Wagner, 2021) 19
Table 2.3: The summary of coking coal parameters required in a blast furnace (Satyendra *et al*., 2013a) 27
Table 3.1: Experimental process parameters for each test run 42
Table 3.2: Various coal compositions 43
Table 4.1: Characterisation of the raw Grootegeluk and Moatize coal samples 46
Table 4.2: Summary of functional groups for the infrared spectra of the Moatize and Grootegeluk coal samples 48
Table 4.3: The Density functional theory textural properties of Grootegeluk (GG) and Moatize coals 52
Table 4.4: Results of the hydrothermally treated Grootegeluk coal at varying residence times, temperatures, and masses. 53
Table 4.5: The Density functional theory textual properties of 100% Grootegeluk (GG), GG-HTC-30-3, GG-HTC-90-9 and GG-HTC-180-1 55
Table 4.6: Results of the hydrothermal treatment of Moatize coal at various residence times, temperatures and masses 56
Table 4.7: The Density functional theory textual properties of 100% Moatize, M-HTC-30-9, M-HTC-90-9 and M-HTC-180-1 57
Table 4.8: Results of raw Grootegeluk (GG)/Moatize (M) and the hydrothermally treated GG/Moatize coal blends at 600g, 200ºC and 90 minutes 59
Table 4.9: The Density functional theory textual properties of the Grootegeluk (GG)/Moatize (M) coal blends 60
Table 4.10: Characterisation of the 90-(50%GG+50%M) blend 61
Table 4.11: Summary of functional groups for the infrared spectra of 100% Moatize (M), 100% Grootegeluk (GG), GG-HTC-600-B2, M-HTC-600-B2 and 90-(50%GG+50%M) 63
Table 4.12: The physiochemical and particle reactivity index of produced coke from Grootegeluk (GG), Moatize (M) and their coal blends 66
Table 4.13: The Density functional theory textural properties of 100% GG-C and GG-HTC-600-B2-C 67
Table 4.14: The Density functional theory textural properties of 100% Moatize (M)-C and M-HTC-600-B2 68
Table 4.15: The Density functional theory textural properties of the carbonised hydrothermal blended coal samples 69
Table A1: Grootegeluk sample nomenclature 24
Table A2: Moatize sample nomenclature 25
Table A3: Maceral group analysis 26
Table A4: Vitrinite reflectance analysis 27
Table A5 Microlithitype 28
Table A6: The Grootegeluk/Moatize coal bend nomenclature 29

NOMENCLATURE

%: Percent

ºC- Degrees Celsius

BET: Brunauer-Emmet-Teller

Bt: Billion Tonnes

cc/g: Cubic Centimetre per Gram

CO: Carbon Monoxide

CO_2: Carbon Dioxide

CRI: Coke Reactivity Index

CSR: Coke Strength after Reaction

ddpm: Dial Divisions per Minute

DFT: Density Functional Theory

DRI: Direct Reduced Iron

EAF: Electric Arc Furnace

Fe^{2+}: Ferrous Cation

Fe^{3+} : Ferric Iron

Fe_2O_3: Hematite

FSI: Free Swelling Index

FTIR: Fourier-Transform Infrared Spectroscopy

g: Grams

GG: Grootegeluk

H_2: Hydrogen

H_2O: Water

HBI: Hot Briquette Iron

HDBI: Hot Direct Reduced Iron

m^2/g: Square Metre per Gram

min: Minutes

mg: Milligram

ml: Millilitres

mm: Millimetre

Mt: Million tonnes

nm: Nanometres

PCI: Pulverised Coal Injection

PRI: Particle Reactivity Index

TGA: Thermogravimetric Analysis

wt%: Weight Percentage

CHAPTER ONE: INTRODUCTION

1.1 RESEARCH BACKGROUND AND MOTIVATION

Global steel production depends on coking coal, and about 71.5% of the crude steel world production in 2018 was through the basic oxygen furnace route (World Steel Association, 2018). World steel production increased from 800 million tonnes (Mt) in 2000 to 1.87 billion tonnes (Bt) in 2019 (World Steel Association, 2019). As much as the world population continues to grow, so shall the demand for steel needed in construction, automobiles, renewable applications (wind turbines), etc. The use of coal is beyond electricity generation; it has been an energy source for the industrialisation of the West, and the backbone of their nation-building and economies. The relevance of coal is critical to the carbon and metallurgical industry to produce ferroalloys, aluminium, cement and glass, as well as fuel in other energy-demanding industrial sectors. With the depletion of coking coal in South Africa and the country's reliance on importing coking coal, the future of the steel and ferroalloys industry is quite bleak. It is extremely significant that research into an alternative approach to upgrading the available semi-soft coking coal in the country should be conducted.

With the closure of Tshikondeni mine in 2014, the remaining steel manufacturers in South Africa now seek to import prime coking coals from Australia and North America, as well as from Moatize in Mozambique (Musiiwa, 2018). The high cost incurred from importing and blending the local semi-soft coking coal from Grootegeluk (GG) has not been of great benefit in reducing the operation cost, as well as meeting the required coal quality. In terms of the quality required for metallurgical applications, the steel-making plants could not push the amount of local coking coal in the blend (local + imported) above 30% (Musiiwa, 2018). With the high proportion of imported coking coal required in the blend to produce a suitable coke, there is a need to find an alternative technique to utilise the local coal (GG) in large quantities while still maintaining the required product quality for metallurgical applications. In the past few years, several steel companies have either closed or moved to other countries due to the input costs for primary steel production in South Africa. Likewise, midstream companies like MacSteel, Trident and Scaw metals are being affected by the high cost of buying steel to produce other products (Creamer Media, 2020).

The current research focused on upgrading the semi-soft coking coal (GG) available in the country, along with the imported Moatize coking coal individually, as well as upgrading the blend of both coals at different percentage ratios. Coal with low coking properties is of no

commercial value to the steel industry, and with the availability of this quality of coal in South Africa, a thorough study is required to investigate upgrading its coking attributes. The approach proposed was hydrothermal carbonisation, and the product obtained from this test was compared to the imported prime coking coal. With little data in the open domain on the pre-treatment of non-coking coal through hydrothermal processes, it was, therefore, important to determine if the coking and caking properties of semi-soft coking coal could be improved using this technique. If successful, this would reduce expensive imported prime coking coals (mostly from Australia) and would guarantee a more cost-effective product for use in South Africa's essential iron and steel making process.

1.2 PROBLEM STATEMENT

The iron and steel industry is a key strategic industry in South Africa as it contributes around 1.5% to the gross domestic product and employs 190 000 people directly and an additional 100 000 people indirectly. In 2015, cheap steel imports from China started to flood South Africa, forcing South African steel companies to liquidate (de Villiers, 2015). The Chinese steel was 25% below the cost of local steel. This is because there is no available prime coking coal locally, so it must be imported (Ratshomo & Nembahe, 2019). The transport cost and the price of prime coking coal contribute to the elevated cost of steel production in the country (Ratshomo & Nembahe 2019).

South Africa has huge coal reserves that are mainly untapped, but the required prime metallurgical grade coal has depleted. The Grootegeluk Waterberg coal has sufficient semi-soft coking coal (Jeffrey, 2005), but a limited amount of this coal is required in the blend for making coke, up to 30% maximum, as any blend above this value tends to produce metallurgical coke with less strength (Musiiwa, 2018). In addition, the amount of Moatize coal required in the blend for making metallurgical coke is limited to 15%; any ratio above this value tends to lead to high "wall pressure" and could damage the coke oven (Musiiwa, 2018, p.1). The percentage of these coals in the blend needs to be improved to reduce the costs of importing prime coking coal further and to produce metallurgical grade coke that meets the industry specification. The hydrothermal treatment of this coal intends to increase the blending ratio, reducing the challenges associated with high wall pressure caused by this coal. The parameters associated with this challenge are low permeability, leading to the restriction of volatile matters (evolving gases), compaction and plastic layer formation with trapped gases leading to internal gas pressure build-up in the plastic layer.

Another challenge associated with using semi-soft coking coal is its chemical composition. The alkalis forming minerals and zinc within this coal have an extremely negative effect as they consume the reducing agent, reducing the productivity of the blast furnace and the hot metal's uniformity. A high ash content leads to a high slag content, hence higher energy consumption. As the blast furnace uses more energy, it becomes less productive (Gómez-Casero *et al*., 2021). Chlorine and moisture increase the dew point at the top of the gases formed in the blast furnace and causes the process to have higher top gas temperatures, becoming thermally inefficient and causing equipment corrosion. Physically, the coke must have sufficient permeability to easily allow slag and hot metal to flow down while also having enough strength for the coke not to crack (Satyendra, 2019).

This study addressed some of the challenges stated above by upgrading GG, Moatize and the GG/Moatize blends using the hydrothermal process to improve the molecular structure, and the coals' chemical and physical properties. The hydrothermal process can remove the inorganic minerals into the liquid phase and enhance the plasticity of carbonaceous materials.

1.3 HYPOTHESIS

The hydrothermal process will disrupt weak covalent bonds, thereby eliminating side chains through hydrolysis, as well as removing cross-links of the macromolecular network at elevated temperatures, leading to improved coalescence and enhanced coking qualities.

1.4 RESEARCH QUESTIONS

I. What is the impact of upgrading the coking quality of GG and Moatize coals and their blends on the coal's coking qualities?
II. What are the optimum set parameters (temperatures, residence time, pressure and GG/Moatize blend composition) for upgrading the coals effectively?
III. To what extent will the physicochemical characteristics and molecular structure of GG, Moatize and GG/Moatize blends change with hydrothermal treatment?
IV. Will the upgraded GG, Moatize and GG/Moatize blends meet the required specification for metallurgical application?

1.5 RESEARCH AIMS AND OBJECTIVES

This study aimed to upgrade the GG, Moatize and GG/Moatize coal blends through the hydrothermal process to produce a metallurgical coal grade. The aim was achieved by:

I. Determining the physiochemical, rheological and micro-molecular structural properties of the as-received coals;
II. Determining the influence of hydrothermal treatment on the characteristics of GG, Moatize and GG/Moatize blended products;
III. Determine the quality of carbonised coal (coke) produced from modified coal at optimal set hydrothermal conditions.

1.6 DISSERTATION OUTLINE

Chapter 1 explains the background information and the motivation behind the research.

Chapter 2 is a literature review, giving a brief history of steel production, considering direct and indirect steel-making processes. The chapter also reviews literature on coal characterisation techniques, coal upgrading techniques, alternative reducing agents, and the recent advancement in the reduction of iron ore for steel making.

Chapter 3 explains the materials and methods used.

Chapter 4 presents the results of the methods outlined in chapter three, as well as a discussion of the significant results. The results include the characterisation of raw coal samples, and the hydrothermal treatment of coal samples and coal sample blends. Lastly, the coking results of the optimum coal samples are presented.

Chapter 5 provides findings, as well as recommendations for additional research.

CHAPTER TWO: LITERATURE REVIEW

This research focused on upgrading semi-soft coking coal through the hydrothermal treatment process, along with the caking and structural properties of the coal and coke produced. This chapter provides an overview of steel production and a more detailed discussion of the theory of direct and indirect reduction processes. Characterisation of coal in the form of proximate analysis, Fourier-transform infrared spectroscopy (FTIR), petrography, pore surface and size, rheological properties and coke strength test are discussed. Finally, the chapter elaborates on other techniques for upgrading coal and other reducing agents and their future use.

2.1 STEEL PRODUCTION

Steel is an alloy of iron and carbon, in which its carbon content can be up to 2%, but alloys with iron and carbon content above 2% are known as cast iron (Nutting *et al*., 2019). Steel is produced from iron ore, a mineral aggregate that is economically converted to iron or scrap (ArcelorMittal, 2015). Iron ore is naturally found in the earth's crust in its oxidised state (Fe^{3+}) as hematite (Fe_2O_3) or as a combination of the two oxidised states (Fe^{3+} and Fe^{2+}) in magnetite (Beukes *et al*., 2003; Nikolaeva *et al*., 2021). Iron ore reduction requires contact with a reagent that has a greater affinity for oxygen than iron (Kunitomo *et al*., 2006). Carbon is usually used to reduce iron in its gaseous, liquid and most common solid phase. Under certain thermodynamic conditions, carbon has more affinity for oxygen than iron (Demirel & Gerbaud, 2019; Harvey & Gheribi, 2014), and this is exploited in a blast furnace (Steenkamp & Du Preez, 2015). The primary source of carbon and fuel widely used for steel making is coking coal (World Steel Association, 2019).

Steel production involves various stages, including the iron-making stage, primary steel making, secondary steel making and continuous casting, and primary and secondary forging (MetroSteel, 2016). Iron making is the first and one of the most energy-intensive stages (Díaz *et al*., 2020). During this stage, hot metal production is in a blast furnace. Due to the high cost of raw material used, and processing time, several alternative technologies available in the market are reviewed in the following sections.

2.1.1 Direct Reduction Process

Steel can be produced directly in an electric arc blast furnace or indirectly in a basic oxygen furnace. The direct steel production process reduces iron ore in a solid-state (lump ores or fines) by using a reducing gas or carbon that may be obtained from natural gas or coal at a

temperature below iron's melting point (Haranda & Tanaka, 2011). The advantage of using the direct reduction process includes the reduced need for feedstock preparation; pelletised iron ore or lumpy iron ore are used. Contaminated natural gas can also be used for a low-cost process. The drawback is that the gas quality reduces the thermal efficiency of the process (Gojić & Kožuh, 2006).

The direct reduction process may use DRI (direct reduced iron), HBI (hot briquette iron) and HDBI (hot direct reduced iron). HBI is a compact form of DRI designed to allow easy shipping and storage due to the susceptibility of unprotected DRI to oxidation and the possibility of exothermic auto-ignition (Michishita & Tanaka, 2010), whereas HDBI is iron that is directly transported to an electric arc furnace (EAF) after being discharged from a reduction furnace. DRI, HBI and HDBI all have gangue that is later removed in an electric furnace, unlike pig iron (Maia Star, 2020). The purity of the iron produced from DRI is 97% (Maia Star, 2020). Due to the attractive size of the blast furnace, not a lot of direct reduction furnaces were commissioned even though there were a large number of them built in the pilot stages (Maia Star, 2020). Three of the commercialised direct reduction processes are outlined below.

2.1.1.1 The Mindrex process

The Mindrex process is one of the most famous commercially direct reduction processes, which uses reforming gas from natural gas to reduce iron ore (Atsushi *et al*., 2010). DRI is then used as a raw material fed into the EAF as a clean substitute source instead of scrap (Atsushi *et al*., 2010). The process flow diagram of the Mindrex process is illustrated in Figure 2.1.

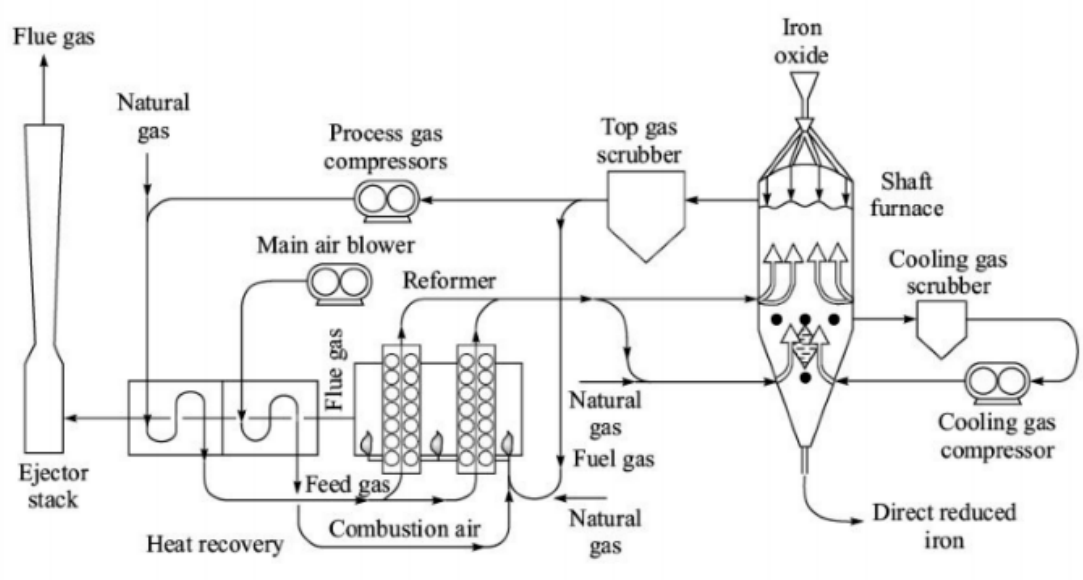

Figure 2.1: Mindrex process flow diagram (Hamadeh *et al*., 2018, p.2)

As seen in Figure 2.1, the natural gas feedstock is fed into the reformer, while the lump ore, powder or iron ore pellets are charged from the top of the shaft furnace as the raw material. The iron ore is reduced in the shaft furnace with the reduced iron discharged from the bottom of the furnace, while a cooling gas is continuously injected to prevent the iron from reaching its molten state. According to Béchara *et al.* (2018), the following reactions (equations 2.1 and 2.2) take place in the reactor.

$$Fe_2O_3 + 3CO \rightarrow 2Fe + 3CO_2 \quad (2.1)$$

$$Fe_2O_3 + 3H_2 \rightarrow 2Fe + 3H_2O \quad (2.2)$$

The exhaust gas (top gas) is emitted from the top of the furnace; the wet scrubber then cleans and cools it prior to re-circulation (Atsushi *et al*., 2010). The top gas containing carbon dioxide and water is compressed, preheated and fed to the reformer furnace. The gas mixture react with with natural gas in the reformer according to equations 2.3 and 2.7 (Béchara *et al*., 2018).

$$CH_4 + CO_2 \rightarrow 2CO + 2H_2 \quad (2.3)$$

$$CH_4 + H_2O \rightarrow CO + 3H_2 \quad (2.4)$$

$$2CH_4 + O_2 \rightarrow 2CO + 4H_2 \quad (2.5)$$

$$CO + H_2O \rightarrow CO_2 + H_2 \quad (2.6)$$

$$CH_4 \rightarrow C(S) + 2H_2 \quad (2.7)$$

In the Mindrex process, both carbon monoxide (CO) and hydrogen (H_2) are utilised to reduce hematite (Fe_3O_3) into solid iron. Equations 2.3 to 2.4 show the reaction of natural gas with the exhaust gas leading to the formation of the reducing gases.

2.1.1.2 The Corex process

The Corex process (Figure 2.2) is similar to the Mindrex process; however, it has a shaft and a gasifier. Unlike the Mindrex process, the Corex process uses non-coking coal instead of natural gas for reduction. In the Corex process, non-coking coal is used directly as a reductant and fuel, unlike in the basic oxygen furnace where coking coal is used. In the Corex process, coal is fed into the gasifier instead of natural gas to produce the reductant (gases) (Zhou *et al*., 2015). A bit of coke (around 15%) can also be used along with oxygen as its main fuel (Assis *et al*., 2008). Pure oxygen is used for this process. The DRI produced from the process has a purity of above 90% and requires further processing to produce steel (Satyendra, 2017).

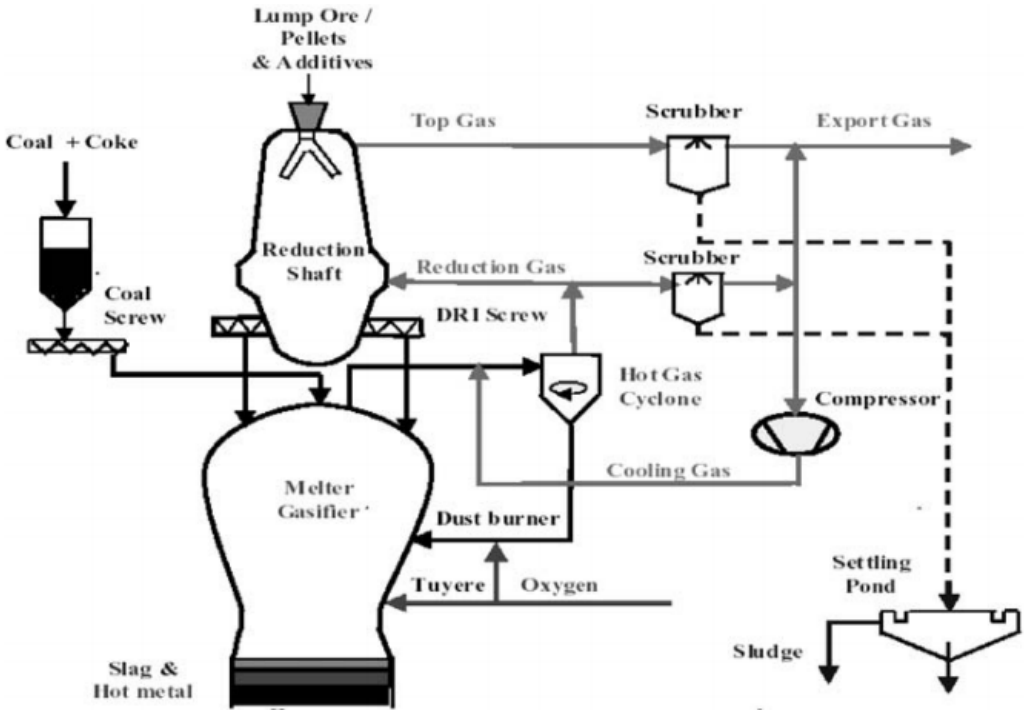

Figure 2.2: The Corex process flow diagram (Liu *et al*., 2019, p.445)

2.1.1.3 The Fastmet process

The Fastmelt process, like the Corex process, is a coal-based direct reduction process. The process converts iron ore in the form of pellets or fines and uses the waste from the metallurgical process to form directly reduced iron. This process uses the Mindrex process integrated with an electric iron melting furnace that produces hot metal (Michishita &

Tanaka, 2010). In this process, the DRI is released straight from the rotary hearth furnace into the electric iron melting furnace (Satyendra, 2013b). Figure 2.3 further explains the Fastmet process.

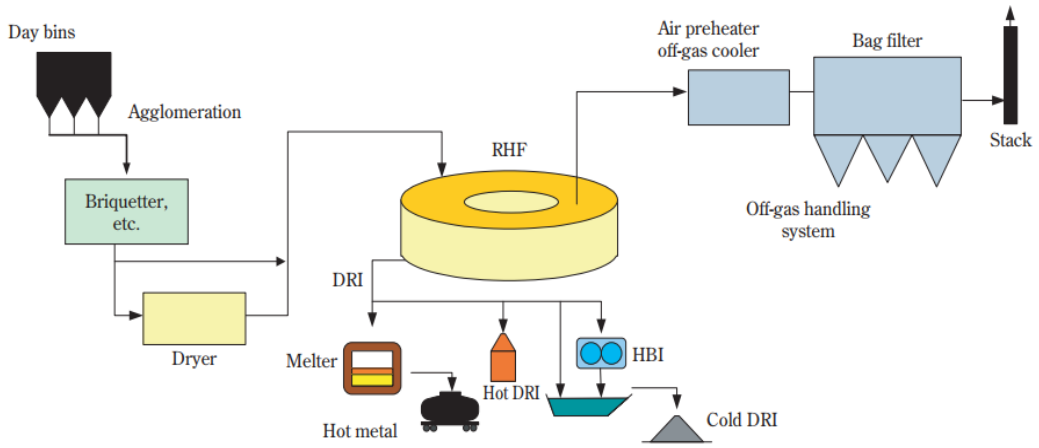

Figure 2.3: A visual description of the fastmet process (Michishita & Tanaka, 2010, p.71)

As seen in Figure 2.3, pulverised coal and iron ore fines are mixed in the day bins and the reduced iron (DRI) is transferred into a melter to produce hot metal in which the metallisation can be reached within 20 to 150 minutes. The chemical reactions that occur in the rotary hearth furnace for iron ore reduction when heated at 1350°C to 1450°C are expressed in equations 2.8 to 2.12, which occur simultaneously in the Fastmet process leading to the reduction of iron ore (Béchara *et al*., 2020).

$$Fe_3O_4 + 4C \rightarrow 3Fe + 4CO \quad (2.8)$$

$$CO_2 + C \rightarrow 2CO \quad (2.9)$$

$$Fe_3O_4 + 4CO \rightarrow 3Fe + 4CO_2 \quad (2.10)$$

$$Fe_2O_3 + 3C \rightarrow 2Fe + 3CO \quad (2.11)$$

$$Fe_2O_3 + 3CO \rightarrow 2Fe + 3CO_2 \quad (2.12)$$

According to Tsutsumi *et al*. (2010), 190 000 tonnes per hour of metal can be produced from the Fastmet process with a carbon content of about 1.5% to 5%. The Fastmet process produces and uses HBI downstream compared to Corex and Mindrex, which use DRI. This was implemented as a result of a study by Tsutsumi *et al.* (2010) on the first two Fastmet plants. The study investigated the effect of porosity and apparent density on HBI and their

weathering resistance effect. The results showed that HBI could withstand long-term storage, unlike DRI.

2.1.2 Indirect Reduction Process

Indirect reduction is a two-step process. In the first step, the carbon is reacted with oxygen gas to form carbon monoxide. The carbon monoxide with hydrogen gas is then used as a reductant of iron oxides. The by-products of iron oxide carbon reduction are carbon dioxide and water (Babich & Senk, 2015). Indirect reduction takes place in a basic oxygen furnace, producing 99% pure iron. It is a large-scale production process with mature technology, decreased production costs and high efficiency. The main disadvantage of a basic oxygen furnace is that premium or high-quality metallurgical coal is needed. As coking coal is less accessible globally, particularly in South Africa, using this technology becomes expensive (Ratshomo & Nembahe, 2019). Another challenge facing the technology is the impact of the emitted gases, which are detrimental to the environment. In addition, the production process is long with a high energy consumption rate (Liang *et al*., 2020). Two commercialised indirect reduction processes are described below:

2.1.2.1 Pulverised coal injection

The pulverised coal injection (PCI) method was developed to reduce the volume and cost of coke (Bennett, 2007). In this process, the air (called the conveying gas) transports pulverised coal into the blast furnace. The pulverised coal is injected from the bottom of the furnace through the lance into the tuyere. The hot air (blast) is blown into the tuyere through a blowpipe and then piped to the furnace to create a raceway that is responsible for the coke and coal combustion, hence melting the solid iron ore and releasing molten iron (Mathieson *et al*., 2005; Shen *et al*., 2012). The pulverised coal injection system (Figure 2.4) was added to the blast furnaces because of its various benefits (Carpenter, 2010). The integration of this system increases the efficiency of the boiler and coal particle size.

Another benefit introduced by the PCI system permits the utilisation of pulverised coal of different types and ranks, not just premium metallurgical coal (de Castro *et al*., 2013). Ren *et al.* (2013) investigated the injection of three coals (meager-lean coal, anthracite coal and bituminous coal) into the blast furnace. He found that most effective coal blend that could be used in a PCI system comprises of a higher quantity of bituminous coal. In another investigation, Raygan *et al*. (2010) concluded that Sarakhs (bituminous with moderate volatiles), Sangrood (bituminous with moderate volatiles), Karmozd (bituminous with high

volatiles) and Tabes (bituminous with low volatiles) could all be used for coal injection and their blend improves the furnace combustion.

Even with so many benefits, unfortunately, there are still drawbacks to the system. The complexity of the equipment involved, additional costs and the storage of the fuel, which is pulverised coal, requires more attention than pellets. Also, there is the possibility of an explosion as the coal burns more like a gas (Silva & Assis, 2019). PCI is incorporated into the blast furnace to provide auxiliary fuel for partial coke replacement, and the approach has proven to be viable and cost-effective.

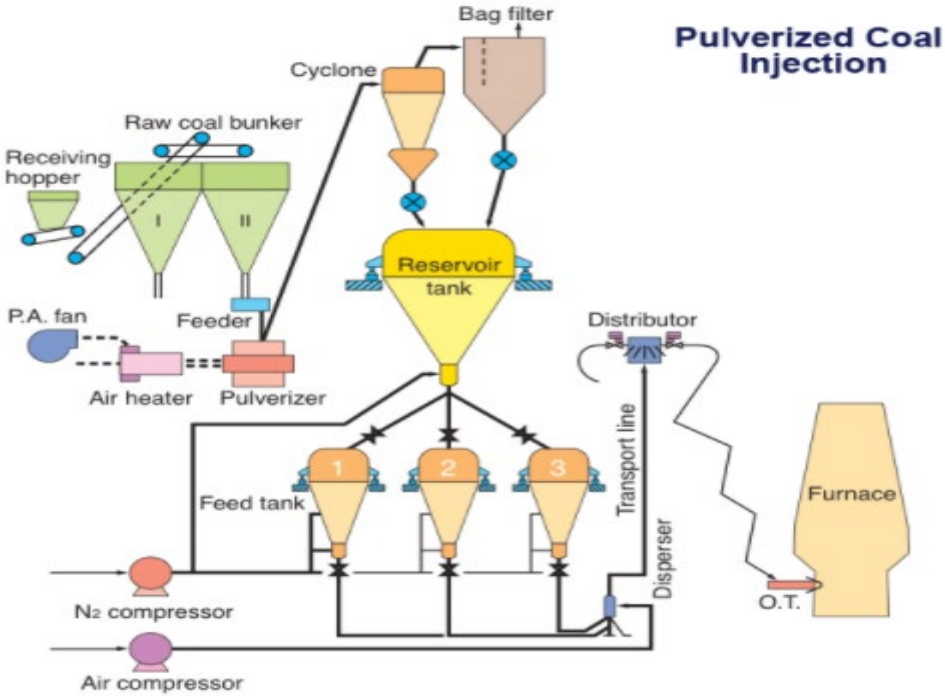

Figure 2.4: Pulverised coal injection (Singh & Rout, 2018, p.9)

2.1.2.2 Basic oxygen furnace

The blast furnace generally uses long shaft-type vessels. The inner wall of the vessel is lined with refractory bricks to prevent degradation of the furnace at high temperature, and it has an overlaying crucible like hearth (Anderson, 2014). The metallurgical coke and iron ore are fed from the top of the furnace. Air is introduced into the blast furnace from the bottom, encountering the coke. This reaction leads to burning the coke, thereby releasing oxygen from the iron ore. The molten iron descends and accumulates in the hearth. Both molten pig iron and slag are tapped from the bottom of the shaft and the hot gas leaves through the top (Puyejovska *et al*., 2013; de Castro *et al.*, 2020). A blast furnace can use other fuels such as tar, coal, oil, gas or processed plastics for it to work effectively (Puyejovska *et al*., 2013).

These fuels may be injected into the blast furnace through the tuyeres along with the air to aid the coke as more cost-effective fuel. These fuels can co-fuel the blast furnace but cannot be used alone in the blast furnace. The coke acts as a support for the burden and allows gaseous movement through the blast furnace (Chukwuleke *et al*., 2009). Figure 2.5 illustrates the blast furnace, while equations 2.13 and 2.14 represent the reactions occurring in the blast furnace.

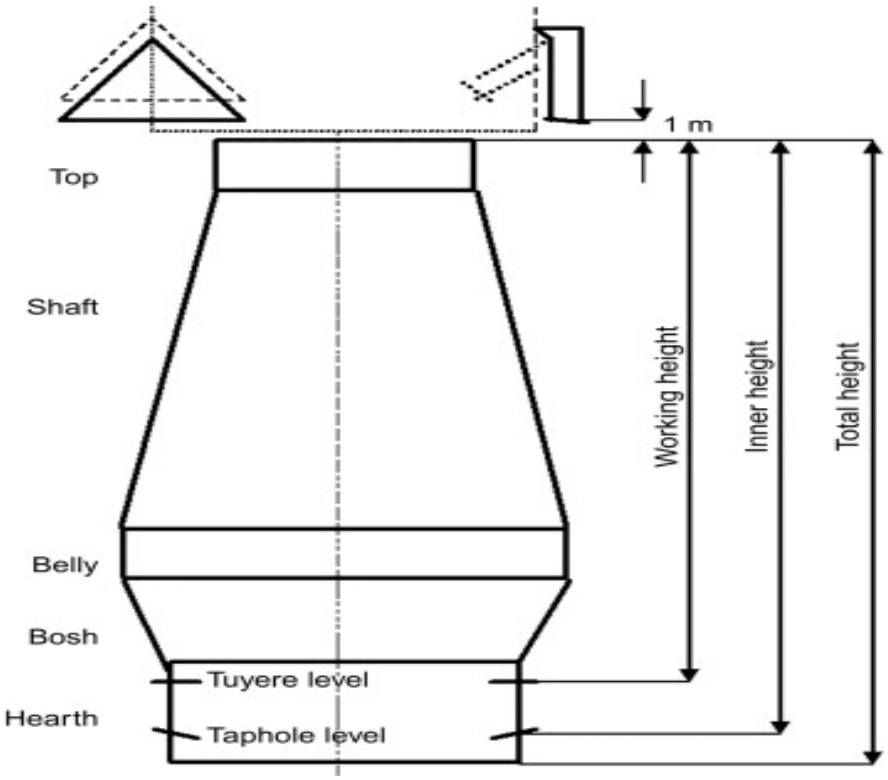

Figure 2.5: A blast furnace (Babich & Senk, 2015, p.510)

$$3Fe_2O_3 + CO \rightarrow 2Fe_3O_4 + CO_2 \quad (2.13)$$

$$Fe_3O_4 + CO \rightarrow 3FeO + CO_2 \quad (2.14)$$

A thermal balance is required in the blast furnace shaft for reactions 2.13 and 2.14 as reaction 2.13 is exothermic and reaction 2.14 is endothermic (Mandal *et al*., 2014). The Boudouard reaction (equation 2.15) takes place by manipulating the thermodynamics within the furnace. As per equations 2.13 and 2.14, the reduction of magnetite to hematite and hematite to wustite is done by carbon monoxide and not carbon. Due to this, the Boudouard reaction is imperative to produce the carbon monoxide that is required to reduce iron ore (Geyer & Halifa, 2014; de Castro *et al*., 2020).

$$C + CO_2 \rightarrow 2CO \quad (2.15)$$

Equation 2.3 ($CH_4 + CO_2 \rightarrow 2CO + 2H_2$) illustrates the methane combustion equation. This may in some instances cause a water-gas shift reaction from the moisture that is found in the coke's volatile matter in the blast. Hydrogen is a better reductant than carbon hence the water-gas shift, found in equation 2.4 ($CH_4 + H_2O \rightarrow CO + 3H_2$) is imperative in a blast furnace (de Castro *et al*., 2020).

$$CO + H_2O \rightarrow CO_2 + H_2 \tag{2.16}$$

The indirect reduction of wustite occurs both in the shaft and in the lower zone (belly and bosh) of the furnace. All the endothermic reactions involved take place in this lower zone of the furnace (de Castro *et al*., 2020).

$$FeO + C \rightarrow Fe + CO \tag{2.17}$$

$$P_2O_5 + 5C \rightarrow P_2 + 5CO \tag{2.18}$$

$$SiO_2 + 2C \rightarrow Si + 2CO \tag{2.19}$$

In this process, it is important to keep the phosphorus content in the melt at a minimum as phosphorus has a negative effect on the steel. Moreover, silicate should also be kept to a minimum since silicates are only necessary for the formation of slag, which must also remain at a minimum for optimal operations in the blast furnace (de Castro *et al*., 2020). Equation 2.17 to equation 2.19 are all endothermic and take place in the lower zone of the furnace. Other reactions that occur in the blast furnace under certain conditions will not be included in this literature review. A summary of the concentration of the most detrimental elements to the quality of steel required for metallurgical applications is provided in the following section.

2.1.2.3 The effect of phosphorus on steel

Phosphorus has detrimental effects on the steel produced. The maximum amount of phosphorus required in higher-grade steel is between 0.03% and 0.05%. The detrimental effects of phosphorus start at 0.10% in low-alloy high-strength steel. Phosphorus makes steel too brittle, increasing the possibility of breakage during steel processing (Jordan, 2006). Most of the phosphorus found in steel can be traced back to the coking coal and coke used in the reduction process. Once it enters the blast furnace, it cannot be removed as it reports to the molten iron. To mitigate this detrimental impact on the quality of the melt, a coke that meets the required phosphorus standard must be charged into the blast furnace (Lu *et al*., 2013).

2.1.2.4 The effect of alkalis in the blast furnace

The percentage concentration of alkalis introduced into the blast furnace is due to the cokes and pulverised coal charged into the furnace. Alkalis are dangerous to the blast furnaces operation and can act as a catalyst to the water-gas shift reaction. This behaviour leads to the accelerated use of carbon and the weakening of the coke at the lower part of the blast furnace (Matsui *et al*., 2005). A study by Lundgren *et al.* (2010) stated that alkalis form a scaffold on the blast furnace walls, thereby reducing the volume inside. This leads to an elevation in the gas velocity required in the furnace; hence increasing the particles that are blown out from the top of the blast furnace by the off-gas and material loss in the furnace. The breaking of the scaffolds from the furnace walls into the hearth of the furnace inhibits the flow of the gas fed into the furnace. Liu *et al*. (2021) also discussed how alkalis support the physio-chemical properties of the slag, hence an abundance of it could initiate slag production prematurely, decreasing the molten metal production. Lastly, alkalis erode the refractory lining of the blast furnace walls, shortening the blast furnace's lifespan.

2.1.2.5 The effect of sulphur on pig iron

The sulphur content should be closely monitored in coking coal as it might end up having detrimental effects on the downstream process (Makgato, 2013). The sulphur content in coke charged into the blast furnace ought to be kept to a minimum, due to its negative effects on steel if present above the minimum required in certain steel. Sulphur does not have a direct effect on pig iron, but it affects the final product, which is steel. The maximum machinability allowable percentage of sulphur is 0.05% (Steel Dynamics, 2021). A value greater than 0.05% causes brittleness and reduces weldability. Free machine steel can have sulphur levels of up to 0.04% because the free machine steel is not as ductile as other steel alloys (Steel Dynamics, 2021). The total sulphur content is dependent on the amount of other forms of sulphur in coal that can be found via characterisation.

2.2 COAL CHARACTERISATION

Coking coal characterisation is imperative to understand and determine the impact of the coal properties in the blast furnace. Several techniques are employed to characterise the physiochemical, micro-molecular and rheological properties of coal. The origin of the coal contributes significantly in its inherent properties, and Gondwana coals have been found to vary excessively in rank and organic composition. The Northern hemisphere (Lasarian) coal formed during the carboniferous period under hot and humid swamp conditions has a superior characteristic to that formed in the Southern hemisphere (Gondwana). The Southern

hemisphere coals are formed under sub-artic to cold temperature deciduous forest to warm savannah woodlands (Wagner *et al*., 2018). For this reason, the characteristics of the coals from different regions of the world are different. The following section provides some of the analytical techniques for characterising coal:

2.2.1 Proximate Analysis

One of the fundamental methods of analysing coal is proximate analysis. This analytical technique determines inherent moisture, ash content and volatile matter in coal with the fixed carbon calculated by difference. Inherent moisture is the water retained in coal pores and fissures (Mahapatra, 2018), while the ash content is the remaining material following total combustion combustion of coal. The volatile matter is the gas eliminated from coal at elevated temperatures and the fixed carbon is the char that remains after the removal of inherent moisture, ash and volatile matter (Theron & le Roux, 2015). The data obtained from the proximate analysis of coal can be used along with its petrographic data, FTIR and other analyses to classify the coal and its suitability as coking coal.

2.2.2 Fourier-Transform Infrared Spectroscopy

The FTIR is an analytical technique used to determine the infrared spectrum of absorption or emission of a solid, liquid or gas (Petit & Madejova, 2013). The FTIR method provides good-quality infrared spectra on opaque materials like coal and char (Petit & Madejova, 2013). It offers various advantages that can extend the usefulness of infrared for studying the properties of coal and other hydrocarbons. Its high sensitivity is due to its high energy throughput. In addition, FTIR has digital storage of data and numerous analysis routines, allowing comparative results for coal as a complex structure.

With the aid of FTIR, Liu and Zhang (2020) investigated the hydrothermal treatments effect on the oxygen functional groups in a coal carbon structure. The FTIR results showed that hydrothermal treatment was an efficient method for upgrading coal. According to the study, the decomposition of oxygen functional groups was noted at low temperatures, hydrolysis of functional groups at higher temperatures and lastly covalent bond breakage. Yao *et al*. (2011) also used FTIR to identify the oxygen groups and alkyl side-chains of coal subjected to cracking at different temperatures. Using FTIR, newly formed structures were identified as carboxylic groups and aromatic rings. However, further analysis is required to look into the microstructure of coal.

2.2.3 Petrography

Coal petrography is a microscopic technique used to determine the coal rank and type (Richards *et al*., 2013). It is a method of characterising coal type (amount of macerals), mineral matter and coal rank using a highly technical reflected microscope. An accurate petrographic analysis is imperative to find the optimum bituminous coal and various coal blends for producing blast furnace coke (Ward & Suárez-Ruiz, 2008). The coal petrographic data is of importance as it not only offers maceral composition and reflectance but also illustrates parameters that can be used in the correlation between the coal's physical and chemical characteristics (Jordan, 2006). The importance of reactive macerals in the blast furnace is their ability to become plastic, evolve volatile matter, swell, bubble, and finally harden (Richards *et al*., 2013). Inert macerals remain solid during the coking process and do not possess the quality derived from a reactive semi-fusinite maceral (lower volatile matter) and vitrinite. Richards *et al*. (2013) reported that there needs to be a balance between reactive and unreactive maceral components for coke stability in a blast furnace. Reactive macerals are inclusive of vitrinite and liptinite, while in Southern African coals, their semi-fusinite content also acts as a reactive maceral. The semi-fusinite is a low-reflecting form of inertinite that can be reactive, contributing to the reactivity of the coal during carbonisation.

The coke strength is one of the most important properties required of a reductant in the blast furnace. Petrography predicts the coke strength from coals and coal blends (Sutchu *et al*., 2009). The rank and maceral composition of coal influences its coking strength and expansion or contraction characteristics. These characteristics influence the blast furnace wall pressure; therefore, a balance is for a smooth process (Richards *et al*., 2013). Advanced optics and digital cameras connected to the petrography microscope enable high-quality resolution images to be captured down to a micron scale, enabling detailed qualification and quantification of the organic and inorganic constituents of the examined coal (Makukule *et al*., 2016). This technique also provides detailed information on the condition (oxidation) of the coal (Ward & Suárez-Ruiz, 2008).

An investigation conducted by Oboirien (2012) using petrographic analysis shows the reactive maceral transformation in South African coals: GG, Matla and Duvha. The author showed that GG coal's porous chars have higher reactive macerals (vitrinite), while Matla and Duvha coal's denser chars (non-porous) are predominantly inertinite. In contrast, a study on four Australian coals illustrated that the inertinite present in the coal is more reactive than the rich vitrinite content of the coals. According to the authors, this was caused by the large

micropore surface area of the inertinite related to that of the vitrinite within the coal (Grigore *et al.*, 2012). Therefore, it is imperative to note that coals from different sources and regions behave differently. The coal rank does not affect the coal's characteristics alone; the maceral composition is also imperative, especially in metallurgical coals (Richards *et al*., 2013). The coal rank and maceral composition affect the coal strength and swelling properties (Denge & Baiyengunhi, 2021).

2.2.3.1 Coal ranking

Coal rank is dependent on vitrinite reflectance. The coals' characteristics change with rank, and the rank presents the possible area of application for a particular coal. The free swelling index (FSI) of coal is a rank-dependent parameter, which is also associated with the coal's volatile matter content. The coal rank also affects the molecular structure of coal and the coke formed for metallurgical applications. The increment in coal rank leads to a more aromatic structure and decreasing aliphatic carbon structure. The rank directly impacts the coal's volatile matter, carbon content, vitrinite reflectance and the carbon to hydrogen ratio. The carbon content, vitrinite reflectance and carbon to hydrogen ratio have a proportional relationship with the rank while the volatile matter has an inverse relationship with the rank. In the metallurgical industry, volatile matter and vitrinite reflectance are the two most imperative parameters to rate the coal rank. Metallurgical coal of good quality has a volatile matter of 15% to 45% at a dry mineral matter-free basis and a vitrinite reflectance of 0.7% to 1.8% (Lu *et al*., 2013).

2.2.3.2 Maceral composition

Maceral is a microscopically recognisable organic coal constituent with characteristic physio-chemical properties (Viljoen *et al*., 2015; Kandiyoti *et al*., 2017). These constituents are coalified plant remains preserved in coal (Viljoen *et al*., 2015). Macerals are classified according to their reflectance, morphology, colour, shape and size (Matjie *et al*., 2016). There are three main maceral groups: liptinite, vitrinite and inertinite. The vitrinite maceral is an intermediate between liptinite and inertinite in the form of their physical and chemical properties (Moroeng, 2018). Table 2.1 illustrates the effect of macerals and rank on the volatile matter for bituminous coal.

Table 2.1: The effect of rank and macerals on the volatile matter (Wagner, 2021)

	Vitrinite reflectance	Liptinite	Vitrinite	Inertinite including reactive semifusinite
High volatile	0.60	77.5	44.0	36.0
	0.80	68.8	40.4	28.2
Medium volatile	1.00	57.2	35.4	23.0
	1.20	43.9	29.6	19.7
Low volatile	1.40	31.5	25.3	17.5
	1.60	21.6	21.2	17.2

The inertinite maceral group consists of several macerals, predominantly semifusinite, fusinite and inertodetrinite (Moroeng *et al*., 2019). Semifusinite appears to be available at various reflectance levels. The low-reflecting semifusinite is abundantly available in South African coals, and it is called reactive semifusinite. This reactive semifusinite has appeared to increase the coking ability of medium-rank bituminous coals (Malumbazo *et al*., 2012). The inertinite group is more aromatic than the vitrinite group in South African coals (Falcon & Ham, 1988; Moroeng *et al*., 2019). Das *et al*. (2016) conducted a study to determine the suitability of low vitrinite and high inertinite coal for its application in a blast furnace. The results exhibited that under top-charging blast furnace conditions, the coal had improved M10 and M40 values, meeting the blast furnace requirements. In contrast, Kalkreuth *et al*. (2005), found an inverse relationship between a Brazilian coal's inertinite content and char reactivity. This illustrates the importance of investigating coals to determine their attributes before being utilised. Table 2.2 summarises the three major maceral groups: vitrinite, liptinite and inertinite.

Table 2.2: A summary of maceral group qualities (Wagner, 2021)

Maceral group			
	Description	Rank	Reflected light %
Vitrinite	Dark to medium grey	High to medium-volatile bituminous	0.5 to 1.1 and 1.1 to 1.6
	Pale grey	Low-volatile bituminous	1.6 to 2.0
	White	anthracite	2.0 to 10.0
Liptinite	Black-brown	High-volatile bituminous	-0.0 to 0.5
	Dark grey	Medium-volatile bituminous	-0.5 to 1.1
	Pale grey	Low-volatile bituminous to anthracite	-1.1 to 1.6
	Pale grey to white shadows	High-volatile bituminous	-1.6 to 10
Inertinite	Medium grey	High-volatile bituminous	0.7 to 1.6
	Pale grey	All bituminous coals and anthracite	1.6 to 10
	White		
	Yellow white		

As shown in Table 2.2, each maceral group is differentiated from another by reflectance (% of reflected light) and colour, and each maceral group is a coal rank identifier. The maceral groups can also be distinguished from each other by their morphology, shape, size, polishing hardness and fluorescence (Oboirien, 2012).

2.2.4 Coal Surface Area and Pore Volume

The microstructure of coal provides distinctive information regarding the width of the coal cell wall, its pore size, pore volume and micro-fissures (Li *et al*., 2019). The coal rank plays a big role in the types of pores in the coal microstructure. When dealing with a porous material, the external surface is defined as a non-porous material, while the internal surface area is defined as the surface of all pore walls (Thommes *et al.,* 2015). Porosity is defined as the volume of the total pore to the particle or agglomerate particle. The pore structure of coking coal is developed during the plastic range of carbonisation (Duad & Ali, 2000). Initially, the pores appear in large particles during the softening range. The medium particle only becomes porous at higher temperature ranges. The rise in temperature increases the pore size and pore numbers (Howaniec, 2016), causing particles to become well-rounded and swell. There are three pore types: micro-pores, mesopores and macro-pores (Pan *et al*., 2019). Mesopores are found in the low to medium-rank coals while micropores are generally found in the higher-rank coals (Schwanke *et al*., 2017). Macropores have a pore width that exceeds 50nm

(nanometre), mesopores have a pore width between 2nm and 50nm and micropores do not exceed 2nm (Thommes *et al.,* 2015). Since the coal rank plays a role in porosity, low-rank coals with good fluidity produce a porosity of about 50% to 60% while medium-rank coals have a slightly less porous coke of around 54% by volume (Cheng *et al*., 2017).

According to the study conducted by Thommes *et al*. (2015), the increase in coals inertinite content leads to a decrease in the coke anisotropy; hence inertinites are responsible for forming isotropic coke. Several techniques, including electron microscopy, mercury intrusion porosimetry and physical adsorption of gases, have been utilised to determine the coal micro-molecular structure. The BET (Brunauer-Emmett-Teller) technique was used to analyse the molecular structure of coke produced in the current study. Pore characteristics of a coal sample with bursting proneness were studied by Li *et al*. (2021a). They used mercury intrusion alongside low-temperature nitrogen adsorption and desorption to study the pore size distribution and pore volume of the coal specimen. The increment in bursting showed many mesopores and macropores in the coal sample. Similarly, Casal *et al*. (2021) investigated nine coals with coking abilities to determine the coals with a tendency to have high coking pressure during carbonisation. The porosity of the plastic layer and the semi-coke produced within the temperature range of 500°C to 800ºC was investigated. The results showed that some coals are dangerous and could not be used as semi-coke due to the high porosity and lower mercury apparent density.

2.2.5 Rheological Properties of Coking Coal

Coking coals could swell and then solidify. The rheological properties, known as the plastic properties of coal, provide information on the coal's swelling and solidifying capability (Glushkov *et al*., 2019). The rheological property of coal plays a big role in coal blends. The plastic zone (350ºC to 500ºC temperature range) and the post-plastic contraction zone (500ºC to 750ºC) are two conditions that have a major effect on coke. The caking capacity and the volatile matter of the coal in the post-plastic zone allow for the forecast of the coke quality. For coals with a caking capacity (dilation) above 75%, the coke blends produced from these high and low-volatile matter coals have a better caking capacity than the original respective coals in the blend(de Cordova *et al*., 2016) . However, coals with a caking capacity of less than 75% are incompatible, suppressing the plasticity of other coals (de Cordova *et al*., 2016; Jiao *et al*., 2019). Bridging coals can combine two incompatible coals with an insufficient overlap or similarity in the plastic zone. The bridging coals, called prime coking coals, have a surplus plastic range that overlaps the two coals (Grainger & Gibson, 2012). Laboratory

results have shown that increasing the resistance to the volatile matter escape in the plastic temperature range increases the plasticity of the coal (Casal *et al*., 2021). Due to this reason, stamp charging of coals into a specialised oven can make good-quality coke from poor coal with a high bulk density.

2.2.5.1 Gieseler Plastometer test

The Gieseler Plastometer test determines the maximum fluidity and plastic range of coals. The maximum fluidity of the coal is reported in dial divisions per minute (ddpm) (SGS, 2021). The data determined from the Gieseler Plastometer test includes the softening temperature (temperature when the stirrer begins to rotate), maximum fluidity temperature (the temperature at which the stirrer reaches maximum rotation rate), resolidification temperature (the temperature at which the stirrer stops) and the maximum fluidity (Guelton, 2017). The plastic range is defined as the positive difference between the maximum fluidity temperature and the softening temperature (Sciazko *et al*., 2020). Figure 2.6 illustrates the Gieseler Plastometer test's temperature range.

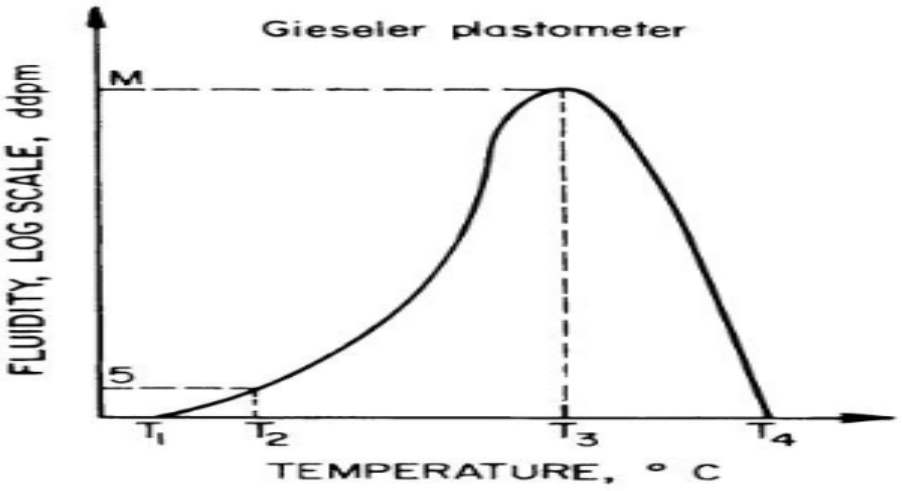

Figure 2.6: The Gieseler Plastometer temperature curve (Eun, 2012, p.70)

Figure 2.6 illustrates the Gieseler Plastometer test's temperature range where:

- T_1 is the softening temperature
- T_2 is the fusion temperature
- T_3 is the maximum fluidity temperature
- T_4 is the solidification temperature
- T_4-T_1 is the plastic temperature range

- M is the maximum fluidity

One of the important aspects of this test is that it enables the coal user to select coals with the maximum appropriate fluidity to be used in the blend. Each coal's softening and re-solidification temperatures are monitored very closely, and their characteristics are taken into account. If coal resolidifies before other coals, then the coal cannot be used in the blend with those coals (Sciazko *et al*., 2020). The maximum fluidity of the coal defines the coal's ability to mix, bond and bind with other coals (Kumar *et al*., 2008). The fluidity of bituminous coal is categorised into three: the minimum volatiles ranging from 20ddpm to 1000ddpm, medium volatiles range from 200 to 20 000ddpm and high volatiles range from 5000ddpm to 30 000ddpm (SGS Minerals Services, 2013). Even with all these ranges, metallurgical coal has a maximum fluidity of between 200ddpm and 1000ddpm(Jordan, 2006).

Arslan & Kemal (2006) studied blending a medium-ranked Zonguldak coal with a volatile matter of 32% at a dry ash-free basis with various low-volatile matter coals. The fluidity of the low-volatile matter coals was low but wide enough to overlap with that of the Zonguldak coal. The optimum coal blend had 20% to 50% Zonguldak coal and the rest was the low-volatile matter coals. The fluidity can also be utilised to determine the effect of blending coal with other materials such as char and coal tar. The addition of coal tar increases the plastic range but the addition of char decreases the coal's plastic range (Fraga *et al*., 2020). Similarly, an investigation conducted by Adeleke *et al*. (2007) on American coking coal showed that the coal had a large plastic range. This means that the coal could not only be used alone but as a blend with weak and probably non-coking coals. The fluidity test alongside the FSI was used by the authors in classifying if the coal was prime coking coal.

2.2.5.2 Ruhr Dilatation

The Ruhr Dilatation test is used to establish the swelling properties of coal when heated under certain conditions. The test uses 5g (grams) of coal moulded into a 60mm (millimetre) pencil. The pencil is placed in the tub and a sliding fit rod is then placed on top of it. The tub is placed into a furnace at 300°C and heated to the coal's maximum dilation temperature, which is usually below 600°C (Jordan, 2006). The coal's thermodynamic movement is reported and used to explain its behaviour during the fusion, softening and contraction of semi-coke (Eun *et al*., 2012). The initial shrinking temperature is the dilatation softening temperature (T_1). When the probe goes down to the minimum point, the temperature is recorded as the maximum contraction temperature (T_2). The temperature at the highest point

is the end of swelling temperature (T_3). The total dilatation is then calculated as an average value between the contraction and dilatation. According to Makgato *et al*. (2019), a minimum of 29.6% dilation is required to obtain a fused coke. Figure 2.7 illustrates the Ruhr Dilatation test's temperature range.

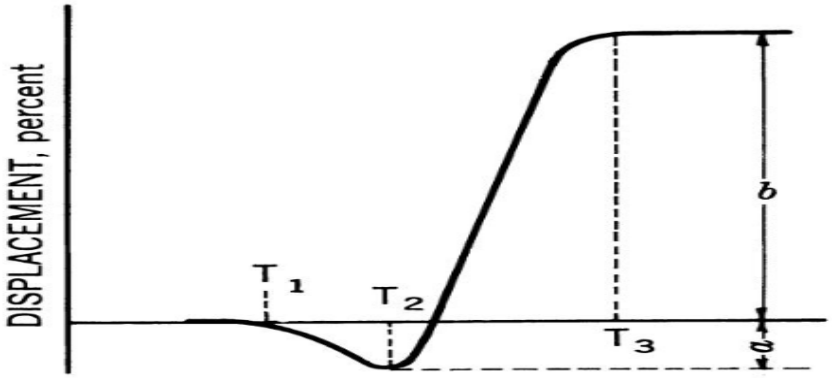

Figure 2.7: The dilatation test of coal (UNT Digital Library, 2021, p.21)

The following temperatures are illustrated in Figure 2.7:

- T_1 is the softening temperature
- T_2 is the maximum contraction temperature
- T_3 is the maximum dilation temperature
- T_3-T_1 is the plastic temperature range
- a is the maximum contraction and
- b is the maximum dilatation

2.2.5.3 Roga Index

The Roga Index, also called the G power or caking capability, describes the coke strength by evaluating the bonding strength between the inert and the reactive maceral groups. Rzychoń *et al*. (2021) conducted a study to predict a caking ability model of coal blends. The results showed that the Roga Index is a non-cumulative variable. It depends more on other coal parameters such as carbon, moisture, volatile matter and vitrinite. The more the vitrinite content in the blend of coal, the higher its Roga Index. Volatile matter has an inverse relationship with the Roga Index; between 29% and 34%, the volatile matter does not affect the Roga Index (Rzychoń *et al*., 2021). It is also imperative to note that the Roga Index only indicates the caking ability of the coal, not how much cake or coke nor the strength that will be formed (Jordan, 2006). A study by Fedorova *et al*. (2017) showed that the Roga Index of coals with different vitrinite reflectance was more dependent on the vitrinite reflectance. The

Roga Index of weakly coking coal lies between 5 and 20. Medium coking coals have a Roga Index of 20 to 50, while strongly coking coals have a Roga Index of 50 (Speight, 2013).

2.2.5.4 Swelling Index

For the swelling index determination of coal, the coal is first heated without any external disturbances, and the heating of the coal gives off volatile matter that causes the coal to swell. After re-solidification, a porous coke button lighter in weight than the original sample is formed. This button, compared to a series of standard profiles, numbered 1-9, can be used to determine the coal swelling index, as shown in Figure 2.8.

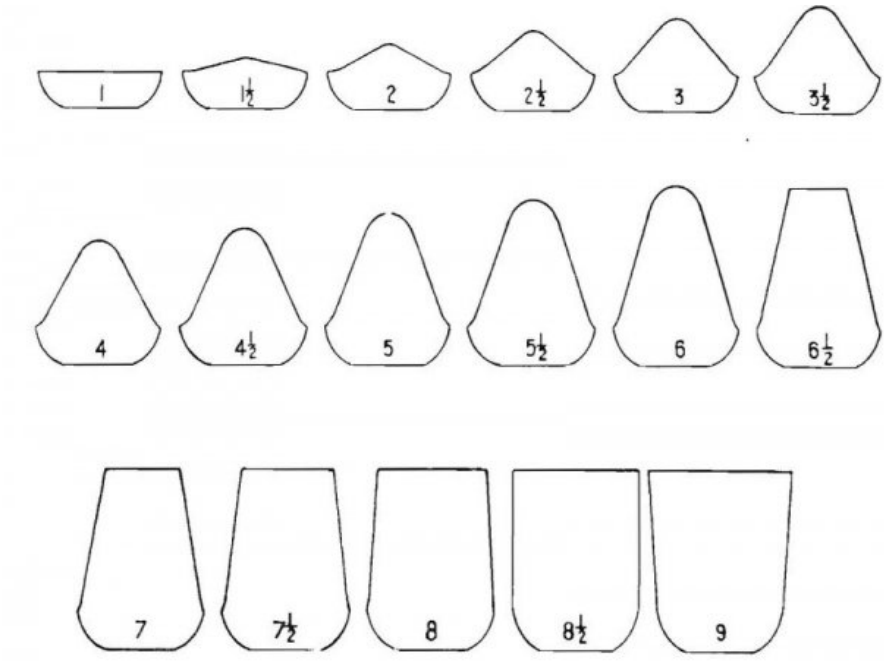

Figure 2.8: The standard 'buttons' for the free Swelling Index (FitzGerald & Zambrowski, 2023, p.23)

Figure 2.8 shows the different coal indexes. An FSI greater than four means that the coal can produce good coking coals, and any FSI above seven produces high-quality coking coals (Battle *et al*., 2014).

2.2.5.5 Rheological properties summary

The results from the rheological properties of coal mentioned above (Gieseler Plastometer, Ruhr Dilatation, FSI and Roga Index) can be used in the interpretation of the coke's CSR and Coke Reactivity Index (CRI). There is usually a proportional relationship between the rheological properties and CSR for coking coal (Dash *et al*., 2011). The CSR tends to increase with increasing rheological values. The CRI is, however, inversely proportional to

the rheological values and tends to decrease with increasing rheological properties. A high rheological index, i.e., the caking index, total dilation and Gieseler Fluidity, can agglomerate the coal; for example, a high fluidity would mean that the coal will have a stronger bond during carbonisation, unlike a smaller fluidity value (Dash *et al*., 2011). Figure 2.9 shows the relationship between the rheological properties and the coke strength properties.

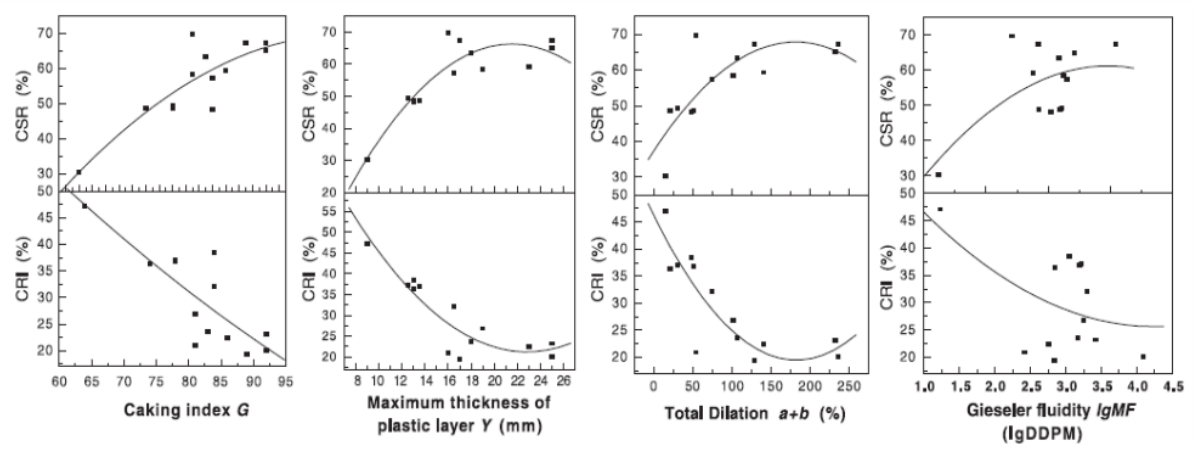

Figure 2.9: The effect of rheological properties on coke strength properties (Eun *et al*., 2012, p.74)

2.2.6 Coal Reactivity Index and Strength After Reaction

The strength of coke in a blast furnace is dependent on two main characteristics, the CRI and the CSR (Probierz & Marcisz, 2019). Coke strength after reaction, also known as the hot strength, is a quality determined in simulated blast furnace conditions. The procedure was developed by Nippon Steel (Probierz & Marcisz, 2019). The test includes reacting 200g of 1mm to 200mm sized coke samples for 2 hours at 1100°C in carbon dioxide gas (Probierz & Marcisz, 2019). Post the reaction, the sample is tumbled in an I-type tumbler, and the percentage of the particles left that are greater than 9.5mm is used to determine the CSR. The change in weight loss is defined as the CRI.

$$CRI = \frac{A-B}{A} x100 \quad (2.20)$$

Equation 2.20 illustrates the CRI equation where:

- A is the original weight of the test sample before the test, and
- B is the weight of the sample after its reaction in carbon dioxide.

A good-quality coke is expected to have a CRI value equal to or below 20% to 30%. The CSR can be obtained using equation 2.21 (Rodero *et al*., 2015):

$$CSR = \frac{C}{B}x100 \quad (2.21)$$

Where:

- B is the weight of the sample after its reaction in carbon dioxide, and
- C is the sample weight greater than 9.5mm after tumbling.

According to Todoshuk *et al*. (2004), Arcelor Mittal has used the CSR method to predict coals and their blends that are allowable for usage in the blast furnace. By integrating various characterisation methods, including proximate analysis, petrography, coal sulphur and ash, Arcelor Mittal was able to change their coal blends, producing strong, long-lasting cokes. Figure 2.10 shows how the CSR has evolved over the years at Arcelor Mittal.

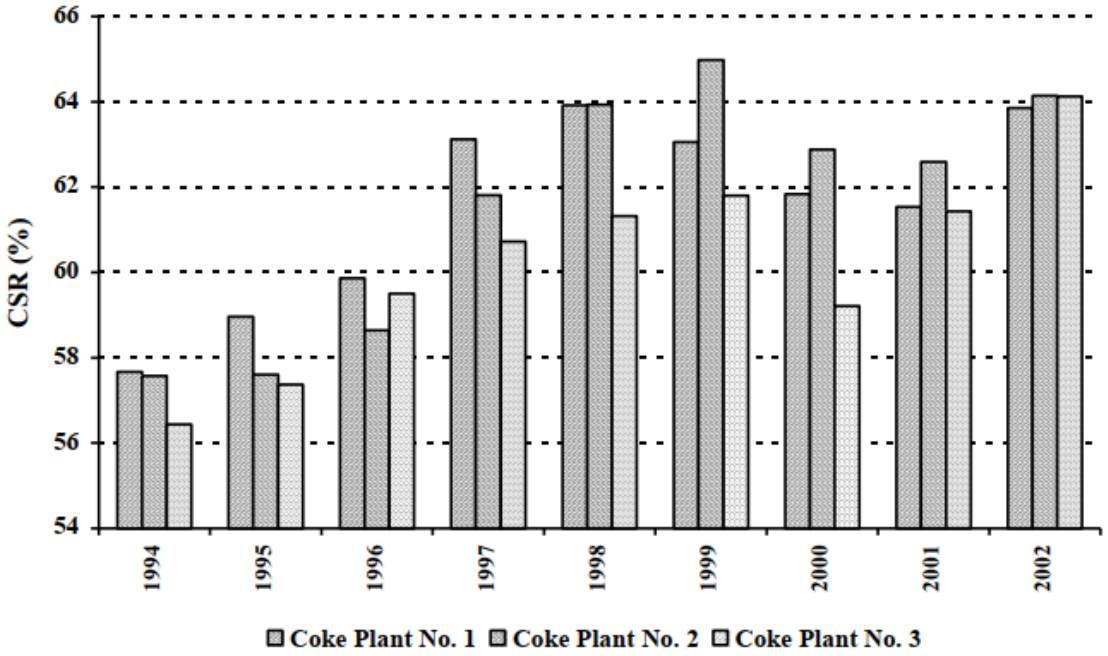

Figure 2.10: The coke strength after reaction (CSR) evolution over the years at Arcelor Mittal (Todoshuk *et al*., 2004, p.16)

As seen in Figure 2.10, the CSR values have evolved and increased over the years. A high CSR means the coke is strong and does not react easily with carbon dioxide. This is imperative in the blast furnace as the coke is expected to last long while all the reactions occur. Coke is important as a reductant, fuel and burden support in the blast furnace, so coke loss must be avoided. Therefore, the CSR values must remain as high as possible. The CRI, however, is the opposite of the CSR and must be kept at a minimum, as stated above (Todoshuk *et al*., 2004).

To determine the CRI, the Salem Box Test has become more prevalent. The Salem Box Test uses 18 kilograms of coal milled to 3mm and stamped into a cake with 10% moisture. The stamped cake is placed into a steel box, charged into an oven for carbonisation, and removed and quenched in the water. The cake is then air-cooled, crushed and sieved to a particle size range of -21 + 19 mm. A CRI of less than 25% and CSR greater than 64% were the only accepted coke parameters. The Salem Box coke method was comparable to the standard used in the industry; hence the method was approved (Nagashanmugam *et al*., 2015).

2.2.7 Typical Characteristics of Coking Coal

For the conditions in the blast furnace to be effective, certain properties are required of the coking coal used. Table 2.3 presents the required coking coal specifications and limits in the blast furnace.

Table 2.3: The summary of coking coal parameters required in a blast furnace (Satyendra *et al*., 2013a)

Parameter	Limit	Reason
Total moisture	10% maximum as-received	High moisture lowers available carbon
Ash	10% maximum	High ash reduces the blast furnace productivity
Volatile matter	Between 20% and 35% air-dried	High volatile matter decreases the blast furnace yield
Sulphur	0.6% maximum air-dried	Part of the sulphur reports to the hot metal
Phosphorus	0.1% air-dried	Reports to hot metal making it difficult to remove it
Free Swelling index (FSI)	three minimum, six maximum	hard coking coals have a higher FSI
Maximum dilatation	55% minimum	
Maximum fluidity	600ddpm minimum	Higher fluidity gives better flow in coke ovens
Alkalis	2% maximum in ash	High alkalis reduce the blast furnace productivity
Ash fusion temperature	1450°C per minute	It needs to be higher than the coking temperature
Mean maximum reflectance	0.85% to 1.35%	
Vitrinite	50% minimum	45% maximum for medium coking coals
Vitrinite distribution	70% minimum	

Table 2.3 indicates the limits of the quality of coking coal accepted in the blast furnace. The quality of the coal used in the blast furnace is imperative and each parameter must be within

its limit. The characteristics of the coal and the efficiency of the blast furnace largely depend on these parameters (Table 2.3). The total moisture, for instance, is largely associated with the blast furnace's efficiency. Yan *et al*. (2020) stated that the high moisture content in coal leads to an energy usage that is both high and inefficient. Fang *et al*. (2019) studied the coal moisture effect on the quality and yield of coke products from carbonisation. The results illustrated that for the moisture content varied from 1.8% to 10.13% and the yield decreased from 77.16% to 75.90%. There was also deterioration in the CSR, CRI, M10 (abrasion index) and M25 (fragmentation index) as the moisture content increased. According to Gridavos *et al*. (2016), high alkalis in the coal also lead to an attack on the refractory lining and cause excess slag and coke usage. Kurunov *et al*. (2009) stated that for each kilogram of alkali that reports into the blast furnace, the furnace productivity decreases by 4.5% and the coke depletion rate increases by 11.3kg. Without utilising a coal or coke that meets the specifications outlined in Table 2.3, the furnace's efficiency continues to decline. It is, therefore, essential to carry out research to improve the available coals quality, especially in South Africa, which no longer has coking coal.

2.3 TECHNIQUES FOR UPGRADING LOW-GRADE COAL AS A COKING COAL

Lower-quality coals are abundant and unsuitable for various processes. The lack of coals suitable for metallurgical application has led to the study on upgrading coal using several techniques as presented in the literature. These technologies include coal briquetting and tar replacement, microwave drying, carbonisation and pyrolysis and hydrothermal treatment as described in the following sections.

2.3.1 Coal Briquetting and Tar Replacement

Briquetting is a technique used to compress coal or other combustible material to produce a densified fuel that can be stored and transported easily. An investigation conducted by Kudo, *et al*. (2018) using hot briquetting and carbonisation on 12 lignite coals improved the quality of briquetted products. The tensile strength of the coal briquette increases as the aliphatic carbons in the lignite coals form stronger bonds. In a recent study by da Assis (2019), using tar as a binder improved the coal oven characteristic. The apparent density of the briquettes produced using this approach increased by 42.5% with good inertinite-rich chemical and physical characteristics, leading to increased productivity in the coke oven. In another study, lignosulphonate and resin were used as binders along with an, low-grade coal to produce strong water-resistant briquettes. The briquettes produced showed adequate strength, cohesiveness and water resistance for industrial usage (Leokaoke *et al*., 2018). Using coal tar

pitch, which is a residue from coal tar formed by high-temperature pyrolysis (Bermudez *et al*., 2017) can also be used in upgrading the quality of a coking coal for metallurgical applications. Coal tar pitch has a more aromatic structure, making it more stable than a thermal pitch. Makgato and Falcon (2013) also utilises coke oven tar as a possible substitute for imported premium coking coal. Their results showed that coke oven tar can improve metallurgical coke qualities, leading to improved quantity and reduced cost of imported coking coal.

2.3.2 Microwave Drying

Microwave drying is a technology that could improve and upgrade coal for different applications. A microwave generates heat to remove moisture extensively from a material and upgrade it thermally (Punathil & Basak, 2016). A review by Zuo *et al*. (2016) described coal microwave drying as both a thermal and non-thermal process, with the thermal process leading to crack formation and changes in pore structure. The non-thermal process effects include removing oxygen functional groups, improved coal rank and mineral decomposition. Both the thermal and non-thermal effects significantly impacted the upgrading of lignite coal using the microwave technique (Zhixiu *et al*., 2019). According to the authors, the scanning electron microscopy analysis results showed an increase in the number of pores, cracks and fractures in the upgraded coal after being microwaved. In addition, FTIR showed a decrease in the oxygen functional group, while the BET showed a 30-fold increase in the specific surface area. The authors observed that most pores had evolved from macropores to mesopores.

Recently, a study was carried out by Williams *et al*. (2019), exhibiting 5 coking and non-coking coal samples being densified prior to being microwaved. The cokes produced from this process were compared with cokes produced from industrial processes. The fused coke lumps were produced within two minutes compared to the industrial coke produced through the conventional method in 16 to 24 hours. Three samples produce a coke with reactivity indices between 20 and 30, which is within an acceptable range for the blast furnace. In addition, from the morphological analysis conducted, the structure of the coke formed from the non-coking coal samples was acceptable and could be used for metallurgical applications.

2.3.3 Carbonisation and Pyrolysis

Carbonisation is the transformation of a three-dimensional macro-molecular network into a three-dimensional macro-atomic network by heating (Marsh & Rodriguez-Reinoso, 2006;

Ogishi *et al*., 2021). It is a process which involves producing metallurgical coke as a reductant for iron making and other smelting processes (Grainger & Gibson, 2020). Carbonisation is essential as it removes the volatile matter and increases the carbon content (Diez *et al*., 2002). This process entails heating coal to about 1300°C in the without oxygen.

The residue left post carbonisation is called coke. The coke that remains generally consists of carbon in various forms and thermally modified mineral remains referred to as ash. There are three temperature levels in which carbonisation may take place. The first level is low-temperature carbonisation. Normally the temperature range is between 500°C and 700°C. The product from this low-temperature process has abundant liquid products and a limited amount of gaseous products. This product is initially used to provide residential town gas for street lighting and domestic or industrial heating. Mazumder (2012) established that the char produced from this carbonisation process could be used as blends in coking oven feeds, leading to pyrolysis being used to upgrade coal.

A study on low-temperature pyrolysis was conducted on Shenmu sub-bituminous coal without a caking property. The pyrolysis results showed an increase in the caking property; the highest caking property was at 450°C. The mechanical strength and coke strength after the reaction also improved (Liu *et al*., 2018). The second level is the medium-temperature carbonisation, which is around 800°C, and the last range is the high-temperature carbonisation range. The high-temperature carbonisation range is between 900°C and 1200°C, whereby all the volatile matter is released as liquid and gas, leaving behind carbon with minimal impurities (Morley *et al*., 2017).

2.3.4 Hydrothermal Treatment

Hydrothermal treatment displays a high moisture content material to high temperatures and pressures to improve its quality. It is imperative to examine the temperature and other factors used for the hydrothermal treatment of coal to find out what conditions may further affect coal during hydrothermal treatment. Temperature is part of the major parameters that affect coalification over time alongside pressure (Stepheson, 2013). Low-rank coals can be upgraded to produce clean fuel. Increasing the temperature can increase the coal's carbon content (Yu *et al*., 2018). A study of hydrothermal treatment of lignite coal conducted between 130°C and 190°C illustrated that temperature adequately inhibited the reduction of hydrogen and oxygen and the decomposition of carboxyl and phenolic hydroxyl groups in lignite (Yu *et al.,* 2018). The author also observed mesopore formation, improving the coal

rank. In another study by Shui *et al*. (2012), temperature increased the coking parameters such as the coals' micro-strength index, particle reactivity index (PRI) and post-reaction strength. The micro-strength index and post-reaction strength increased for coal treated at a temperature range of 150° to 300°C, leading to an increased coke strength. Another hydrothermal test was conducted on Naiyinhua lignite coal, improving the coalification of the coal at a temperature of 250°C. This also led to a decrease the oxygen to carbon and hydrogen to carbon atomic ratios (Shi *et al*., 2017).

Hydrothermal treatment conducted at elevated temperatures with water acting as a catalyst allows for the elimination of oxygen groups, mainly the hydroxyl groups, promoting the breakage of hydrogen bonds in the molecular network (Shui *et al*., 2013; Zhao *et al*., 2016). This generated lighter fragments, which are stabilised by hydrogen from water. The structure of coal is dissociated effectively, increasing caking capacity and solvent extraction (Shui *et al*., 2012). Disrupting hydrogen bonds may further form the rearrangement of atomic rings that could form plastic materials (Zhao *et al*., 2016). Even though temperature significantly affects the coal's behaviour, the coal particle size has been found to have little or no effect on the hydrothermal treatment (Shui *et al*., 2012).

Temperature is not the only variable that affects the upgrading of coal. The effect of water on hydrothermal treatment and pyrolysis was studied by Li *et al*. (2019). They used two models to investigate the effect of water at high temperatures on the structure of lignite coal while using either hydrothermal treatment or pyrolysis to upgrade the coal. The water molecules formed hydrogen bonds with the oxygen-containing groups, destroying the intermolecular bonds in lignite, improving the coal product.

A study on transforming lignite into caking coal by hydro-modification in subcritical water–CO system illustrated that the disruption of weak covalent bonds, such as ether, ester and side chains, by hydrolysis and pyrolysis changed the distribution of non-covalent bonds, such as hydrogen bonds (Zhao *et al*., 2016). This disruption was able to form plastic materials in lignite coal by rearranging the atomic rings, increasing the caking property of the lignite with an index from 0 to 96 (Zhao *et al*., 2016). At 200°C, similar effects were evident on lignite treated hydrothermally in the hope of producing coke from this lignite. When this lignite coal was acid washed before the hydrothermal treatment, the porosity and ash content reduced while the plasticity increased (Mori *et al*., 2013). A small change in other parameters, such as

a decrease in hydrogen content and ash, is still an indicator of pre-treated coal (Wang *et al*., 2008).

2.4 ALTERNATIVE REDUCING AGENTS

Coking coal (coke) is the most widely used reducing agent currently used in a blast furnace. The depletion of metallurgical coal has led to various studies on alternative reducing agents for use in the steel production processes. This section provides insight into other reducing agents, such as hydrogen and shredder residue material, that can be used as a substitute in metallurgical applications.

2.4.1 Hydrogen

Hydrogen is proposed as a future reductant for the steel industry. The current technology used for steel making releases a large amount of carbon dioxide because carbon is a reductant (He *et al*., 2017). The steel industry is one of three major carbon dioxide-producing industries (McKinsey & Company, 2020). To overcome this major emission, many studies on the use of hydrogen as alternative reductant to carbon are on-going (Noussa *et al*., 2021). Hydrogen is researched because water is the by-product of the process. Four types of primarily produced hydrogen can be used as a reductant: brown, grey, blue and green hydrogen (Figure 2.11). Brown and grey hydrogen are produced from fossil fuels that emit carbon dioxide (Wood, 2020). The production of brown hydrogen is from coal and oil while the production of grey hydrogen is from natural gas reforming process. Blue hydrogen is also produced from fossil fuels, but the process is integrated with carbon dioxide capture technology (Jovan & Dolanc, 2020. The sequestrated carbon dioxide from the blue hydrogen process is either deposited underground or used by industry to produce other products. Renewable energy sources like wind and solar energy produce green hydrogen (Jovan & Dolanc, 2020).

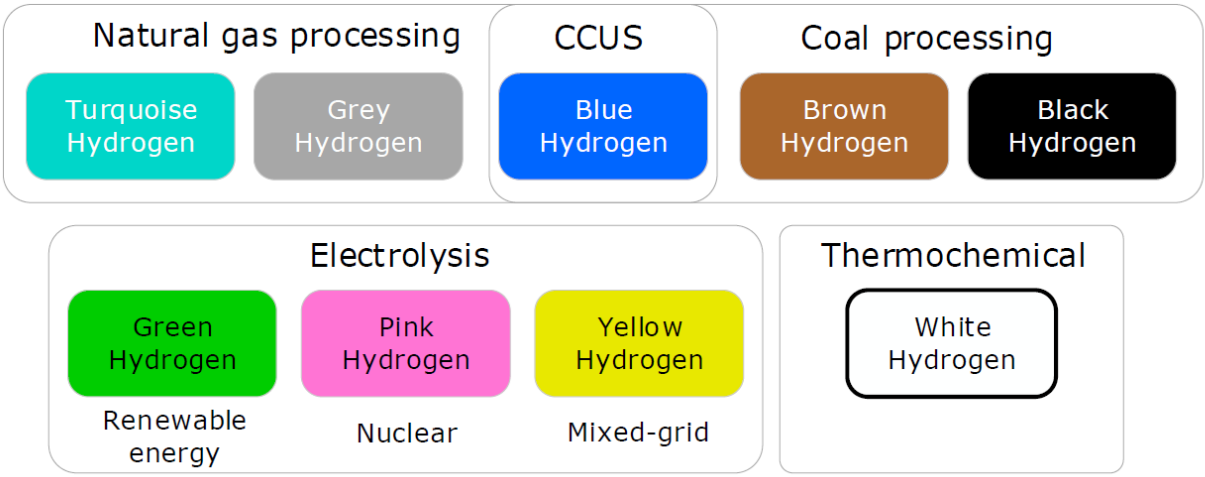

Figure 2.11: Hydrogen colour based on production method (Panic', *et al.*, 2022, p.5)

In the production of brown hydrogen, carbonaceous material is processed into carbon dioxide, hydrogen and carbon monoxide by applying temperatures above 700ºC with a controlled amount of steam or oxygen (Kumar, 2013; Energy Information Administration, 2022). Additional or more hydrogen can be produced using the water-gas shift reaction ($CO + H_2O \rightarrow CO_2 + H_2$). Coal gasification is the most popular method to produce brown hydrogen. Syngas containing hydrogen, carbon monoxide and a trace of carbon dioxide are produced during gasification, while absorbers and membranes are used to separate the hydrogen from the rest of these contaminants (Giovannini, 2020). Hydrogen may be further classified as brown or black based on the coal type used (CsiroScope, 2021). Brown hydrogen is produced from lignite (brown coal) and black hydrogen is produced from bituminous coal. Grey hydrogen is produced from natural gas by steam reforming. Synthesis gas (syngas) is produced from natural gas and steam (U.S Department of Energy, 2020). With the recorded high emission from the production of grey hydrogen, "steam methane reforming" produces about 95% of the world's hydrogen to date (Wood, 2020). Blue hydrogen has an industrial carbon capture system to capture the carbon dioxide formed. A maximum of 80 to 90% of the carbon can be captured. The process is carbon neutral because of the minimal pollution. Another hydrogen, turquoise hydrogen, is made through methane pyrolysis, but this is still in the experimental phase (Figure 2.11). The process is aimed at decomposing methane at high temperatures generating hydrogen and solid carbon (Harrison, 2022). Finally, there is a water electrolysis technology that comprises three colours of hydrogen: pink, yellow and green. All three are produced using electricity. Pink hydrogen is

produced from nuclear energy, yellow from any combination of available energy and green from renewable energy (Kshirsagar & Malladi, 2021). The current production of green hydrogen is 1%, and the world is moving towards the production and use of green hydrogen (Wood, 2020).

Hydrogen has several advantages, such as having water as a by-product and faster reaction rates compared to carbon (coal). The current limitation is that hydrogen production is costly. As a result, hydrogen is not used as a reducing agent for steel production, nickel reduction and the reduction of refractory metal oxides (Antrekowtsch & Steinlenchner, 2010; Birol, 2019). Several strategies have been put in place by different companies over the years to move to zero-carbon steel production (McKinsey & Company, 2020; POSCO, 2021). European companies have reached the lifespan of their basic oxygen furnaces and various companies have started setting up pilot plants for carbon-free steel production. As a result of the McKinsey & Company (2020) report, hydrogen can be injected into a PCI system. Coking coal will still exist, but its contribution will decrease as the world is moving into decarbonised steel production. POSCO (2021) already uses FINEX (Fine Iron Ore Reduction), a fluidised bed reactor with a melter or gasifier that produces molten iron. It uses 25% hydrogen and 75% carbon monoxide, and it is the primary technology behind the breakthrough of HyREX (Hydrogen Reduction), which aims to use 100% hydrogen. SSAB, LKAB (Sweden's largest iron producer) and Vattenfall (Sweden's energy producer) constructed a hydrogen electrolysis and storage facility, as well as the pilot steel factory in 2018, with the first commercial sales of fossil-free steel expected in 2026 (Pei, 2021). The EAF technology is fuelled by renewable electricity and fed by DRI. According to Pei *et al*. (2020), HyBRIT expects that due to carbon tax, the cost of coal will equate to that of hydrogen by 2028 in Europe.

Other companies like ArcelorMittal are also investigating green hydrogen for steel production. One of the studied technologies includes installing an electrolyser in the DRI-EAF route to produce hydrogen, reducing carbon used and mitigating carbon dioxide emissions (ArcelorMittal, 2020). To reduce their emissions by 30% by the year 2030, ArcelorMittal has employed hybrid blast furnace/DRI technology, which injects hydrogen-rich coke gas to reduce iron (ArcelorMittal, 2021). This technology would inject gases from various parts of the plant and has a carbon capture system. The system is currently using grey hydrogen but aims to move to green hydrogen and renewable energy.

As mentioned above, various companies (especially in Europe) are starting to decarbonise the steel-production industry. Their carbon-neutral plants are expected to be at full capacity by between 2048 and 2050. Huxham *et al*. (2019) and Tollip (2021) reported that South Africa has abundant and potentially low-cost renewable energy. South Africa may store and export renewable energy to Europe in the second phase of going green between 2027 and 2030 (Huxman *et al*., 2019). I disagree with the authors because the hydrogen produced will be too expensive, as we are a country without adequate water, electricity, and hydrogen gas storage facilities. Even though the hydrogen economy is important for the country's growth and energy security, the country has not yet begun to build its low-carbon steel production plant.

2.4.2 Shredder Residue Material

Automotive shredder residue materials obtained from discarded car components, along with the steel, iron and non-ferrous scrap, can be used as an alternative reductant (Steinert, 2021). Shredder residue material, with the inclusion of plastic, has been investigated as a possible alternative reducing agent to coke (Lotfian *et al*., 2017b). Although the char produced from the shredder residue materials have a lower fixed carbon to coal char, char is more reactive due to its higher surface area, but also contains high ash content. A study by Lotfian (2018) demonstrated that the conversion time of plastic materials was longer than that of coal. Plastic-containing material can be co-injected into a zinc-fuming furnace to replace coal without decreasing the rate of reduction (Lotfian *et al*., 2019). With all the attractive characteristics displayed by the shredder residue material, Lotfian *et al*. (2017a) suggested that it should only be used in a nonferrous blast furnace operation. This is because, with the chemical composition of shredder residue material, if used in the ferrous blast furnace application, it will detrimentally affect the quality of the pig iron produced (Nourredine, 2007).

2.5 SUMMARY

This chapter provided details of the various techniques used for coal upgrade and the specifications required for applications in the blast furnace. The chapter also highlighted different techniques for categorising coking coal and coke. In addition, the importance of hydrogen as an alternative reducing agent of the future and the different processes involved in producing hydrogen were discussed. Information on the use of shredding residues in the production of steel and non-ferrous metals along with the limitation of the reductant is well elucidated. With hydrogen being the most realistic future reductant, more funding needs to be provided in this area of research to investigate replacing coal as a reductant.

CHAPTER THREE: RESEARCH METHODOLOGY

3.1 INTRODUCTION

The coal samples, equipment, and methods employed in this study are described in this chapter. The GG semi-soft coking coal and Moatize coking coal were used as the feeds. Both coals were subjected to various physicochemical, rheological, and micro-molecular analyses to characterise their initial properties. The raw coal samples were hydrothermally treated and characterised. Based on the results of the physiochemical and micro-molecular analysis, the optimum parameters to run the hydrothermal reactor were chosen. The coals were used to produce blends that were hydrothermally treated at the optimum parameters. This allowed the optimum blend to be chosen to run the coking tests on this blend. The overall methodology is illustrated in Figure 3.1.

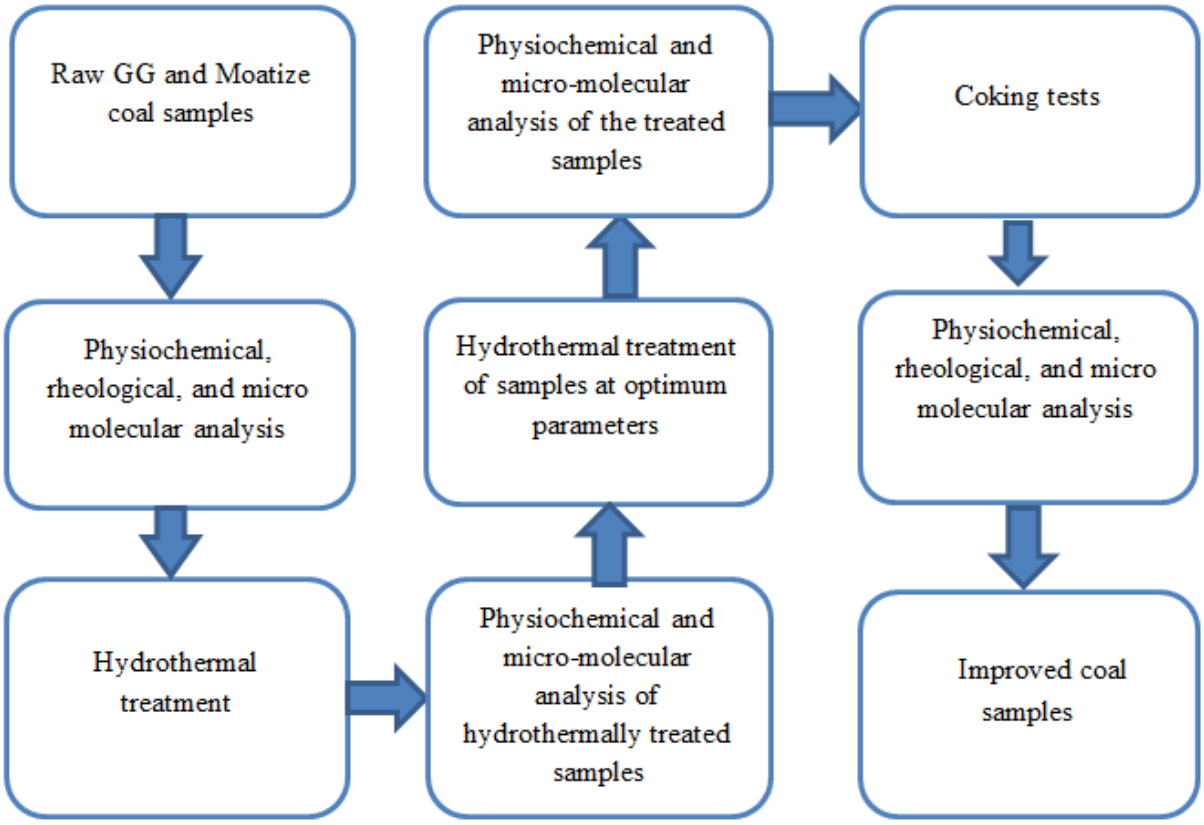

Figure 3.1: The process flow diagram

Each coal sample, GG and Moatize, was characterised before hydrothermal treatment. Physiochemical analysis, including proximate analysis, ultimate analysis, total carbon and sulphur, and FTIR analysis, were conducted on the raw coal samples. Furthermore, the raw coals were subjected to rheological analyses, such as the crucible swelling index, and the

Gieseler Fluidity and Ruhr Dilatation tests. Also, the raw coals were subjected to micro-molecular analyses, such as petrography and pore size distribution.

Hydrothermal treatment was conducted under varying temperatures, coal mass samples and residence times. The hydrothermally treated coal samples were further subjected to physiochemical and micro-molecular analysis to determine the optimum conditions. The coal at optimum hydrothermal conditions were blended, subjected to hydrothermal tests, and carbonised alongside the raw coal samples. The micro-molecular analyses, including BET pore surface area and pore volume, were conducted on the selected hydrothermally treated samples, their blends and carbonised coals. Lastly, the full characterisation was conducted on the upgraded coal blend.

3.2 EQUIPMENT

The following equipment was used for the experimental tests:

i. Pulveriser
ii. LECO TGA701
iii. Berghof BR-1500 High-Pressure Laboratory Reactor with accessories
iv. LECO SC632 Sulfur/Carbon Series.
v. Gieseler Plastometer
vi. Ruhr Dilatometer
vii. Elementar vario EL cube analyser
viii. Perkin Elmer Spectrum Two FTIR Spectrometer
ix. Leica DM4500 polarisation microscope
x. Autosorb-iQ gas sorption analyzer

3.3 CHARACTERISATION

3.3.1 Proximate Analysis

The sample's inherent moisture, volatile matter content and ash content were determined by proximate analysis. In addition, the fixed carbon content was calculated using equation 3.1, and values were expressed in percentages. The analysis was conducted according to ASTM D-5142 on a LECO TGA-701 instrument, where each sample was measured at approximately 1g using a ceramic crucible in the instrument. Moisture determination analysis commenced at 25ºC and heated up to 107ºC in a nitrogen atmosphere at a 6ºC/min temperature ramp rate, and the uncovered samples were held at 107ºC for 15 minutes until there was no change in

the sample mass. In a nitrogen atmosphere, the determination of the volatile matter commenced at 107ºC, crucibles were covered, and the temperature was raised to 950ºC at a 43ºC/min temperature ramp rate, where it was held for 7 minutes. For ash determination, the temperature was first reduced to 600ºC, before being raised to 750ºC at a heating rate of 3ºC/min in an oxygen atmosphere.

$$FC = 100 - IM - VM - Ash \quad (3.1)$$

Where FC is the fixed carbon content (%),

IM is the inherent moisture content (%),

VM is the volatile matter content (%) and

Ash is the ash content (%).

3.3.2 Ultimate Analysis

The ultimate analysis was conducted according to ISO 12902 in the Elementar vario EL cube analyser. The equipment carousels that can accommodate about 80 samples were loaded with tin foil capsules that could each accommodate a 50mg sample. After that, the sample was automatically sent to the combustion vessel where it was first flushed with helium, a carrier gas that removes atmospheric nitrogen. Combustion took place at 1150ºC. Before being delivered to the thermal conductivity detector for elemental concentration detection, the gases nitrogen, CO_2, H_2O and sulphur dioxide were once more divided into their component parts in the gas separation columns (Elementar, 2021). The percentage of carbon, hydrogen, nitrogen and sulphur was determined analytically, whereby oxygen was calculated by equation 3.2:

$$O = 100 - (C + H + N + S + Ash) \quad (3.2)$$

Where O is the oxygen content,

C is the carbon content,

H is the hydrogen content,

N is the nitrogen content,

S is the sulphur content, and

Ash is the ash content.

3.3.3 Total Carbon and Sulphur

Total carbon and sulphur determination was done according to ASTM D4239 using a LECO SC632 Sulfur/Carbon Series. The ceramic boat was tared on the scale and a sample was weighed to around 0.25g. The analyse button was pressed and when the system was ready, the boat with the sample was pushed into the furnace. Oxygen was used at 1350ºC to analyse the total carbon and sulphur in the material.

3.3.4 Fourier-Transform Infrared Spectroscopy

The FTIR analysis of the raw coal samples was performed to identify the functional groups using the Perkin Elmer Spectrum Two FTIR Spectrometer with attenuated total reflectance. Approximately 0.2g of the crushed coal sample was placed on the instrument, which applied pressure on the sample, and the spectra were displayed on the screen. Each sample's spectrum was obtained at the wavelength range of 4000cm^{-1} and 450cm^{-1}.

3.3.5 Gieseler Fluidity

Bureau Veritas uses a Gieseler Plastometer extensively to measure the fluidity of coal. The instrument's rotating ramble arm stirrer was held under constant torque in a packed sample of ground coal that was heated at 3ºC/min through the plastic range. Softening temperature (ºC), the temperature of maximum fluidity (ºC), the resolidification temperature (ºC) and the maximum fluidity in ddpm were obtained.

3.3.6 Ruhr Dilatation Test

The Ruhr Dilatation test was carried out according to SANS 881:2009 at Bureau Veritas. Coal crushed and pulverised to 250 microns was used to form a 60 mm pencil that was inserted into an accurately calibrated retort tube with a graduated piston on top. The sample was then placed in a furnace and heated at 3ºC/min. The piston movement as the coal pencil contracted and dilated was recorded.

3.3.7 Free Swelling Index

The FSI, also termed the crucible swelling index, measures the increase in the volume of coal when heated in the absence of air. The samples obtained are reported in numbers from 0 to 9, with the higher value considered higher quality for coking coal applications. The FSI was done by milling and sieving coal to 250 microns. One gram of the 250-micron coal was heated under specified conditions in a 17ml silica crucible with a regular lid. The caking characteristic of the coal samples was determined according to ISO 501:2012 (Hard coal – Determination of the crucible swelling number).

3.3.8 Roga Index

One gram of coal greater than 2mm was mixed with 5g of standard anthracite. The mixture was carbonised in an inert atmosphere for 15 minutes to 850ºC (Gagarin, 2009). The obtained coke was subjected to three drum tests and the Roga Index was determined.

3.3.9 Surface Area, Pore Volume and Pore Area

The multipoint BET model was used to obtain the specific surface area and the pore volume on the Autosorb-iQ gas sorption analyzer. The Quantachrome® ASiQwinTM software was then used for data processing and to enable data extraction. The surface area was analysed according to ASTM D6556-14. Approximately 0.2g of each sample was degassed at 300ºC for ten hours. The degassed sample analysis was carried out at 77 Kelvin (K) for surface area, pore volume and average pore size with 20 adsorption and desorption points chosen.

The pore size distribution is commonly used to describe and characterise the internal structure of activated carbons and other porous materials (Wang *et al*., 2019). The adsorption isotherm is commonly used to describe the pore size distribution of carbons. The non-local density functional theory is the frequently used calculation for pore size distribution based on the nitrogen adsorption data. A study by Abdulsalam (2019) illustrated that the Density functional theory (DFT) accurately determines the pore size distribution even though there are other methods, such as Barrett-Joyner-Halenda, so DFT was used in this research.

3.3.10 Petrographic Analysis

The petrographic analysis was done according to ISO 7404. The coal sample was crushed to -1mm, mixed with epoxy resin and hardener, and moulded as a block mount (Wagner *et al*., 2018). Maceral analysis was done according to ISO 7404-3 on well-polished block mounts. A Leica DM4500 polarisation microscope with a J and M spectrolytic system was used for maceral analysis and vitrinite reflectance. The macerals were counted in groups, and the results were stated in volume %. The microlythotype was carried out similarly to the maceral analysis but with a 20-point graticule in the microscope's ocular. The vitrinite reflectance was done according to ISO 7404-5. The vitrinite reflectance measurements were taken on a smooth polished surface under a monochromatic green light by photomultipliers and detectors. The results were reported as random reflectance, a standard deviation of the reflectance and a reflectance histogram.

3.4 HYDROTHERMAL TREATMENT

The hydrothermal treatment was conducted in a Bergof BR-1005 High-Pressure Laboratory Reactor Figure 3.2. This high-pressure system has a 1.75-litre vessel, magnetic stirrer, pressure gauge, standard fittings, temperature regulator, heating jacket, seals and data loggers, and it can go up to 300ºC and 90 bars.



Figure 3.2: Berghof BR series reactor and accessories (DKSH Group, 2018, p.3)

3.4.1 Hydrothermal Treatment of Coal

The coal particle size is not imperative in hydrothermal treatment. Even so, the particle size used was - 6mm. Moisture also plays no effect in the hydrothermal treatment of coal as water is added to the process. The tests were conducted under various conditions, with the residence time ranging from 30 minutes to 90 minutes, the raw coal sample mass ranging from 300g to 600g, and the temperature ranging from 100ºC to 200ºC. The reactor was pressurised to 20 bar under nitrogen or argon for each test, and 800ml of distilled water was used to mix with the raw coal. Upon receiving the results, a further test at 280ºC, 180 minutes and 600g was conducted to see the effect of higher temperature and residence time on the samples. Table 3.1 illustrates the parameters used for tests run on the hydrothermal reactor. Table A1 and Table A2 in appendix A illustrate the GG and Moatize nomenclature respectively.

Table 3.1: Experimental process parameters for each test run

Sample ID	Coal sample	Temperature (ºC)	Time (min)	Pressure (bar)	Mass (g)	Water (ml)
GG-HTC-300A	GG	100	30	20	300	800
GG-HTC-450A	GG	100	30	20	450	800
GG-HTC-600A	GG	100	30	20	600	800
M-HTC-300A	M	100	30	20	300	800
M-HTC-450A	M	100	30	20	450	800
M-HTC-600A	M	100	30	20	600	800
GG-HTC-300-A1	GG	150	30	20	300	800
GG-HTC-450-A1	GG	150	30	20	450	800
GG-HTC-600-A1	GG	150	30	20	600	800
M-HTC-300-A1	M	150	30	20	300	800
M-HTC-450-A1	M	150	30	20	450	800
M-HTC-600-A1	M	150	30	20	600	800
GG-HTC-300-A2	GG	200	30	20	300	800
GG-HTC-450-A2	GG	200	30	20	450	800
GG-HTC-600-A2	GG	200	30	20	600	800
M-HTC-300-A2	M	200	30	20	300	800
M-HTC-450-A2	M	200	30	20	450	800
M-HTC-600-A2	M	200	30	20	600	800
GG-HTC-300B	GG	100	90	20	300	800
GG-HTC-450B	GG	100	90	20	450	800
GG-HTC-600B	GG	100	90	20	600	800
M-HTC-300B	M	100	90	20	300	800
M-HTC-450B	M	100	90	20	450	800
M-HTC-600B	M	100	90	20	600	800
GG-HTC-300-B1	GG	150	90	20	300	800
GG-HTC-450-B1	GG	150	90	20	450	800
GG-HTC-600-B1	GG	150	90	20	600	800
M-HTC-300-B1	M	150	90	20	300	800
M-HTC-450-B1	M	150	90	20	450	800
M-HTC-600-B1	M	150	90	20	600	800
GG-HTC-300-B2	GG	200	90	20	300	800
GG-HTC-450-B2	GG	200	90	20	450	800
GG-HTC-600-B2	GG	200	90	20	600	800
M-HTC-300-B2	M	200	90	20	300	800
M-HTC-450-B2	M	200	90	20	450	800
M-HTC-600-B2	M	200	90	20	600	800

M: Moatize, GG: Grootegeluk, min: minutes, g: grams, ml: millilitres

3.4.2 Coal Blending for Further Hydrothermal Treatment

Based on the analytical results from the hydrothermal treatment outlined in section 3.4.1, the optimum temperature and raw coal mass for the GG and Moatize coal samples were determined. The two raw coal samples GG and Moatize were blended at varying compositions from a GG composition of 15% to 50%. The blends were subjected to hydrothermal treatment at the optimum conditions from section 3.4.1, as shown in Table 3.2.

Table 3.2: Various coal compositions

Sample ID	Coal composition (wt-%)	Temperature (ºC)	Time (min)	Pressure (bar)	Mass (g)	Water (ml)
90-(15%GG+85%M)	15%GG, 85%M	200	90	20	600	800
90-(30%GG+70%M)	30%GG, 70%M	200	90	20	600	800
90-(50%GG+50%M)	50%GG, 50%M	200	90	20	600	800

wt-%: weight percentage, GG: Grootegeluk, M: Moatize, min: minutes, g: grams, ml: millilitres

3.5 COKING TESTS

The coking tests were conducted on the LECO TGA701 under an inert atmosphere by adding 0.1g of sample into a ceramic crucible and allowing the sample to be raised to 400ºC at 5ºC/min and to a further 950ºC by ramping it at 4ºC/min (Flores *et al*., 2017). The sample was then held at 950ºC for 30 minutes. The coke reactivity was also determined using the LECO TGA701, from room temperature to 1000ºC at a heating rate of 30ºC/min in a nitrogen atmosphere. At 1000ºC, the atmosphere was changed from nitrogen to carbon dioxide and the temperature was held for two hours (Díez & Borrego, 2013; Flores *et al*., 2017). The change in mass with respect to time was recorded and used to calculate the particle reactivity index using equation 3.3 (Shui *et al*., 2012):

$$R = \frac{1}{m_0}\frac{dm}{dt} \qquad (3.3)$$

Where $dm = m_0 - m$

Therefore, $R = \frac{m_0 - m}{(m_0).(dt)} = \frac{dX}{dt}$

Where $X = \frac{(m_0 - m)}{m_0} x100;$

R is expressed in %/min;

m_0 is the coke's starting mass following the removal of all moisture and volatile substances and before the conversion from a nitrogen atmosphere to a carbon dioxide atmosphere in mg (milligram).

m is the mass of the coke at any specific time and temperature in mg;

$\frac{dm}{dt}$ is the conversion in %.

3.6 SUMMARY

This chapter presented the methods used to characterise the raw GG and Moatize coal samples, the hydrothermal treatment procedure, the blending of the two coals at various compositions, coke production and the coking tests for coal. The analytical methods for physiochemical analysis of the coal included proximate, ultimate, total carbon and sulphur and FTIR. The rheological analytical methods included Ruhr Dilatation, Gieseler Fluidity, FSI and Roga Index. The micro-molecular analysis techniques included surface area, pore size, pore volume and petrography. The results and the discussion of the aforementioned experiments are presented in Chapter 4.

CHAPTER FOUR: RESULTS AND DISCUSSIONS

4.1 INTRODUCTION

This chapter presents the experimental data from this research. The data consists of the physiochemical properties of the as-received coal samples and their micro-molecular and rheological properties. The results obtained from the hydrothermally treated coals at various temperatures (100°C to 280°C) and various masses (300g to 600g) are presented. The physiochemical analysis and micro-molecular data from the effect of blending the Moatize coal with the 15%, 30% and 50% GG coal on mass ratio are also presented in this chapter. Lastly, the coke produced from the blend of the hydrothermally treated samples and their reaction in carbon dioxide is discussed.

4.2 CHARACTERISATION OF THE RAW COAL SAMPLES

4.2.1 Physiochemical Characterisation of the Raw Coal Samples

The physiochemical, rheological and micro-molecular properties of the two coals utilised in this research were done to determine the suitability and the coking potential of the coals. These results are presented in Table 4.1.

The inherent moisture content of the coals was 5.31% and 2.23% for GG and Moatize, respectively. For effective coke production, the inherent moisture content of the coal must be below 8% (Das *et al*., 2016; Makgato & Falcon, 2013). According to Fang *et al*. (2019), a decrease in the moisture content of coking coal influences the overall property of a coke, enhancing the CSR and carbon yield, hence decreasing the CRI. A good coking coal must also have a volatile content between 20% and 35%, with the most appropriate coal having a volatile matter in the lower range (Satyendra, 2013a). The Moatize coal had a volatile matter content of 20.35% (Table 4.1), which is within the required range for a suitable coking coal. The same coal can be used as a pressure reducer when blended with coal such as the GG coal of higher volatile matter to reduce the negative impact of a highly swelling coal.

Table 4.1: Characterisation of the raw Grootegeluk and Moatize coal samples

Coal	**Grootegeluk coal**	**Moatize coal**
Proximate (% adb)		
Inherent moisture (IM)	5.31	2.23
Ash content (Ash)	10.72	10.6
Volatile matter (VM)	35.02	20.35
Fixed carbon (% calculation*)	51.84	67.36
Ultimate (% adb)		
Carbon content (C)	69.5	76.5
Hydrogen content (H)	4.90	4.22
Nitrogen content (N)	1.41	1.84
Oxygen content (% calculation**)	7.03	4.61
Total sulphur (S) (%)	1.13	1.19
Maximum dilatation (%)	-10.0	59.0
Crucible swelling index	5.5	9.0
Maximum fluidity (ddpm)	3.0	24
Petrographic composition (% in.mm)		
Vitrinite content	72.5	75.0
Inertinite content	9.20	13.6
Liptinite content	2.0	0.0
Mineral matter content	16.3	11.4
Microlythotype (%in.mm)		
Vitrinite content	66.6	68.6
Inertinite content	4.20	10.8
Liptinite content	0	0
Intermediates	10.8	10.6
Minerals	18.4	10.0
Reflectance random	0.720	1.28
Standard deviation	0.169	0.095
Rank category	Medium-rank C bituminous	Medium-rank B bituminous
Total pore volume (cc/g)	$1.11e^{-2}$	$9.48e^{-3}$
Average pore size (nm)	7.05	7.70
Specific surface area (m^2/g)	5.75	4.92

% adb: % air-dried basis, ddpm: dial divisions per minute, in.mm: including mineral matter, cc/g: cubic centimetre per gram, nm: nanometre, m^2/g: square metre per gram, *FC=100-(IM+Ash+VM), **O=[100-(Ash+H+C+N+S+IM)]

The ash content of the two coals was between 10.60% and 10.72%, and a good-quality coking coal is expected to have an ash content of less than 10% (Ryemshak & Jauro, 2013. According to Ryemshak and Jauro (2012), a 2wt% (weight percentage) to 3wt% decrease in metal production can be caused by 1wt% increment in the coke ash content. From the

ultimate analysis result, the Moatize coal had a higher total carbon content of 76.50% compared to 69.50% from GG coal. Moatize coal also ranked higher than GG coal; this is due to its higher carbon content, less volatile matter and more vitrinite composition. Moatize coal is arguably more mature and has more carbon as a reductant than GG coal.

The FTIR spectra of the raw GG and Moatize coal (Figure 4.1) and the summary of the coals functional groups are presented in Table 4.2. This provides an insight into the difference in the structural and functional groups within the two coals. As seen in Figure 4.1 and Table 4.2, the peaks of an O-H stretch, aliphatic and aromatic C-H, CH_2, CH_3 and Si-O deformations. Peak 1, between 3693cm^{-1} and 3679cm^{-1}, shows O-H vibrations. The Moatize coal sample exhibited more intense O-H bonds, which can be attributed to higher hydrogen (1.80%) bonds than GG coal (1.41%). Moatize coal also exhibited a more intense peak than GG coal in the 1934cm^{-1} to 1602cm^{-1} range (peaks 4, 5 and 6), which shows the aromatic segment of C-H. This is supported by the higher elemental carbon in the sample (76.5%) than in GG coal (69.5%). The fingerprint region from 560cm^{-1} to 500cm^{-1} shows peaks of a similar range for both samples. According to the petrographic result, GG coal had a higher mineral content than Moatize, but both coals had similar ash content.

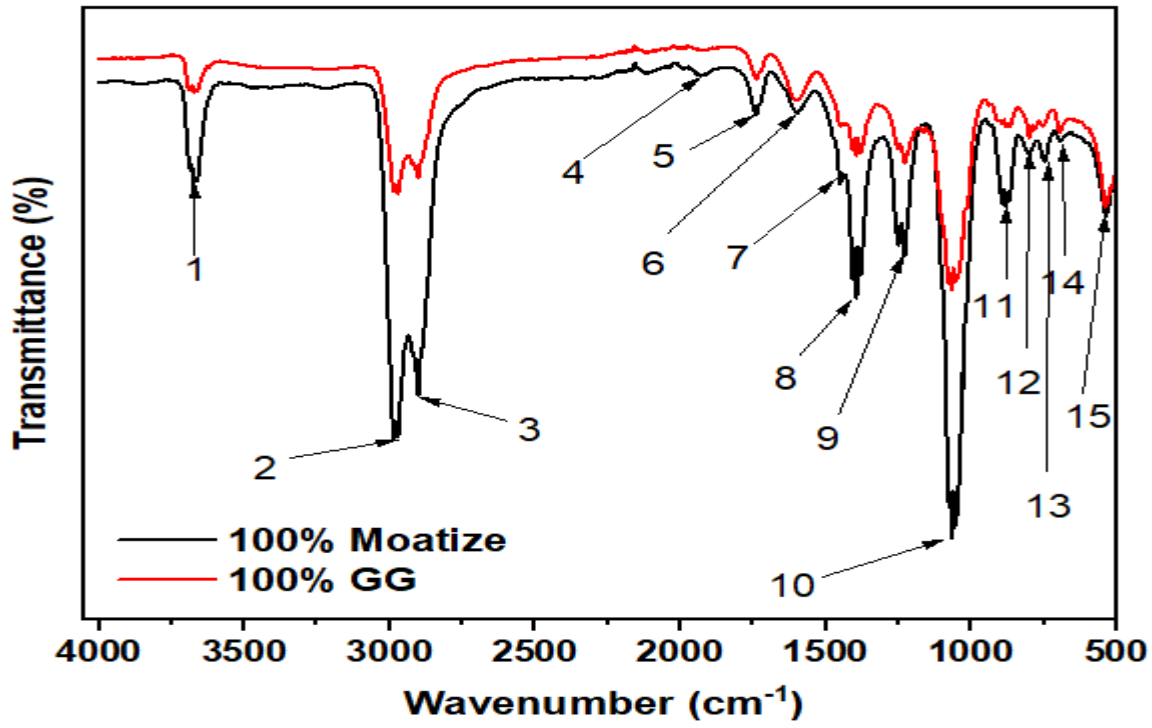

Figure 4.1: The Fourier-Transform Infrared Spectroscopy spectra of Moatize and Grootegeluk (GG) coal samples

Table 4.2: Summary of functional groups for the infrared spectra of the Moatize and Grootegeluk coal samples (Khan *et al*., 2018; Merk, 2022)

Wave number (cm^{-1})	Peak/vibration	Functional groups/band assignments
3693-3679	1	O-H stretching vibrations
2990-2900	2,3	Aliphatic C-H stretch
1934-1602	4,5,6	Aromatic C-H stretch
1452-1403	7	CH_2, CH_3 bend vibrations
1390	8	CH_3
1300-1000	9,10	C-O stretch and O-H bending vibrations in phenol structures
900-700	11,12,13	Out of plane aromatic C-H vibrations
560-500	14,15	Si-O and Si-O-Si deformations associated with kaolinite and quartz

4.2.2 The Rheological Characterisation of Grootegeluk and Moatize Coals

The rheological property of the coal signifies its area of application. The coal used in a blast furnace must produce a coke that exhibits a rheological property that conforms to the required standard maximum dilatation, fluidity, caking index and crucible swelling index. From Table 4.1, the maximum dilatation of GG coal was -10%, while that of Moatize coal was 59%. The negative maximum dilation was due to the contraction of coal when exposed heat instead of the usual expansion. This phenomenon is called negative thermal expansion (Cong *et al*., 2023). According to Makgato *et al*. (2019), the required minimum dilatation percentage for a coking coal to make a fused coke is 29.6%. Furthermore, coal with dilatation between 0 and 40 is weakly coking and above 50 is a strongly coking coal (Speight, 2013). The Moatize coal was found to be above 50. The maximum fluidity temperature for the GG coal sample and the Moatize coal sample used in this study was 420℃ and 474℃, respectively.

The plastic range of a coal sample is highly dependent on its chemical composition (Sciazko *et al*., 2020). The GG coal was within the coking coal crucible swelling index limits of three to six, while the Moatize coal was within the prime coking coal limit of 6-9 (Battle *et al*., 2014). According to the swelling index standard, a weak caking coal has a swelling index below 2.5, and a weak to moderate caking coal has an index between three and 3.5. A moderate caking coal is between four and 6.5, and a swelling index above seven provides high caking power. The cokes with high caking power are too strong to be used in a blast furnace; hence the moderate caking power cokes are used. From the maximum fluidity test result, both coals were not within the metallurgical coal range for maximum fluidity. The maximum fluidity range for metallurgical coal is between 200ddpm and 1000ddpm (Jordan,

2006); the study coals were 3ddpm and 24ddpm for the GG and Moatize coal samples, respectively. The study coals had a Roga Index of 36 for GG and 56 for Moatize, and both indices do not comply with the range for metallurgical coking coal. Their micro-molecular parameters were investigated to conclude the quality and suitability of these coals for metallurgical application.

4.2.3 The Micro-Molecular Characterisation of Grootegeluk and Moatize Coal

The GG coal sample was discovered to be a medium-rank C bituminous coal with a vitrinite content of 72.5% and a mineral matter content of 16.3%. The Moatize coal sample was discovered to be a medium-rank B bituminous coal with a vitrinite content of 75% and a mineral matter of 11.4 The full maceral group analysis, vitrinite reflectance and microlythotypes can be seen in Table A3, Table A4 and Table A5 in Appendix A. According to the micrograph in Figure 4.2c, the sample of Moatize coal indicates the presence of natural coke.

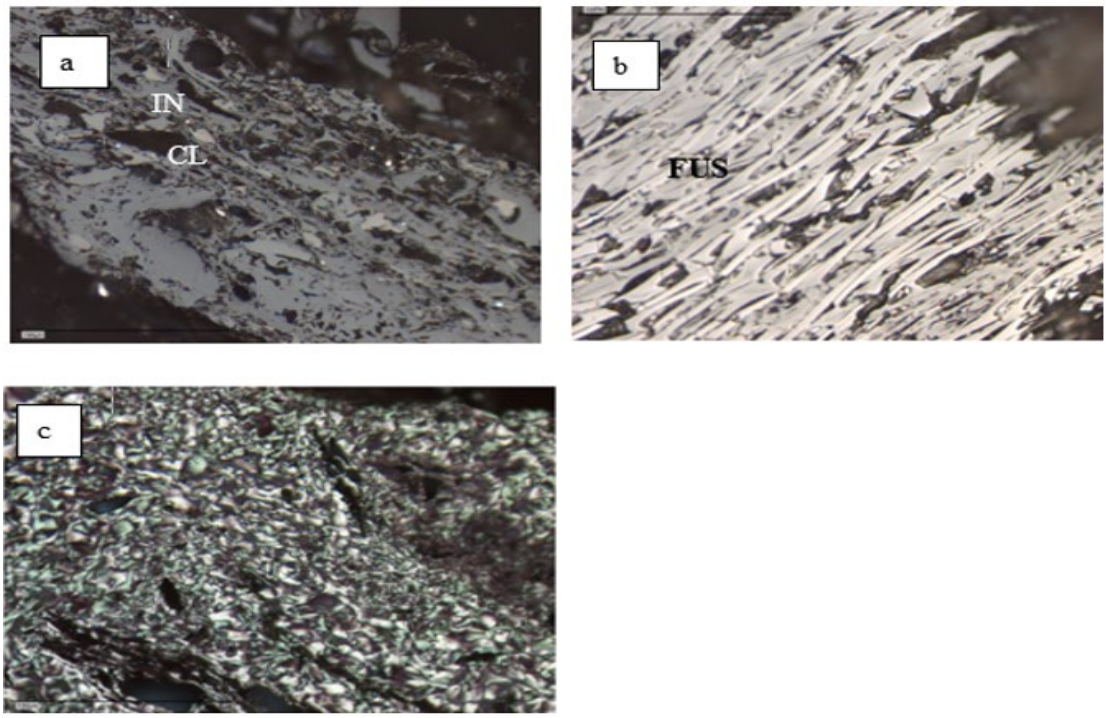

Figure 4.2: Moatize coal sample with (a) inertinite (IN) and clay (CL), (b) fusinite (FUS) and (c) natural coke

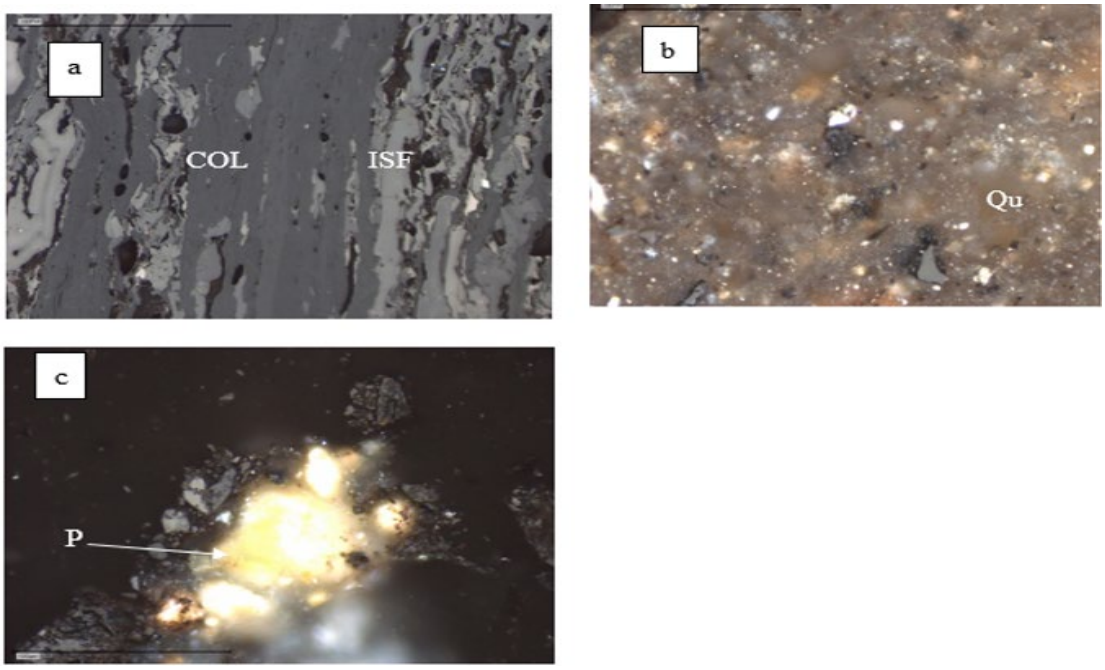

Figure 4.3: Grootegeluk coal with (a) colledilite (COL) and inert semifusinite (ISF), (b) quartz (Qu) and (c) pyrite (P)

Figures 4.2 and 4.3 show the composition of the Moatize and GG samples in terms of their maceral constituents and mineral matter contents. Vitrinite is the main and valuable maceral in a coking coal that determines the quality of the coke (Makgato, 2013). The Southern African coking coals have semi-reactive fusinite, which also enhances the quality of coking coal. Vitrinite is also known to appear as thick bands in light grey and dark grey, which can be seen in Figures 4.2a and 4.3a. The Moatize and GG coal samples were abundant in vitrinite, and collotelinite dominates over collodetrinite. This exhibits similar behaviour to South African coals previously studied by Kruszewska (2003) and Mphaphuli (2017).

The Moatize coal sample also exhibited natural coke, as seen in Figure 4.2(c), which is supported by the higher carbon content and coking coal reflectance in the Moatize, as well as its higher reactive fusinite content than GG coal. Both samples were dominated with inertinite macerals (fusinite and inertodetrinite) (Figures 4.2b and 4.3b. This corresponds to the higher inertinite content (13.6%) for Moatize, with 1.2% of that being reactive semifusinite and GG (10.9%) of inertinite and only 0.2% of the reactive semifusinite. In terms of the mineral contents, the Moatize and GG coal samples were composed of clay, quartz, pyrite, and carbonate, including traces of other minerals, but Moatize had higher inertinite. Even though Figure 4.3c shows some pyrite content, the percentage pyrite from both samples was as low as 0.4%.

The BET was used to analyse the specific surface area, pore volume and pore size distribution of the two samples. According to Wang *et al*. (2019), the internal structure of a coal can be characterised based on its pore size distribution. Table 4.3 presents the summary of the textural properties of the two coals. The pore size distribution of the coals was generated using the DFT model. Since coal structure is very complex, determining its pore size distribution for micro, meso and macro-pores requires DFT rather than Barrett-Joyner-Halenda, which has limitations for evaluating micropores. Studies have shown the DFT pore size distribution to be more accurate for calculating the pore size distribution (Horvat *et al*., 2022).

Table 4.3 and Figure 4.4 provide an overview of the DFT textual properties of the raw GG and Moatize samples. The 100% Moatize exhibited a higher micropore volume than 100% GG at the micropore region (0 to 2nm). Furthermore, the micropore volume for 100% Moatize was 7.18×10^{-3}, and it was 4.40×10^{-3} for 100% GG. Raw GG exhibited a larger mesopore volume (5.60×10^{-3}) than 100% Moatize (2.30×10^{-3}). The average pore diameter of 100% GG was 7.06nm, while that of Moatize was 2.50nm. The Moatize coal has a micropore surface area of 4.42 m^2/g, higher than that of GG coal. This agrees with the notion that higher-rank coal has more micropores and a higher micropore surface area than lower-ranked coal. Even though the Moatize coal sample was higher ranking and had a higher carbon content than the GG coal sample, neither can individually be used in a blast furnace because they do not meet the required standard for making coking coal individually. Therefore, the samples were subjected to hydrothermal processes to enhance their properties. Hydrothermal treatment can dissolve and leach inorganic minerals, reducing ash and volatile matter content, particularly important for the GG coal. This opens more pores in the coal, reducing the micro-molecular pore volume and increasing the mesopore volume (Wang *et al.*, 2008; Li *et al*., 2021d Su *et al*., 2022). Blending both coals could also enhance the rheological properties of the blend (Duffy *et al*., 2009; Hu *et al*., 2016), and this was investigated in this study.

Table 4.3: The Density functional theory textural properties of Grootegeluk (GG) and Moatize coals

Sample	S_{BET} (m^2/g)	V_{Total} (cc/g)	S_{Micro} (m^2/g)	S_{Meso} (m^2/g)	V_{Micro} (cc/g)	V_{Meso} (cc/g)	D_{ave} (nm)
100% GG	5.75	$1.00x10^{-2}$	1.56	4.19	$4.40x10^{-3}$	$5.60x10^{-3}$	7.06
100% Moatize	4.92	$9.48x10^{-3}$	4.42	0.50	$7.18x10^{-3}$	$2.30x10^{-3}$	2.50

nm: nanometres, m^2/g: square metre per gram, cc/g: cubic centimetres per gram, S_{BET}: specific surface area, V_{Total}: total pore volume, S_{Micro}: micropore surface area, S_{Meso}: mesopore surface area, V_{Micro}: micropore volume, V_{Meso}: mesopore volume, D_{ave}: average pore diameter

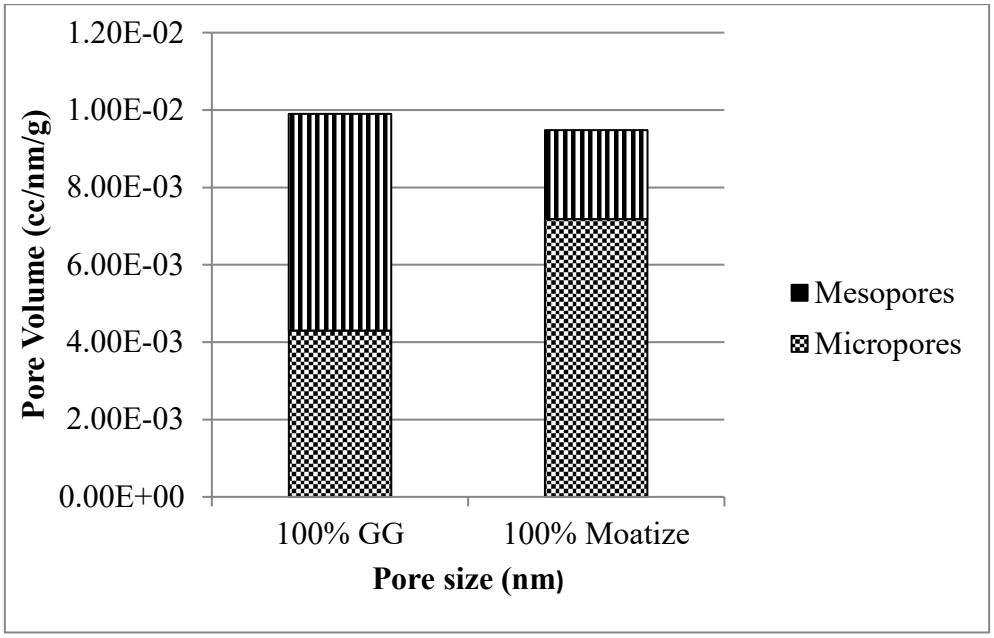

Figure 4.4: The Density functional theory pore size distribution of the raw Grootegeluk (GG) and raw Moatize coal

The following section presents the results obtained following the hydrothermal treatment of the two coals. The textural properties of the upgraded samples are presented for comparison. Based on these results, the best optimal parameters were determined and used to produce more samples for the carbonisation studies.

4.3 CHARACTERISATION OF HYDROTHERMALLY TREATED SAMPLES

Table 4.4 presents the results obtained from the hydrothermal treatment of GG coal at various temperatures (100 to 280ºC), residence times (A to C) and mass ratios (300 to 600g), illustrating the altering properties of the GG coal based on the results obtained at different hydrothermal treatment conditions. The GG sample had an initial ash content of 10.20% (Table 4.1), and after hydrothermal treatment at 280°C, 600g and 180 minutes, the ash

content decreased to 7.85%. Another sample with low ash content (GG-HTC- 450-B2), was treated at 200°C, 450g and 30 minutes. Lastly sample GG-HTC-600A, which was treated at 100°C, 600g and 30 minutes also had an ash content lower than 10%. A decrease in ash was also noted by Wang *et al*. (2008) when they studied the hydrothermal treatment of lignite coal at various temperatures and found that the hydrothermally treated coals had an ash content that was below that of the raw coal except for the highest treatment temperature at 350ºC. Various studies suggested that hydrothermal treatment is the best method to upgrade high-ash coal due to the ability of the water to leach out inorganic minerals under pressure, reducing ash content (Butler *et al*., 2007; Favas & Jackson, 2008; Zhang *et al*., 2016).

Table 4.4: Results of the hydrothermally treated Grootegeluk coal at varying residence times, temperatures, and masses.

Sample	IM (% adb)	Ash (% adb)	VM (% adb)	FC (%)	TC (% adb)	TS (% adb)	Condition	
							Time (min)	Temperature (ºC)
GG-HTC-300A	3.03	10.77	32.68	51.84	64.4	1.13	30	100
GG-HTC-450A	5.86	10.15	32.40	51.77	68.2	0.83	30	100
GG-HTC-600A	3.75	9.88	33.58	52.79	69.55	0.81	30	100
GG-HTC-300-A1	2.77	9.58	33.24	54.14	68.40	1.05	30	150
GG-HTC-450-A1	3.56	11.39	33.68	51.42	67.80	0.86	30	150
GG-HTC-600-A1	3.04	10.72	33.95	52.29	68.80	0.79	30	150
GG-HTC-300-A2	3.54	11.63	32.61	51.97	68.25	0.89	30	200
GG-HTC-450-A2	5.04	9.57	32.70	52.69	68.05	0.88	30	200
GG-HTC-600-A2	3.47	11.47	32.60	52.46	68.05	0.80	30	200
GG-HTC-300B	2.78	11.2	33.29	52.91	68.50	0.90	90	100
GG-HTC-450B	5.37	11.54	32.06	51.03	67.68	0.92	90	100
GG-HTC-600B	3.65	11.40	32.06	52.89	69.25	0.90	90	100
GG-HTC-300-B1	2.58	10.37	33.66	53.4	67.30	0.83	90	150
GG-HTC-450-B1	2.59	11.49	32.53	53.39	68.85	0.76	90	150
GG-HTC-600-B1	3.60	10.30	32.74	53.36	68.90	0.88	90	150
GG-HTC-300-B2	3.71	11.57	32.81	51.91	67.08	0.83	90	200
GG-HTC-450-B2	3.10	11.07	32.07	53.76	68.04	0.82	90	200
GG-HTC-600-B2	3.05	10.96	32.15	53.84	69.55	0.80	90	200
GG-HTC-600C	3.16	7.85	32.48	56.51	68.50	0.92	180	280

% adb: % air-dried basis; FC=100-(IM+Ash+VM); IM: inherent moisture; VM: volatile matter; FC: fixed carbon, Ash: ash content; TC: total carbon; TS: total sulphur; min: minutes

The volatile matter content decreased in all samples from 35.02% in the original sample (Table 4.1). The samples with the lowest volatile matter content were GG-HTC-450B, treated at 100°C, 450g and 90 minutes, and GG-HTC-600A, treated at 100°C, 600g and 90 minutes. The reduction of volatile matter in the low-rank coal after hydrothermal treatment was

concluded to be due to the expansion of new pores and the collapse of old pores in the coal sample (Li *et al*., 2021c; Su *et al*., 2022). The reduction of volatile matter was also accompanied by the loss of alkanes, alkenes and alkynes (Su, *et al*., 2022). The decreased ash content, volatile matter and moisture content increased the coal's fixed carbon. This agrees with a study by Nonaka *et al*. (2011) where a blend of low-rank coal and biomass was hydrothermally treated at 300ºC. Even though the blends had various compositions, the increase in fixed carbon was evident in all the hydrothermally treated blends. Zhang *et al*. (2016) also saw a 5% to 7% increase in fixed carbon after the hydrothermal treatment of a lignite coal. Both samples GG-HTC-600-B2 and GG-HTC-600A had the highest total carbon content of 69.55%. Two samples with total sulphur above 1% were GG-HTC-300A and GG-HTC-300-A1, which were treated at 100°C, 300g and 30 minutes and 150°C, 300g and 30 minutes, respectively. When comparing all samples with respect to their ash content, volatile matter content and total carbon, GG-HTC-600-B2, GG-HTC-600A and GG-HTC-600C were the most improved samples.

With the three most improved samples determined based on their physicochemical properties, further analysis was conducted to determine their pore size distribution and suitability. Table 4.5 and Figure 4.5 present the pore size distributions of the three best thermally treated GG coals from the DFT model. In accordance with the results, the BET surface area gradually increases from 5.75m^2/g (100% GG) to 12.56m^2/g (GG-HTC-600A) when treated at 100ºC. A further increase in surface area to 49.47m^2/g (GG-HTC-600-B2) was noted as the treatment temperature increased to 200ºC and a less steep increase in surface area to 52.94m^2/g (GG-HTC-600C) at 280ºC.

The micropore surface area also increased from 1.56m^2/g (100% GG) to 36.28m^2/g as the hydrothermal treatment temperature increased to 280ºC. The increase observed in the total volume, micropore volume and mesopore volume (Table 4.5) as the temperature increased shows that hydrothermal treatment influences the coals' structure. The micropore percentage for each sample was calculated (Figure 4.5), and GG-HTC-600A had the lowest micropores of 5.28%, while GG-HTC-600C had the highest micropores of 52.94%. According to the literature, coals with high mesopore distribution are more suitable coking coals for coke production (Li *et al*., 2021b; Fang *et al*., 2022; Lingling *et al*, 2022). In other words, coal with a higher ratio of mesopores to micropores is more favourable for coke production. Consequently, GG-HTC-600-B2 and GG-HTC-600A were selected to be more appropriate for coke production. Mesopores are more pronounced in low to medium-rank coals, while

micropores are generally found in higher-rank coals (Schwanke *et al*., 2017). Low-rank bituminous coal has a more loosened coal structure, as its pores are developed under shallow depth, low temperature and low pressure (Ju *et al*., 2005; Xinglong *et al*., 2010; Jienan *et al*., 2019). Increasing the temperature, pressure and depth of the coal decreases the mesopore volume gradually. This is noted in an anthracite; as the temperature and pressure during coalification increases, large micropore volume and specific surface area are formed due to the high degree of aromatisation (Schwanke *et al*., 2017). As observed in this study, the hydrothermally treated Moatize coal, which is a high-rank coal, had a higher micropore surface area than the hydrothermally treated GG.

Table 4.5: The Density functional theory textual properties of 100% Grootegeluk (GG), GG-HTC-30-3, GG-HTC-90-9 and GG-HTC-180-1

Sample	S_{BET} (m^2/g)	V_{Total} (cc/g)	S_{Micro} (m^2/g)	S_{Meso} (m^2/g)	V_{Micro} (cc/g)	V_{Meso} (cc/g)	D_{ave} (nm)
100% GG	5.75	$1.00x10^{-2}$	1.56	4.19	$4.40x10^{-3}$	$5.60x10^{-3}$	7.06
GG-HTC-600A	12.56	$2.69x10^{-2}$	1.70	10.86	$1.94x10^{-3}$	$2.50x10^{-2}$	2.79
GG-HTC-600-B2	49.74	$3.52x10^{-2}$	7.76	41.98	$5.49x10^{-3}$	$2.97x10^{-2}$	2.56
GG-HTC-600C	68.53	$5.60x10^{-2}$	36.28	32.25	$2.96x10^{-2}$	$2.63x10^{-2}$	3.06

nm: nanometres, m^2/g: square metre per gram, cc/g: cubic centimetres per gram, S_{BET}: specific surface area, V_{Total}: total pore volume, S_{Micro}: micropore surface area, S_{Meso}: mesopore surface area, V_{Micro}: micropore volume, V_{Meso}: mesopore volume, D_{ave}: average pore diameter

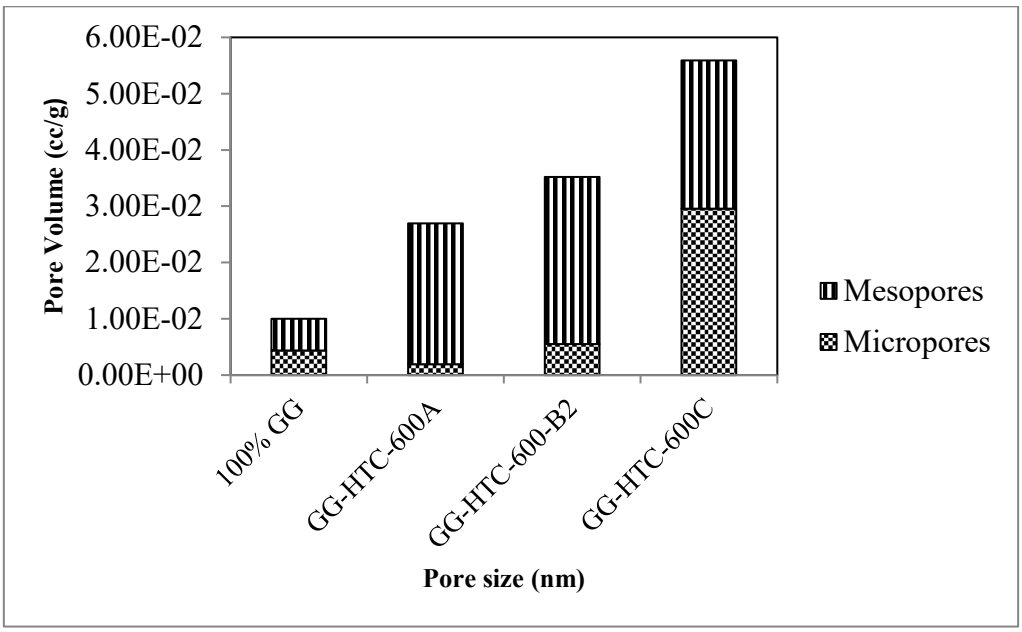

Figure 4.5: The pore size distribution of 100% Grootegeluk (GG), GG-HTC-600A, GG-HTC-600-B2 and GG-HTC-600C

Table 4.6 presents the results from the hydrothermal treatment of Moatize coal at similar conditions to that of GG coal exhibited in Table 4.5. There was a negligible change in the

volatile matter of the raw Moatize coal (20.35%; Table 4.1). The sample with the highest volatile matter was M-HTC-450-B, while M-HTC-600C had the lowest volatile matter content. M-HTC-600-A2 and M-HTC-600-B2 had the highest total carbon content, while M-HTC-600C had the lowest ash content. When comparing the samples with respect to their volatile matter, ash content, total carbon content and fixed carbon content, M-HTC-600C was the most improved sample, closely followed by M-HTC-600-B2.

Table 4.6: Results of the hydrothermal treatment of Moatize coal at various residence times, temperatures and masses

Sample	IM (% adb)	Ash (% adb)	VM (% adb)	FC (%)	TC (% adb)	TS (% adb)	Condition	
							Time (min)	Temperature (ºC)
M-HTC-300A	2.32	10.06	20.35	67.36	76.40	1.03	30	100
M-HTC-450A	1.32	10.04	20.44	68.20	74.80	1.04	30	100
M-HTC-600A	1.35	10.08	20.44	67.40	72.40	1.03	30	100
M-HTC-300-A1	0.97	9.23	20.49	69.31	76.60	1.02	30	150
M-HTC-450-A1	1.22	9.43	20.47	68.88	77.35	1.00	30	150
M-HTC-600-A1	0.78	9.99	20.29	68.95	76.80	0.99	30	150
M-HTC-300-A2	1.04	9.39	20.31	69.27	77.60	1.00	30	200
M-HTC-450-A2	1.52	9.93	20.61	68.39	77.10	1.02	30	200
M-HTC-600-A2	0.99	9.79	20.31	68.91	77.75	1.03	30	200
M-HTC-300B	1.25	10.11	20.20	68.44	77.65	1.03	90	100
M-HTC-450B	1.32	10.04	20.09	68.55	76.80	1.06	90	100
M-HTC-600B	0.99	9.32	20.56	69.13	76.35	1.03	90	100
M-HTC-300-B1	1.21	9.60	20.33	69.06	76.95	1.04	90	150
M-HTC-450-B1	1.00	9.17	20.25	69.58	77.30	1.03	90	150
M-HTC-600-B1	1.05	9.91	20.26	68.78	77.60	1.05	90	150
M-HTC-300-B2	1.45	9.36	20.35	68.83	77.30	1.01	90	200
M-HTC-450-B2	0.99	9.79	20.31	68.91	77.55	0.93	90	200
M-HTC-600-B2	1.35	9.84	20.49	68.83	77.75	1.03	90	200
M-HTC-600C	1.07	8.40	21.10	69.43	74.95	0.971	180	200

% adb: % air-dried basis; FC=100-(IM+Ash+VM); IM: inherent moisture; VM: volatile matter; FC: fixed carbon, Ash: ash content; TC: total carbon; TS: total sulphur; min: minutes

Table 4.7 and Figure 4.6 present the pore size distribution of the three best thermally treated Moatize samples. Raw Moatize had a higher micropore surface area than raw GG, which is expected as Moatize is a higher-rank coal. As the hydrothermal treatment temperature increased, the Moatize micropores increased, which is to the pore size distribution exhibited by GG. M-HTC-600C (treated at 280ºC) had the largest micropore volume, 62.55% of the pore size distribution, as seen in Figure 4.6.

Since coals with high mesopore distribution and higher mesopore-micropore ratio are better suited to coke production, M-HTC-600A and M-HTC-600-B2 were selected. Both samples had a lower micropore volume percentage than M-HTC-600C. The best parameters observed in this study to produce GG/Moatize coal blends were 200ºC, 600g and 90 minutes.

Table 4.7: The Density functional theory textual properties of 100% Moatize, M-HTC-30-9, M-HTC-90-9 and M-HTC-180-1

Sample	S_{BET} (m^2/g)	V_{Total} (cc/g)	S_{Micro} (m^2/g)	S_{Meso} (m^2/g)	V_{Micro} (cc/g)	V_{Meso} (cc/g)	D_{ave} (nm)
100% Moatize	4.92	$9.48x10^{-3}$	4.42	0.50	$7.18x10^{-3}$	$2.30x10^{-3}$	2.50
M-HTC-600A	10.56	$9.59x10^{-3}$	0.80	9.76	$7.24x10^{-4}$	$8.87x10^{-3}$	3.09
M-HTC-600-B2	54.83	$2.16x10^{-2}$	5.34	49.49	$2.10x10^{-3}$	$1.95x10^{-2}$	4.57
M-HTC-600C	64.53	$5.24x10^{-2}$	40.36	24.17	$3.28x10^{-2}$	$1.96x10^{-2}$	3.06

nm: nanometres, m^2/g: square metre per gram, cc/g: cubic centimetres per gram, S_{BET}: specific surface area, V_{Total}: total pore volume, S_{Micro}: micropore surface area, S_{Meso}: mesopore surface area, V_{Micro}: micropore volume, V_{Meso}: mesopore volume, D_{ave}: average pore diameter

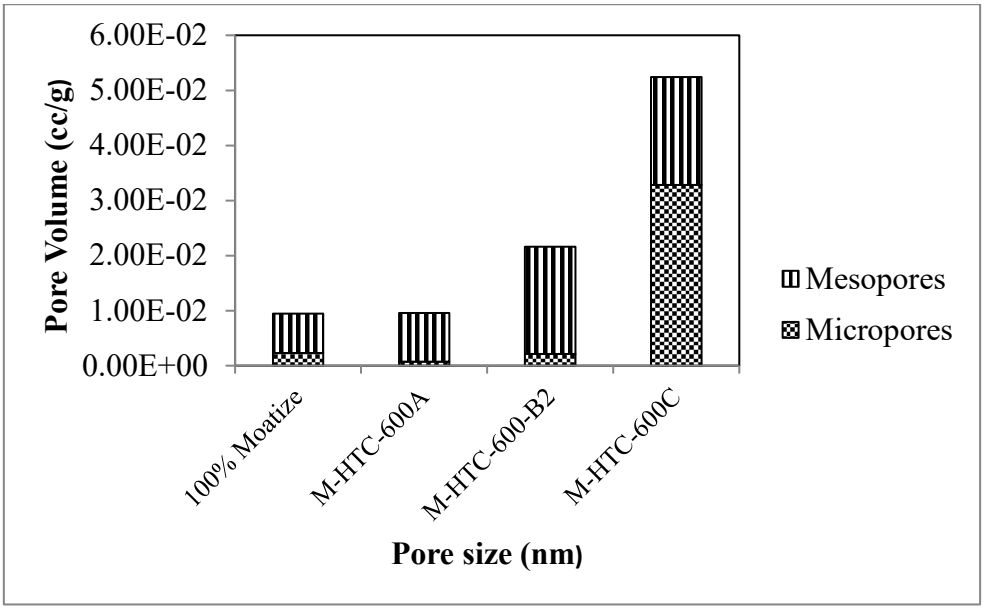

Figure 4.6: The Density functional theory pore size distribution of the 100% Moatize, M-HTC-30-9, M-HTC-90-9 and M-HTC-180-1

4.4 CHARACTERISATION OF HYDROTHERMALLY TREATED COAL BLENDS

The GG and Moatize coal samples were blended at various GG/Moatize percentages. For each test, 600g of the blend was hydrothermally treated at 200ºC and a residence time of 90 minutes. The characteristics of the blended samples are presented in Table 4.8.

The volatile matter in the GG coal sample decreased significantly from 32.15% for 100% GG when mixed with the Moatize coal sample at different ratios. A study by Makgato *et al.* (2013) shows that a coke oven tar (lower volatile matter) blended with bituminous coal

(higher volatile matter) can reduce the volatile matter of a coal/coke oven tar. In another study, Arslan & Kemal (2006) confirmed that the addition of low-volatile coal reduced the volatile matter content of a coal blend from 32% to 26%.

The fixed carbon was influenced by the coal composition. The fixed carbon content of the R-(15%GG+85%M) sample decreased from 67.35% to 64.39% in R-(30%GG+70%M) and to 62.74% in R-(50%GG+50%M) by increasing in GG content in the blend. This was an improvement from the fixed carbon content of 51.84% for 100% GG; however, this is below the fixed carbon of 67.36% for 100% Moatize. The volatile matter increased inversely with fixed carbon. Raw Moatize had a volatile matter of 20.35%, while 100% GG had a volatile matter of 35.02%. As the percentage ratio of GG in the blend was increased, the volatile matter also increased from 21.46% for R-(15%GG+85%M) to 23.89% for R-(30%GG+70%M) and 25.60% for R-(50%GG+50%M). High-quality medium bituminous coal with a volatile matter ranging from 22% to 35% is suitable for blast furnace usage (Kentucky Geological Survey, 2019). Based on this, 100% GG, 100% Moatize and R-(15%GG+85%M) are considered unsuitable for blast furnace usage.

The volatile matter increased from 21.46% for 90-(15%GG+85%M) to 22.52% for 90-(30%GG+70%M) and to 23.79% for 90-(50%GG+50%M). According to these results, 90-(15%GG+85%M) cannot be used in a blast furnace, while the other two samples can be used based on their volatile matter, fixed carbon and total sulphur content. To further determine the suitability of the coal blends for metallurgical applications, the pore size distribution, pore volume and specific surface area of the samples were also evaluated.

Table 4.8: Results of raw Grootegeluk (GG)/Moatize (M) and the hydrothermally treated GG/Moatize coal blends at 600g, 200ºC and 90 minutes

Sample	IM (% adb)	Ash (% adb)	VM (% adb)	FC (%)	TC (% adb)	TS (% adb)	Composi-tion (wt%)	Residence time (min)
R-(15%GG+85%M)	1.03	10.15	21.46	67.35	82.10	0.84	15% GG, 85% M	0 (raw coal)
R-(30%GG+70%M)	1.07	10.65	23.89	64.39	79.65	0.78	30% GG, 70% M	0 (raw coal)
R-(50%GG+50%M)	1.26	10.40	25.60	62.74	68.80	0.88	50% GG, 50% M	0 (raw coal)
GG-HTC-600-B2	3.05	10.96	32.15	53.84	69.55	0.80	100% GG	90
M-HTC-600-B2	1.35	9.84	20.49	68.83	77.75	1.03	100% M	90
90-(15%GG+85%M)	2.12	10.24	21.36	66.29	78.00	0.79	15% GG, 85% M	90
90-(30%GG+70%M)	1.94	10.33	22.52	65.21	76.60	0.83	30% GG, 70% M	90
90-(50%GG+50%M)	1.07	10.41	23.79	64.73	78.40	0.71	50% GG, 50% M	90

% adb: % air-dried basis, FC=100-(IM+Ash+VM), IM: inherent moisture, VM: volatile matter, FC: fixed carbon, Ash: ash content, TC: total carbon, TS: total sulphur, R: raw coal; wt%: weight percentage, min: minutes

Table 4.9 and Figure 4.7 exhibit the pore size distribution of the GG/Moatize coal blends. No micropores were detected in the blends. The coal blend and hydrothermal treatment conditions caused an increase in pore size. The reaction of coal with water and carbon dioxide has proven to increase the pore size hence reducing the micropores (Fang *et al*., 2022). Table A6 in Appendix A illustrates the coal blend nomenclature. Blend composition altered the specific surface area; 90-(15%GG+85%M) had the smallest specific surface area of 8.72m^2/g and 90-(50%GG+50%M) had the largest surface area of 14.39m^2/g. However, unlike the temperature effect, increasing the GG% in the blend led to the increment in the mesopore surface area, as expected. Raw GG had more mesopore area, as seen in Table 4.3. Since 90-(50%GG+50%M) had the highest mesopore surface area, further studies were conducted on the physiochemical properties of this coal sample.

Table 4.9: The Density functional theory textual properties of the Grootegeluk (GG)/Moatize (M) coal blends

Sample	S_{BET} (m^2/g)	V_{Total} (cc/g)	S_{Micro} (m^2/g)	S_{Meso} (m^2/g)	V_{Micro} (cc/g)	V_{Meso} (cc/g)	D_{ave} (nm)
90-(15%GG+85%M)	8.72	$3.12x10^{-3}$	0	8.72	0	$3.12x10^{-3}$	4.25
90-(30%GG+70%M)	12.57	$3.18x10^{-3}$	0	12.57	0	$3.18x10^{-2}$	5.09
90-(50%GG+50%M)	14.39	$3.22x10^{-3}$	0	14.39	0	$3.22x10^{-3}$	5.20

nm: nanometres, m^2/g: square metre per gram, cc/g: cubic centimetres per gram, S_{BET}: specific surface area, V_{Total}: total pore volume, S_{Micro}: micropore surface area, S_{Meso}: mesopore surface area, V_{Micro}: micropore volume, V_{Meso}: mesopore volume, D_{ave}: average pore diameter

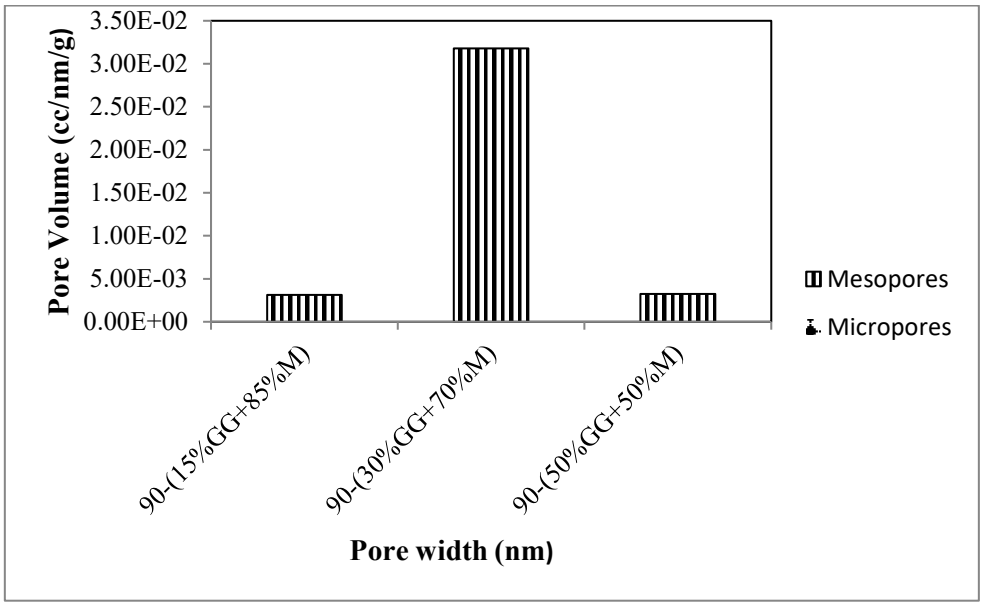

Figure 4.7: The Density functional theory pore size distribution of the Grootegeluk (GG)/Moatize (M) coal blends

4.5 THE EFFECT OF HYDROTHERMAL TREATMENT AND BLENDING OF GROTEGELUK AND MOATIZE COAL SAMPLES ON RHEOLOGICAL PROPERTIES OF 90-(50%GG+50%M) BLEND

According to the test work conducted by Musiiwa (2018) on GG coal as a blend to produce coke, it was found that no more than 39% of GG can be used to produce good coke. In this research, the GG percentage was pushed to 50% with the use of hydrothermal treatment. The micro-molecular and physiochemical properties of the blend 90-(50%GG+50%M) are discussed in this section.

Table 4.10: Characterisation of the 90-(50%GG+50%M) blend

Coal	**90-(50%GG+50%M)**
Proximate (% adb)	
Inherent moisture	1.07
Ash content	10.41
Volatile matter	23.79
Fixed carbon (% calculation*)	64.73
Ultimate (% adb)	
Total carbon content (C)	78.40
Hydrogen content (H)	4.68
Nitrogen content (N)	1.66
Oxygen content (% calculation**)	4.75
Total sulphur (%)	0.71
Maximum dilatation (%)	8
Crucible swelling index	5.5
Maximum fluidity (ddpm)	13
Total pore volume (cc/g)	
Average pore size (nm)	3.41
Specific surface area (m^2/g)	27.66

% adb: % air-dried basis, ddpm: dial divisions per minute, cc/g: cubic centimetre per gram, nm: nanometre, m^2/g: square metre per gram, *FC=100-(IM+Ash+VM), **O=[100-(Ash+H+C+N+S+IM)]

From the physiochemical analysis data presented in Table 4.10, 90-(50%GG+50%M) had the lowest total sulphur content. Its volatile matter and fixed carbon content were within the range require for metallurgical applications. The sample's maximum dilatation was 8%, which increased from -10% obtained for 100% GG but still less than 59% for 100% Moatize coal. According to Speight (2013), dilatation between 0% and 40% exhibits medium coking coal properties. The maximum fluidity of the blend increased to 13ddpm, higher than 3ddpm obtained for 100% GG coal. The addition of Moatize coal to the GG coal significantly increased the overall coking properties of the coal. This contrasts with the observation made when biochar is added to coal. According to Yustanti *et al*. (2021), 25% biochar to 75% coal decreased coal dilatation from 78% to 28%. Another study shows that the addition of 5% raw biomass decreased coal fluidity from 669ddpm to 130ddpm (Strugala *et al*., 2022). The use of biomass does not appear to be an alternative to producing a good coke for a metallurgical application.

4.6 FOURIER-TRANSFORM INFRARED SPECTROSCOPY ANALYSIS

FTIR was conducted on the two raw coal samples, the samples at optimum conditions (GG-HTC-600-B2 and M-HT-600-B2), and the 90-(50%GG + 50%M) blend. Table 4.11

illustrates the peaks that are seen in Figure 4.8. Peak 1 and 2, between 3693cm^{-1} and 3400cm^{-1}, are O-H stretching vibrations. These peaks are visible in all samples except the 90-(50%GG+50%M) blend. The aliphatic stretch peaks (3 and 4) in the 100% Moatize coal decreased with hydrothermal treatment, with GG-HTC-600-B2 having the lowest intensity. These peaks generally decrease with increasing coal rank, meaning there may be coal metamorphism during the hydrothermal treatment (Wei & Tang, 2018). There was insignificant change noticed in the aromatic C-H band, which is peak 5 and 6 between 1934cm^{-1} and 1602cm^{-1} for all samples. Overall, 90-(50%GG+50%M) showed a lower aliphatic C-H band than the raw coals (100% GG and 100% Moatize) and no O-H bands, illustrating that the blending and hydrothermal treatment influenced the structural properties of coal.

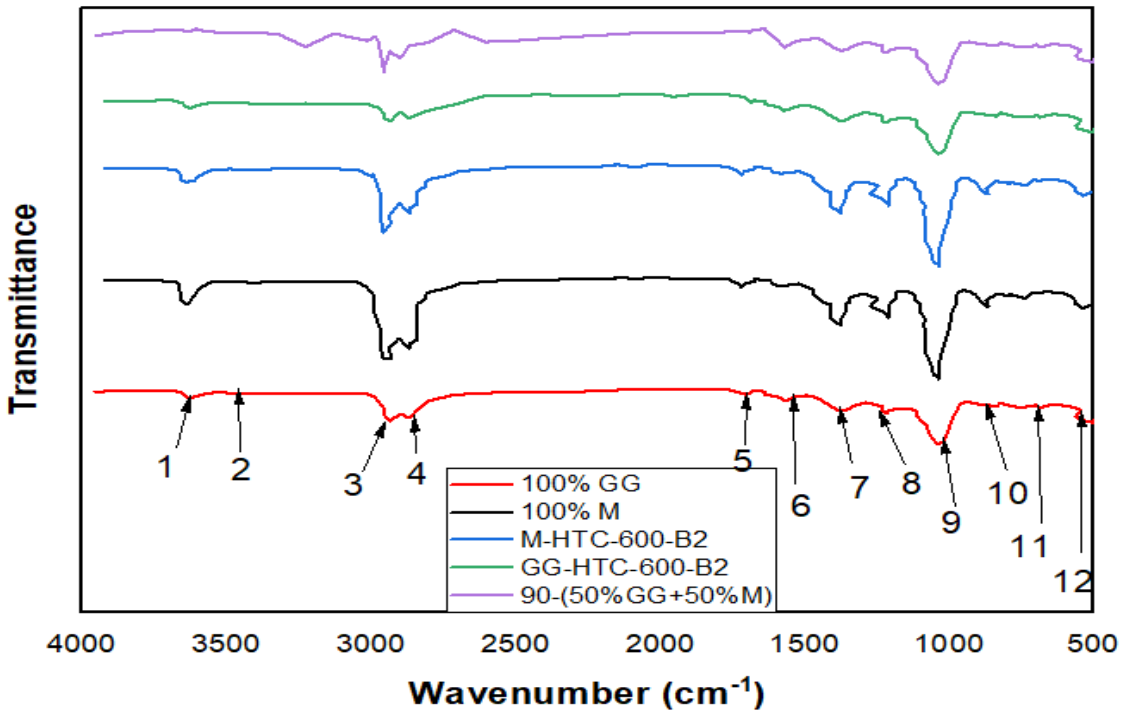

Figure 4.8: The FTIR spectra of the reacted coal blends vs the raw coal samples (Grootegeluk (GG) and Moatize (M))

Table 4.11: Summary of functional groups for the infrared spectra of 100% Moatize (M), 100% Grootegeluk (GG), GG-HTC-600-B2, M-HTC-600-B2 and 90-(50%GG+50%M)

Wave number (cm^{-1})	Peak/vibration	Functional groups/band assignments
3693-3400	1,2	O-H stretching vibrations
2990-2800	3,4	Aliphatic C-H stretch
1934-1602	5,6	Aromatic C-H stretch
1390	7	CH_3
1300-1000	8,9,10	C-O stretch and O-H bending vibrations in phenol structures
900-700	11	Out of plane aromatic C-H vibrations
560-500	12	Si-O and Si-O-Si deformations associated with kaolinite and quartz

4.7 COKE TESTS

The 100% GG and Moatize samples, including specific hydrothermally treated coal samples and their blends, were utilised to produce coke. Proximate analysis, particle reactivity index and pore size distribution were used to characterise the coke produced. The reactivity curves for each sample are provided in Figures 4.9 to 4.11.

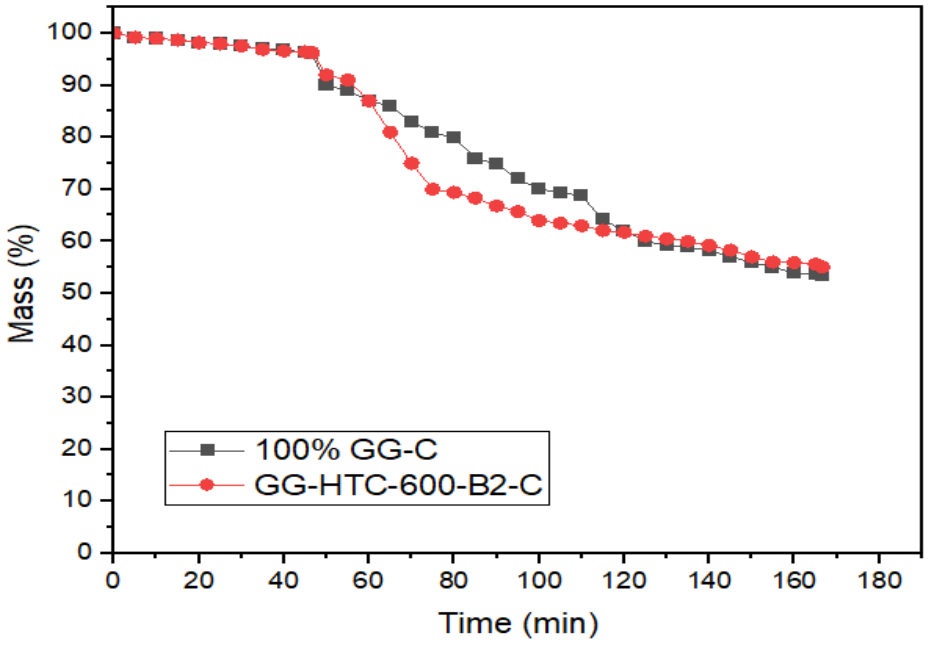

Figure 4.9: The mass loss versus time graph of 100% Grootegeluk (GG-C) and GG-HTC-B2-C

The mass loss over time for the 100% GG-C and GG-HTC-600-B2-C is given in Figure 4.9. Both samples started with a constant mass loss and similar reactivity profiles. The reaction zone denotes the release of moisture from both samples. Gasification commenced as the gas changed from nitrogen to carbon dioxide, and the fixed carbon-rich GG-HTC-600-B2-C had a steeper degradation profile than 100% GG-C. This phenomenon is the result of coke's reaction with carbon dioxide, which is one of the main causes of coke degradation (Huang *et al*., 2020). Both carbonised coal samples showed similar degradation as the reaction progressed.

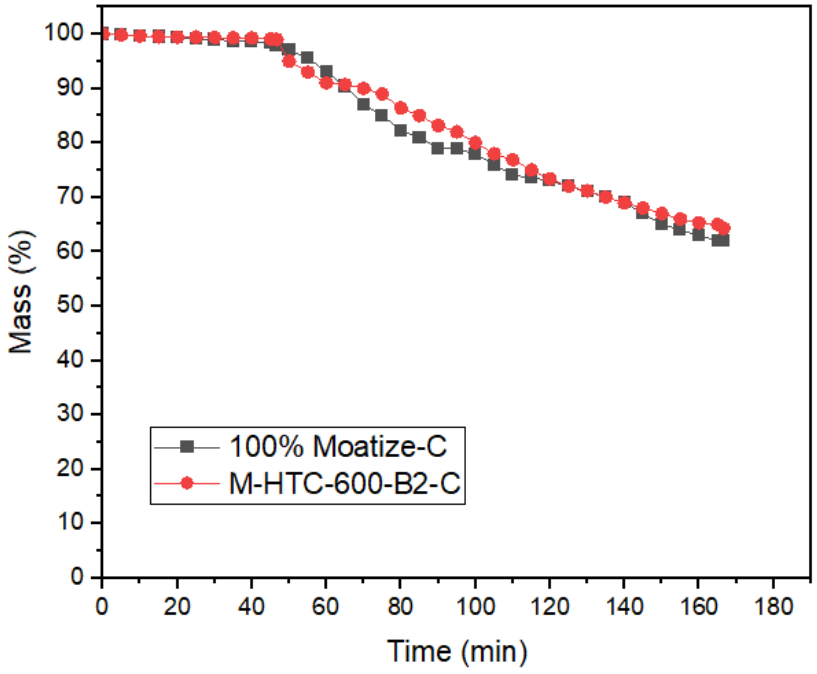

Figure 4.10: The mass loss versus time graph for 100% Moatize-C and M-HTC-600-B2-C

Figure 4.10 shows the mass loss over time for 100% Moatize-C and M-HTC-600-B2-C. The samples' reactivity profile was similar to that of 100% GG-C and GG-HTC-600-B2-C (Figure 4.9). The mass loss increased when the gas was switched to carbon dioxide after 46 minutes in nitrogen. Both samples proceeded with similar degradation profiles.

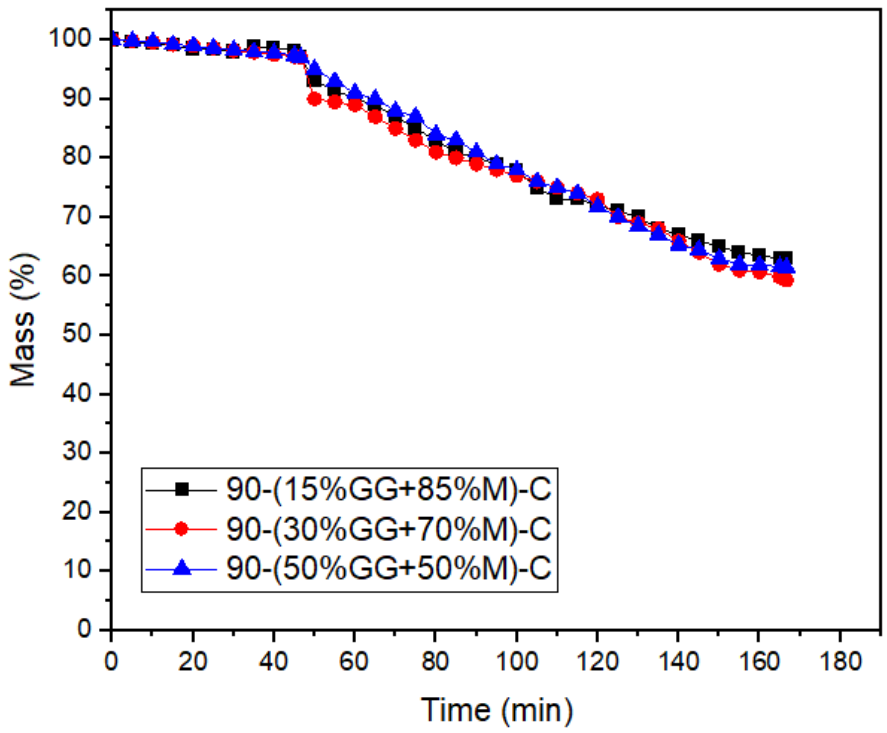

Figure 4.11: The mass loss versus time graph of the carbonised hydrothermal coal blends of Grootegeluk (GG) and Moatize (M) coals

The mass loss of the carbonised coal blends is presented in Figure 4.11. As with other carbonised samples, mass loss increased when the gas was changed to carbon dioxide. The carbonised coal blends followed a similar degradation profile, with 90-(15%GG+855M)-C having the lowest mass loss. The reactivity of coke in carbon dioxide was then calculated using the mass loss data, as shown in Table 4.12.

Table 4.12: The physiochemical and particle reactivity index of produced coke from Grootegeluk (GG), Moatize (M) and their coal blends

Sample	IM (% adb)	VM (% adb)	AC (% adb)	FC (calculation %*)	PRI (%)
100% GG-C	4.03	4.92	17.00	74.05	30.37
GG-HTC-600-B2-C	3.31	2.64	16.68	77.37	29.25
100% Moatize-C	1.67	3.86	14.21	80.26	25.75
M-HTC-600-B2-C	2.08	3.26	15.14	79.52	24.80
90-(15%GG+85%M)-C	2.55	2.03	12.59	82.83	24.35
90-(30%GG+70%M)-C	2.73	2.29	13.20	81.78	26.90
90-(50%GG+50%M)-C	2.85	2.32	13.78	81.05	27.51

% adb: % air-dried basis, *FC=100-(IM+Ash+VM), IM: inherent moisture, VM: volatile matter, FC: fixed carbon, AC: ash content; PRI: particle reactivity index; C-carbonised

The quality of the carbonised coal (coke) produced in this study was determined based on their proximate analysis, PRI and DFT pore size distribution. The coke properties were used alongside the coal's rheological characteristics (fluidity, dilatation, Roga Index and FSI) to determine the strength of the cokes. The results showed that the hydrothermal treatment significantly affected and reduced the reactivity of the coal. Table 4.12 illustrates the reactivity ranges of coal and coke produced from 24.35% (90-(15% GG 85%M)-C) to a maximum of 30.37%, demonstrated by 100% GG-C. The reactivity index of coke suitable for use in blast furnaces varies between 20 and 28 (Musiiwa, 2018). In the current study, the hydrothermal treatment reduced the volatile matter and reduced the reactivity index of the coke. As seen with the 100% GG-C coal sample, its PRI of 30.37% decreased to 29.25% upon undergoing hydrothermal treatment for 90 minutes, while for 100% Moatize-C, the PRI reduced from 25.75% to 24.80%. Similarly, Shui *et al*. (2012) indicated a reduction in the PRI of hydrothermally treated coal from 48.6% to 41.4% at 200ºC. The GG coal sample had a PRI greater than 28%, but all coal blends had a PRI that was between 20% and 28%.

Table 4.13 shows the results of hydrothermally carbonised treated samples based on their distribution of pore size and porous surface. GG-HTC-600-B2-C exhibited more mesopores than micropores (Figure 4.12), possibly due to the hydrothermal treatment and the coking process, causing the promotion of pores and expansion of existing pores. Volatile matter is lost during the carbonisation process, so more pores collapse, and more mesopores were formed, as seen in Table 4.13. As observed in the same table, the surface area increased as

the temperature increased. The 100% GG-C was 27.59m^2/g, and the hydrothermally treated GG-HTC-600-B2-C increased to 217.67m^2/g.

Table 4.13: The Density functional theory textural properties of 100% GG-C and GG-HTC-600-B2-C

Sample	S_{BET} (m^2/g)	V_{Total} (cc/g)	S_{Micro} (m^2/g)	S_{Meso} (m^2/g)	V_{Micro} (cc/g)	V_{Meso} (cc/g)	D_{ave} (nm)
100% GG-C	27.59	$3.20x10^{-2}$	13.34	14.26	$1.55x10^{-2}$	$1.65x10^{-2}$	1.69
GG-HTC-600-B2-C	217.70	$3.85x10^{-2}$	13.40	204.30	$2.35x10^{-2}$	$1.50x10^{-2}$	3.14

nm: nanometres, m^2/g: square metre per gram, cc/g: cubic centimetres per gram, S_{BET}: specific surface area, V_{Total}: total pore volume, S_{Micro}: micropore surface area, S_{Meso}: mesopore surface area, V_{Micro}: micropore volume, V_{Meso}: mesopore volume, D_{ave}: average pore diameter

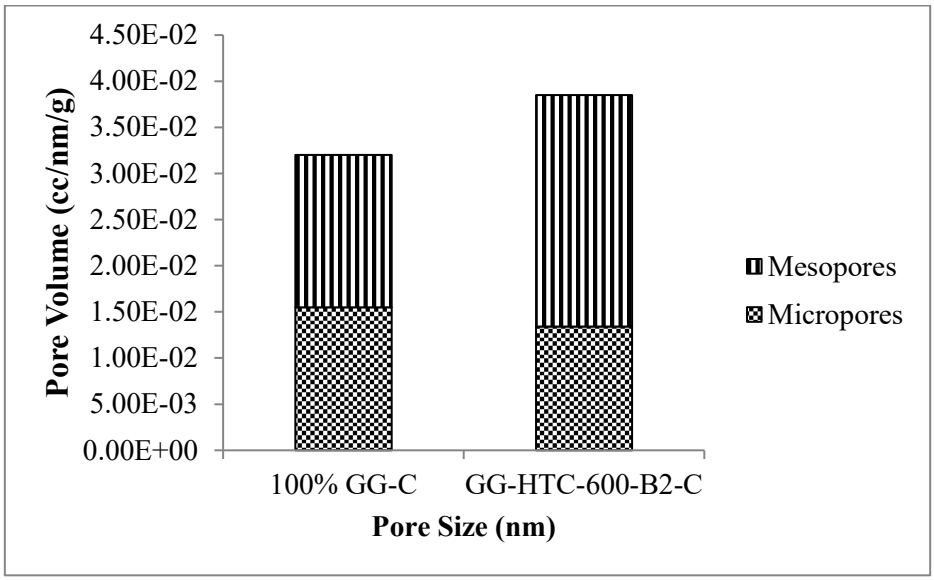

Figure 4.12 The Density functional theory pore size distribution of 100% Grootegeluk (GG)-C and GG-HTC-600-B2-C

The effect of the hydrothermal treatment on the DFT pore size distributions of the 100% Moatize-C and M-HTC-600-B2-C is presented in Figure 4.13. Most of the pores in both samples lay in the mesopore range. From Table 4.14, the surface area of the 100% Moatize-C increased after hydrothermal treatment from 13.59m^2/g to 156.2m^2/g for the coke produced. The total volume of the micropore and mesopore decreased for the carbonised hydrothermally treated samples. This could have been due to collapsing pores in the samples.

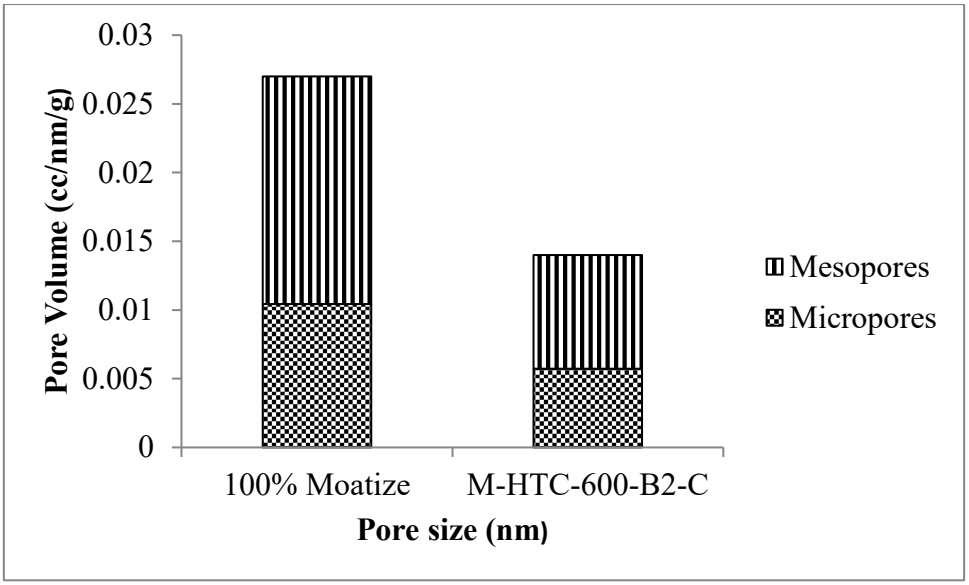

Figure 4.13: The Density functional theory pore size distribution of 100% Moatize (M) and M-HTC-600-B2-C

Table 4.14: The Density functional theory textural properties of 100% Moatize (M)-C and M-HTC-600-B2

Sample	S_{BET} (m^2/g)	V_{Total} (cc/g)	S_{Micro} (m^2/g)	S_{Meso} (m^2/g)	V_{Micro} (cc/g)	V_{Meso} (cc/g)	D_{ave} (nm)
100% Moatize-C	13.59	$2.70x10^{-2}$	5.26	8.33	$1.04x10^{-2}$	$1.65x10^{-2}$	2.08
M-HTC-600-B2-C	156.2	$1.15x10^{-2}$	13.40	92.32	$4.6x10^{-2}$	$6.33x10^{-2}$	3.14

nm: nanometres, m^2/g: square metre per gram, cc/g: cubic centimetres per gram, S_{BET}: specific surface area, V_{Total}: total pore volume, S_{Micro}: micropore surface area, S_{Meso}: mesopore surface area, V_{Micro}: micropore volume, V_{Meso}: mesopore volume, D_{ave}: average pore diameter

Figure 4.14 and Table 4.15 present the DFT pore size distribution of the coke produced from the blends of the carbonised hydrothermally treated coals. The pore size distribution illustrates that the mesopore volume for the three samples was quite similar. The volume lay between $5.00x10^{-2}$ and $5.61x10^{-2}$, with 90-(30%GG+70%M)-C having the lowest mesopore volume percentage. In terms of the ratio of mesopore to micropore, sample 90-(50%GG+50%M)-C exhibited a higher ratio than the other samples. Therefore, 90-(50%GG+50%M)-C considered the most suitable sample. This may be as a result of the higher composition of the GG% in the blend. The 100% GG sample had a higher mesopore volume than the 100% Moatize coal used in this study. Furthermore, since micropores do not provide sufficient gas exchange for carbon materials used in a blast furnace, 90-(50%GG 50%M) could be more appropriate with its lower micropore volume percentage(Guo *et al*., 2020; Casal *et al*., 2021).

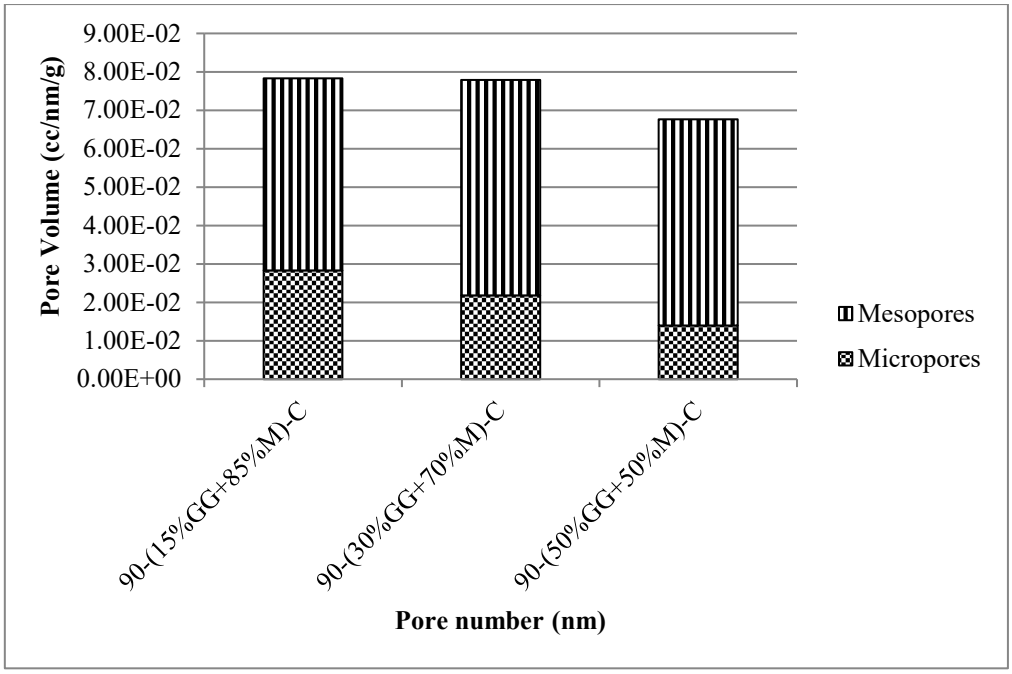

Figure 4.14: The Density functional theory pore size distribution of the carbonised hydrothermal blend coal samples

Table 4.15: The Density functional theory textural properties of the carbonised hydrothermal blended coal samples

Sample	S_{BET} (m^2/g)	V_{Total} (cc/g)	S_{Micro} (m^2/g)	S_{Meso} (m^2/g)	V_{Micro} (cc/g)	V_{Meso} (cc/g)	D_{ave} (nm)
90-(15%GG+85%M)-C	61.02	$7.83x10^{-2}$	23.39	37.62	$2.83x10^{-2}$	$5.00x10^{-2}$	2.08
90-(30%GG+70%M)-C	82.30	$7.79x10^{-2}$	23.03	59.27	$2.18x10^{-2}$	$5.61x10^{-2}$	3.14
90-(50%GG+50%M)-C	90.05	$6.76x10^{-2}$	18.65	71.4	$1.40x10^{-2}$	$5.36x10^{-2}$	3.59

nm: nanometres, m^2/g: square metre per gram, cc/g: cubic centimetres per gram, S_{BET}: specific surface area, V_{Total}: total pore volume, S_{Micro}: micropore surface area, S_{Meso}: mesopore surface area, V_{Micro}: micropore volume, V_{Meso}: mesopore volume, D_{ave}: average pore diameter

In conclusion, by physiochemical, rheological and micro-molecular characterisation, the Moatize coal sample ranked higher than the GG coal sample. Hydrothermal treatment significantly reduced the volatile matter of the GG coal sample, while it increased the specific pore surface area and specific volume of the micropores. The volatile matter of the Moatize coal sample was not improved significantly, but the pore size distribution changed in the same way as the GG coal sample. The parameters that significantly changed the samples were 200ºC, 90 minutes and 600g of sample.

Coal blending decreased the GG volatile matter content while causing an increment in its fixed carbon content. Hydrothermal treatment of the blends decreased volatile matter and total sulphur and increased fixed carbon and total carbon. The DFT pore size distribution

analysis of the coke products exhibited higher mesopore to micropore volume in the 90-(50%GG+50%M)-C coke sample than in all the other coke samples. The 90-(30%GG+70%M)-C and 90-(50%GG+50%M)-C samples had a PRI that could be used in the blast furnace. However, the maximum dilatation and Gieseler Fluidity of the blend were not within the range used in a blast furnace.

CHAPTER FIVE: CONCLUSION AND RECOMMENDATIONS

5.1 CONCLUSION

To date, the bulk of steel production continues to use the basic oxygen furnace route. This means that demand for coking coal will continue to increase as world demand for steel increases. With population growth and steel as the backbone of industrialisation, the demand for steel increases daily. With the depletion of coking coal in South Africa, the country has lost out both financially and industrially. This led to the need for the study to upgrade the existing coal with a new approach to meet the quality required in this application.

This research aimed to upgrade the GG, Moatize and GG/Moatize coal blends through the hydrothermal process to produce a metallurgical coal grade. The aim and the objective outlined in this research were all achieved and the following conclusions were reached:

1. The physiochemical analysis revealed that the 100% GG coal sample exhibited more volatile matter content (35.02%) than Moatize (20.35%). According to the ultimate analysis, the 100% Moatize coal sample had a higher carbon content and less oxygen and nitrogen content.
2. According to the rheological properties, 100% Moatize coal exhibited prime coking coal properties with a maximum dilation of 59, crucible swelling index of 9 and low fluidity at 24ddpm. The 100% GG coal sample exhibited semi-soft coking coal behaviour with a crucible swelling index of 5.5, maximum fluidity of 3 and very low dilation of -10.
3. Micro-molecular analysis found that Moatize had more vitrinite and less mineral matter than GG. The pore size distribution further showed that the 100% Moatize had more micro-molecular pores than 100% GG with a DFT specific area of 4.42m^2/g and 1.16m^2/g, respectively.
4. The hydrothermal treatment decreased the volatile matter of the 100% GG coal to a minimum of 32.15% with a consequential increase in fixed carbon. Moatize showed a decrease in ash content and an increase in total carbon content. The hydrothermal treatment increased mesopores and the specific surface area with the optimal conditions being 200ºC, 90 minutes and 600g.
5. Blending the two coals reduced the volatile matter from a wide range of 14.67 (20.35%-35.02%) to a narrow range of 4.14 (21.46%-25.60%), while the

hydrothermal treatment of the blend decreased the volatile matter range to 2.36 (21.36%-23.79%).

6. The surface area of the coals increased after hydrothermal treatment, with the total volume of the micropore and mesopore decreasing for the carbonised hydrothermally treated samples. This could have been due to collapsing pores.
7. The hydrothermal treatment reduced the individual PRI coals individually and blending led to a further reduction of the PRI to a range of 20% to 28% for blast furnace applications. Furthermore, the 90-50%GG+50%M blend had a PRI of 27.51%.
8. The 90-50%GG+50%M blend exhibited metallurgical application specifications with a crucible swelling index of 5.5, a higher mesopore-to-micropore volume ratio and the maximum dilatation was 8%.

The hydrothermal treatment disrupted weak bonds and eliminated side chains through hydrolysis and removed cross-links of macromolecular network at 200°C which led to the improved coking qualities. Although the overall quality of the improved coal blends did not meet the specifications required for use in the blast furnace, some of the blends were suitable for other metallurgical applications. This study established that hydrothermal treatment could upgrade South African semi-soft coking coal.

5.2 RECOMMENDATIONS

This study had shown that hydrothermal treatment could enhance some of the metallurgical properties of semi-soft coking, but further suggested research based on the results obtained in this study are:

1. A prime coking coal with a maximum fluidity within the range of 200ddpm to 1000ddpm should be blended with the semi-soft coal and subjected to hydrothermal treatment.
2. The blend produced should be pelletised, carbonised and tested for its CSR, M_{20} and M_{50}.
3. The best coke produced should be tested as a reductant for other ferro-alloys.
4. Semi-soft coking coal will still require a higher premium coking coal to achieve a blend with an overall blast furnace specification. Further research is required as this sector is the main pillar of the world economy.

REFERENCES

Abdulsalam, J. (2019). Development of activated carbons from South Africa coal waste for application in natural gas storage. PhD thesis. University of the Witwatersrand.

Adeleke, A. O., Makan, R. S., & Ibitoye, S. A. (2007). Studies on the Gieseler plastometry parameters of the American Pittson Coal for metallugicsl cokemaking at the Ajaokuta Steel Plant, Nigeria. *The Pacific Journal of Science and Technology, 8*(2), 208-211.

Anderson, A. (2014). Thermodynamic study of trace elements in the blast furnace and basic oxygen furnace. MSc dissertation. Luleå University of Technology.

Antrekowitsch, J., & Steinlechner, S. (2010). Potential of hydrogens as potential reducing agent in metallurgical processes. *3rd International Conference on Engineering for Waste and Biomass Volatisation*. 17-19 May 2010. Beijing, China.

ArcelorMittal. (2015). *ArcelorMittal*. *Fact book 2015*. Available: https://storagearcelormittaluat.blob.core.windows.net/media/zs0nxw0h/arcelormittal-ar2015.pdf. [2023, March 29].

ArcelorMittal. (2020). *ArcelorMittal Europe to produce 'green steel' starting in 2020*. Available: https://corporate.arcelormittal.com/media/news-articles/arcelormittal-europe-to-produce-green-steel-starting-in-2020. [2021, July 28].

ArcelorMittal. (2021). *Corporate ArcelorMittal*. *ArcelorMittal Austrias starts coke-oven gas injection for blast furnace B*. Available: https://corporate.arcelormittal.com/media/news-articles/arcelormittal-asturias-starts-coke-oven-gas-injection-for-blast-furnace-b. [2021, July 28].

Arslan, V., & Kemal, M. (2006). The effects of inert matters on low volatile coal addition on the plasticity high volatile Zonguldak coals. *The Journal of the South African Institute of Mining and Metallurgy,106*, 199-204.

Assis, P. S., Gou, L., Fang, J., Mankhand, T. R., & de Assis C.F.C. (2008). Optimisation of the COREX process. *Ironmaking and Steelmaking,* 35(4), 303-307. https://doi.org/10.1179/174328108X269478.

Atsushi, M., Uemura, H., & Sakaguchi, T. (2010). Mindrex Process. *Kolbeco Technology Review, 29*, 50-57.

Babich, A., & Senk, D. (2015). 17 - Recent developments in blast furnace iron-making technology. *Iron Ore: Mineralogy, Processing and Environmental Sustainability*, 505-547. https://doi.org/10.1016/B978-1-78242-156-6.00017-4.

Battle, T., Srivastava, U., Kopfle, J., Hunter, R., & McClelland, J. (2014). Chapter 1.2 The direct reduction of iron. In *Treatise on process metallurgy. Volume 3: Industrial processes.* S. Seetharaman, Ed. Armsterdam: Elsevier. 89-176. https://doi.org/10.1016/B978-0-08-096988-6.00016-X

Béchara, R., Hamadeh, H., Mirguax, O., & Pattison, F. (2020). Carbon impact mitigation of the iron ore direct reduction process through computer aided optimisation and design changes. *Metals*, *10*(3), 367. https://doi.org/10.3390/met10030367.

Béchara, R., Patisson, B., Hamadeh, H., & Mirguax, O. (2018). Optimization of the iron ore direct reduction process through multiscale process modelling. *Materials, 11*(7), 1094. https://doi.org/10.3390/ma11071094.

Bennett, P. (2007). *PCI-Impact on blast furnace operation.* Karana Downs: CoalTech.

Bermudez, V., Likubira, S., & Ogale, A. A. (2017). 1.3 Pitch precursor-based carbon fibres. *Module in Materials Science and Materials Engineering: Comprehensive Composite Materials II, 1*, 41-65. https://doi.org/10.1016/B978-0-12-803581-8.10312-1.

Beukes, N. J., Gutzmer, J., & Mukhopadhyay, J. (2003). The geology and genesis of high-grade hematite iron ore deposits. *Applied Earth Sciences, 112(1)*, 18-25. https://doi.org/10.1179/037174503225011243.

Birol, F. (2019). *The future of hydrogen.* Available: https://www.iea.org/reports/the-future-of-hydrogen. [2023, March 30].

Butler, C. J., Green, A. M., & Chaffee, A. L. (2007). The fate of trace elements during MTE and HTD dewatering of Latrobe Valley brown coals. *Coal Preparation*, *27*(4), 210-229. https://doi.org/10.1080/07349340701640844.

Carpenter, A. M. (2010). *Ínjection of coal and waste plastics in blast furnaces.* Rio Tinto: IEA Clean Coal Centre.

Casal, M., Díaz-Faes, E., & Barriocanal, C. (2021). Permeability and porosity development during the carbonisation of coals of different coking pressures. *Energy and Fuels, 35*(7), 5808-5817. https://doi.org/10.1021/acs.energyfuels.0c04219.

Cheng, Y., Jiang, H., Zhang, X., Cui, J., Song, C., & Li, X. (2017). Effects of coal rank on physiochemical properties of coal and on methane adsorption. *International Journal of Coal Science Technology, 4*, 129-146. https://doi.org/10.1007/s40789-017-0161-6.

Chukwuleke, O. P., Jui-ju, C., Chukwujekwu, S., & Song, X. (2009). Shift from coal to coke using direct reduction method and challenges. *Chinese Journal of Iron and Steel Research International*, *16*(2), 1-5.

Cong, Y., Zhai, Z., Yu, X., Xu, J., Sun, Y., Tang, W., Zheng, Y., & Wu, J. (2023 Study on typical temperature effect mechanism of multi-component coal during low-temperature thermal expansion. *Case Studies in Thermal Engineering,* Volume 43, pp. 1-12. https://doi.org/10.1016/j.csite.2023.102744.

Creamer Media. (2020). *Creamer Media engineering news: Opinion: South African steel industry is an industry in distress*. Available: https://m.engineeringnews.co.za/article/opinion-south-african-steel-industry-is-an-industry-in-distress-2020-03-06/rep_id:4433. [2020, July 22].

CsiroScope, 2021. *Green, blue, brown: the colours of hydrogen explained.* Available: https://blog.csiro.au/green-blue-brown-hydrogen-explained/. [2021, May 27].

Das, T. K., Ghosh, K. N., Misra, S., Sahoo, B. K., Niyogi, O. S., Jha, P. K., & Prasad, B.S. (2016). Studies on the effect of usage of inert-rich coal in coal blend on coke properties through pilot oven carbonization tests. *Transactions of the Indian Institute of Metals, 69*, 1209-1216. https://doi.org/10.1007/s12666-015-0671-0.

Dash, P. S., Guha, M., Chakraborty, D., & Banerjee, P. K. (2011). Prediction of coke CSR from coal blend characteristics using various techniques: A comparative evaluation. *International Journal of Coal Preparation and Utilization, 32(4)*, 169-192. https://doi.org/10.1080/19392699.2011.640301.

de Assis, C.F.C., dos Santos, R., Guilherme, O., da Silva, L.R., & Assis, P.S. (2019). Characterization of coal briquettes using tar as a binding material for use in a coke

oven. *International Engineering Journal, 72*(1), 113-118. https://doi.org/10.1590/0370-44672017720151.

de Castro, J. A., de Mattos Araujo, G., de Oliveria da Mota, I., Sasaki, Y., & Yagi, J. (2013). Analysis of the combined injection of pulverised coal into large blast furnaces. *Journal of Materials Research and Technology, 2*(4), 308-314. https://doi.org/10.1016/j.jmrt.2013.06.003.

de Castro, J. A., de Medeiros, G. A., de Oliveira, E. M., de Campos, M. F., & Nogami, H. (2020). The mini blast furnace process: An efficient reactor for green pig iron production using charcoal and hydrogen-rich gas: A study of cases. *Metals, 10*(11), 1501. https://doi.org/10.3390/met10111501.

de Cordova, M., Madias, J., & Barreiro, J. (2016). Review on modelling of coal blends for prediction of coke quality. *AISTech 2016 Proceedings*. 16-19 May 2016. Pittsburgh, Pennsylvania: D.L. Lawrence Convention Center, 297-309.

de Villiers, E. (2015). *Who owns whom*. *Africa business information* Available: https://www.whoownswhom.co.za/store/info?segment. [2020, July 20].

Demirel, Y. & Gerbaud, V. (2019). Chapter 15 - Probabilistic Approach in Thermodynamics. In: Y. Demirel & V. Gerbaud, eds. *Nonequilibrium Thermodynamics (Fourth Edition).* Nebraska: Elsevier, pp. 711-791.

Denge, E. & Baiyengunhi, C. (2021). Maceral Types and Quality of Coal in the Tuli Coalfield: A Case Study of Coal in the Madzaringwe Formation in the Vele Colliery, Limpopo Province, South Africa. *Applied Sciences, 11*(5), https://doi.org/10.3390/app11052179.

Dering, D., Swartz, C., & Dogan, N. (2020). Dynamic modeling and simulation of basic oxygen furnace (BOF) operation. *Processes, 8*(4), 483. https://doi.org/10.3390/pr8040483.

Díaz, J., Fernández, F. J., & Prieto, M. M. (2020). Hot metal temperature forecasting at steel plant using multivariate adaptive regression splines. *Metals, 10*(1), 41. https://doi.org/10.3390/met10010041.

Díez, M. A., Alvarez, R., & Barriocanal, C. (2002). Coal for metallurgical coal production: Prediction of coke quality and future requirements for coke making. *International Journal of Coal Geology, 50(1)*, 389-412. https://doi.org/10.1016/S0166-5162(02)00123-4.

Díez, M. A & Borrego, A. G. (2013). Evaluation of CO2-reactivity patterns in cokes from coal and woody biomass blends. Fuel. 113. 59-68.

DKSH Group. (2018). *Berghof-High Pressure Reactor-BR series.* Available: https://www.dksh.com/global-en/products/ins/berghof-high-pressure-reactor-br-series. [2021, August 23].

Duad, W. M., & Ali, W. S. (2000). Effects of carbonization temperature on pore development in palm-shell-based activated carbon. *Carbon, 38*(14), 1925-1932. https://doi.org/10.1016/S0008-6223(00)00028-2.

Duffy, J. J., Mahoney, M. R., & Steel, M. K. (2009). Influence of coal thermoplastic properties on coking pressure generation: Part 2 - A study of binary coal bends and specific additives. *Fuel, 89*(7), 1-16. https://doi.org/10.1016/j.fuel.2009.08.035.

Elementar. (2021). *vario EL cube: CHNS elemental analyzer.* Available: https://www.elementar.com/en/products/organic-elemental-analyzers/vario-el-cube. [2021, August 23].

Energy Information Administration. (2022). *Hydrogen explained.* Available: https://www.eia.gov/energyexplained/hydrogen/production-of-hydrogen.php. [2023, March 31].

Eun, K. (2012). *The effect of coal properties on carbonization behavior and strength of coke blends.* MSc dissertation. University of New South Wales.

Fang, H., Han, J., Zhang, H., Zhao, B., & Qin, L. (2019). Effect of coal moisture content on coke's quality and yields of products during coal carbonization. *Journal of Central South University, 26*(12), 3225-3237. https://doi.org/10.1007/s11771-019-4248-7.

Fang, S., Zhu, H., Gao, M., He, X., Liao, Q., & Hu, L. (2022). Evolution of pore characteristics and methane adsorbtion characteristics of Nashn 1/3 coking coal under

different stresses. *Scientific Reports, 12*, 3117. https://doi.org/10.1038/s41598-022-07118-2.

Favas, G., & Jackson, W. R. (2008). Hydrothermal dewatering of low rank coals: 2. Effects of coal characteristics for a range of Australian and international coals. *Fuel, 82*(1), 59-69. https://doi.org/10.1016/S0016-2361(02)00191-6.

Fedorova, N. I., Mikhaylova, E. S., & Ismaglov, Z. R. (2017). Properties of Kuznets Basin gas coal. *Coke and Chemistry, 60*(7), 261-266. https://doi.org/10.3103/S1068364X17070031.

FitzGerald, K., & Zambrowski, K. (2023). *Coal Workshop: Thermal Coal and Coking Coal*. [PowerPoint slides]. WhitehavenCoal. https://whitehavencoal.com.au.

Flores, B. D., Flores, I. V., Guerrero, A., Orellana, D. R., Pohlmann, J. G., Diez, M. A., . . . Vilela, A. C. (2017). Effect of charcoal blending with vitrinite rich coal on coke reactivity. *Fuel Processing Technology*, *155*(1), 97-105.

Fraga, M., Flores, B., Osório, E., & Vilela, A. (2020). Evaluation of the thermoplastic behavior of charcoal, coal and coking coal blends. *Journal of Materials Research and Technology, 9*(3), 3406-3410.

Gagarin, S. G. (2009). Correlation between the Roga index and the free-swelling index of coal. *Coke and Chemistry*, *52*(11), 473-476.

Geyer, P. G., & Halifa, Z. (2014). Blast furnace tapping practice at ArcelorMittal South Africa, Vanderbijlpark Works. *The Southern African Institute of Mining and Metallurgy*, *Furnace Tapping Conference*. 27-29 May 2014. Muldersdrift, South Africa. 97-112.

Giovannini, S. (2020). *Energy Cities 50 shades of (grey and blue and green) hydrogen*. Available: https://energy-cities.eu/50-shades-of-grey-and-blue-and-green-hydrogen/. [2021, July 20].

Glushkov, D. O., Lyrschikov, S. Y., Shevyrey, S. A., & Yashutina, O. S. (2019). Rheological properties of coal water slurries containing petrochemicals. *Thermal Science*, *23*(5B), 2939-2949. https://doi.org/10.2298/TSCI180422191G.

Gojić, M., & Kožuh, S. (2006). Development of direct reduction processes and smelting reduction processes for steel processes. *Journal of Chemists and Chemical Engineers, 55(1)*, 1-10.

Gómez-Casero, M, A, Pérez-Villarejo, ., L., Casto, E., & Eliche-Quesada, D. (2021). Effect of steel slag and curing temperature on the improvement in technological properties of biomass bottom ash based alkali-activated materials. *Construction and Building Materials, 302*. https://doi.org/10.1016/j.conbuildmat.2021.124205.

Grainger, L., & Gibson, J. (2012). *Coal utilisation: Technology, economics and policy.* New York City: Springer. https://doi.org/10.1007/978-94-011-7352-0.

Grainger, L., & Gibson, J. (2020). The carbonisation of coals. In *Coal utilisation: Technology, economics and policy.* L. Grainger, & L. Gibson, Eds. New York City: Springer. 129-160. https://doi.org/10.1007/978-94-011-7352-0.

Gridavos, V. P., Logachev, G. N., Pishnograev, S. N., Pavlov, A. V., Gostenin, V. A., & Chevchelov, A. V. (2016). Behavior of alkalis in blast furnaces. *Metallurgist, 59*, 761-765. https://doi.org/10.1007/s11015-016-0171-4.

Grigore, M., Sakurovs, R., French, D., & Sahajwalla, V. (2012). Properties and CO_2 reactivity of the inert and reactive maceral-derived components in cokes. *International Journal of Coal Geology, 98*(1), 1-9. https://doi.org/10.1016/j.coal.2012.04.004.

Guelton, N. (2017). The prediction of the Gieseler characteristics of coal blends. *Fuel, 209*, 661-673. https://doi.org/10.1016/j.fuel.2017.07.017.

Guo, Y., Zhou, L., Guo, F., Chen, X., Wu, J., & Zhang, Y. (2020). Pore structure and fractal characteristic analysis of gassification-coke prepared at different high temperature residence times. *ACS Omega 5*(35), 22226-22237. https://doi.org/10.1021/acsomega.0c02399.

Hamadeh, H., Mirguax, O., & Patisson, F. (2018). Detailed modelling of the direct reduction of iron ore in a shaft furnace. *Materials, 11*(10), 1865. https://doi.org/10.3390/ma11101865.

Haranda, T., & Tanaka, H. (2011). Future of steelmaking model by direct reduction technologies. *ISIJ International: Transactions of the Iron and Steel Institute of Japan, 51*(8), 1301-1307. https://doi.org/10.2355/isijinternational.51.1301.

Harrison, S. B. (2022). *Turquoise hydrogen production by methane pyrolysis.* Available: https://www.digitalrefining.com/article/1002720/turquoise-hydrogen-production-by-methane-pyrolysis. [2023, April 02].

Harvey, J., & Gheribi, A. E. (2014). Process simulation and control optimisation of a blast furnace using classical thermodynamics combined to a direct search algorithm. *Metallurgical and Materials Transactions B, 45*, 307-327. https://doi.org/10.1007/s11663-013-0004-9.

He, H., Guan, H., Zhu, X., & Lee, H. (2017). Assessment of the energy flow and carbon emission of integrated steelmaking plants. *Energy Reports, 3*, 29-36. https://doi.org/10.1016/j.egyr.2017.01.001.

Horvat, G., Pantić, M., Knez, Ž., & Novak, Z. (2022). A brief evaluation of pore structure determination of bioaerogels. *Gels, 8*(7), 438. https://doi.org/10.3390/gels8070438.

Howaniec, N. (2016). Temperature induced development of porous structure of bituminous coal chars at high pressure. *Journal of Sustainable Mining, 15*(3), 120-124. https://doi.org/10.1016/j.jsm.2016.12.002.

Howarth,. R, W., & Jacobson, M, Z. (2021) How green is blue hydrogen?. *Modelling and analysis, 9,*1676-1687. https://doi.org/10.1002/ese3/956.

Hu, Y., Liu, J., Wang, R., Zhou, J., & Cen, K. (2016). Rheological properties of oil sand slurries and the effect on viscosity of blending with coal. *Petroleum Science and Technology, 34*(14), 1272-1278. https://doi.org/10.1080/10916466.2015.1021010.

Huang, J., Tao, L., Tie, W., Li, Z., Wang, Q., & Liu, Z. (2020). Transport properties of CO_2 in different reactivity coke solution loss reaction based on Stefan Flow Theory. *ACS Omega, 5*(41), 26817-26828. https://doi.org/10.1021/acsomega.0c03913.

Huxham, M., Anwai, M., & Nelson, D. (2019). *Understanding the impact of low-carbon transition on South Africa*. Available:

https://www.climatepolicyinitiative.org/publication/understanding-the-impact-of-a-low-carbon-transition-on-south-africa/. [2021, July 30].

Jeffrey, L. S. (2005). Characterization if the coal resources of South Africa. *Journal of the South African Institute of Mining and Metallurgy, 105*(2), 95-102.

Jiao, H., Wang, M., Kong, J., Guo, J., & Chang, L. (2019). Effects of interactions among coals on the caking ability of blends during carbonization. *Journal of Analytical and Applied Pyrolysis, 138*, 154-160.

Jienan, P., Zhaozhao, Z., Meng, L., Yawen, W., & Kai, W. (2019). Characteristics of multi-scale pore structure of coal and its influence on permeability. *Natural Gas Industry B, 6*(4), 357-365. https://doi.org/10.1016/j.ngib.2019.01.012.

Jordan, P. (2006). Characterisisng coals for coke production and assessing coke. MSc (Eng) dissertation. University of the Witwatersrand.

Jovan, D. J & Dolanc, G. (2020) Can green hydrogen production be economically viable under current market conditions .*Energies*.*13*(24), 1-16. https://doi.org/10.3390/en13246599

Ju, Y., Jiang, B., HouQ, Wang, G., & Fang, A. (2005). Structural evolution of nano-scale pores of techtonic plates in southern North China and its mehanism. *Acta Geophysica Sinica, 79*(2), 269-285.

Kalkreuth, W., Borrego, A. G., Alvarez, D., Menendez, R., Osório, E., & Ribas, M. (2005). Exploring the possibilities of using Brazilian subbituminous coals for blast furnace pulverised fuel injection. *Fuel, 84*(6), 763-772. https://doi.org/10.1016/j.fuel.2004.11.007

Kandiyoti, R., Herod, A. A., & Bartle, K. D. (2017). 6 - Elements of thermal breakdown: Heating rate effects and retrogressive reactions. In *Solid fuels and feavy hydrocarbon liquids: thermal characterization and analysis.* 2nd ed. R. Kandiyoti, A. Herod, K. Bartle, & T. Morgan, Eds. North York: Elsevier. 251-283. https://doi.org/10.1016/B978-0-08-100784-6.00006-0.

Kentacky Geological Survey. (2019). *Earth Resources - Our Common Wealth*. Available: http://www.uky.edu/KGS/coal/coal-for-cokesteel.php. [2022, October 6].

Khan, S. A., Khan, S. B., Khan, L. U., Farooq, A., Akhtar, K., & Asiri, A. M. (2018). Fourier Transform Infrared Spectroscopy: Fundamentals and Application in Functional Groups and Nanomaterials Characterization. . In: S. Sharma, ed. *Handbook of Materials.* New York: Springer, Cham, 317-334

Kruszewska, K. J. (2003). Flourescing macerals in South Africn coals. *International Journal of Coal Geology*, *54*(1-2), 79-94. https://doi.org/10.1016/S0166-5162(03)00025-9.

Kshirsagar, S., & Malladi, K. (2021). *Hydrogen holds promise as an alternative clean energy carrier.* Available: https://wri-india.org/blog/hydrogen-holds-promise-alternative-clean-energy-carrier. [2023, April 02].

Kudo, S., Mori, A., Hayashi, G., Yoshida, T., Okuyama, N., Norinaga, K., & Hayashi, J. (2018). Characteristic properties of lignite to be converted to high-strength coke by hot briquetting and carbonization. *Energy and Fuels, 32*(4), 4364-4371. https://doi.org/10.1021/acs.energyfuels.7b03155.

Kmar, S. (2013).Clean Hydrogen Production and Carbon Dioxide Caapture Methods, Florida. PhD thesis. Florida International University. https://digitalcommons.fu.edu/etd.

Kumar, P. P., Barman, S. C., Singh, S., & Rajan, M. (2008). Influence of coal fluidity on coal blend and coke quality. *Ironmaking ans Steelmaking, 35*(6), 416-420. https://doi.org/10.1179/174328108X335113.

Kunitomo, K., Takamoto, Y., Fujiwara, Y., & Onuma, T. (2006). *Blast furnace ironmaking process using pre-reduced iron ore. Shinnittetsu Giho (Nippon Steel Technical Report), 384*, 121. Shimaada: Nippon Steel.

Kurunov, I. F., Titov, V. N., Emel'yanov, V. L., Lysenko, S. A., & Arzamastesev, A. N. (2009). Analysis of the behavior of alkalis in a blast furnace. *Metallurgist, 53*, 533-542. https://doi.org/10.1007/s11015-010-9210-8.

Leokaoke, N. T., Bunt, H. W., Neomagus, H. W., Waanders, F. B., Strydom, C. A., & Mthombo, T. S. (2018). Manufacturing and testing of briquettes from inertinite-rich low-grade coal fines using various binders. *The Journal of the Southern African Institute of Mining and Metallurgy, 118*(1), 83-88. http://dx.doi.org/10.17159/2411-9717/2018/v118n1a10.

Li, H., Shi, S., Lin, B., Lu, J., Ye, Q., Lu, Y., Wang, Z., Hong, Y., & Zhu, X. (2019). Effects of microwave-assisted pyrolysis on the microstructure of bituminous coals. *Energy, 187*. https://doi.org/10.1016/j.energy.2019.115986.

Li, H., Wang, S., Zeng, Q., Kang, J., Guan, W., & Li, W. (2021a). Effects of pore structure of different rank coals on methane adsorption heat. *Processes, 9*(11), 1971. https://doi.org/10.3390/pr9111971.

Li, H., Wu, S., Wu, Y., Wang, H., Zhang, Z., Huang, S., & Gao, J. (2019). Effects of He Li, Shiliang Shi, Baiquan Lin, Jiexin Lu, Qing Ye, Yi Lu, Zheng Wang, Yidu Hong, Xiangnan Zhu, hydrothermal treatment on physio-chemical structures and liquefaction behaviors of lignite. *Fuel, 263*, 116636. https://doi.org/10.1016/j.fuel.2019.116636.

Li, T., Wu, C., & Wang, Z. (2021b). The dynamic change of pore structure for low rank coal under refined upgrading pretreatment temperatures. *Petroleum Science, 18*, 430-443. https://doi.org/10.1007/s12182-020-00536-9.

Li, T., Wu, J., Wang, X., & Haung, H. (2021c). Particle size effect and temperature effect on the pore structure of low-rank coal. *ACS Omega, 6*(8), 5865-5877. https://doi.org/10.1021/acsomega.0c06280.

Li, Y., Jiang, Y., & Wang, P. (2021d). Investigation on the pore characteristics of coal specimens with bursting proneness. *Scientific Reports, 9*, 16518. https://doi.org/10.1038/s41598-019-52917-9.

Liang, T., Wang, S., Lu, C., Jiang, N., Long, W., Zhang, M., & Zhang R. (2020). Environmental impact evaluation of an iron and steel plant in China: Normalized data and direct/indirect contribution. *Journal of Cleaner Production*, 246.

Liang, T., Wang, S., Lu, C., Jiang, N., Long, W., Zhang, M., & Zhang R. (2020). Environmental impact evaluation of an iron and steel plant in China: Normalized data and direct/indirect contribution. *Journal of Cleaner Production,* 246.

Lingling, Q., Xinshan, P., Zhaofeng, W., Xiangjun, C., & Juhua, D. (2022). Study on the pore structures and adsorbtion characteristics of coking coal of liulin mining in China

under the condition of high temperature and high pressure. *Frontiers in Earth Science, 10*, 1-10. https://doi.org/10.3389/feart.2022.877462.

Liu, X., Liu, C., Wang, B., Ye, F. (2019). Optimization of iron ore blending in the COREX shaft furnace. The Journal of the Southern African Institute of Mining and Metallurgy. 119.445-452. https://dx.doi.org./10.17159/24119717/18/018/2019.

Liu, K., Zhang, Z., & Sun, J. (2021). Advances in understanding the alkali-activated metallurgical slag. *Advances in Civil Engineering*, 1-16. https://doi.org/10.1155/2021/8795588.

Liu, P., & Zhang, D. (2020). Effect of hydrothermal treatment on the carbon structure of Inner Mongolia lignite. *International Journal of Coal Science Technology, 7*, 493-503. https://doi.org/10.1007/s40789-020-00356-7.

Liu, X., Zhao, Z., Xie, R., Lei, Z., Ling, Q., & Cui, P. (2019). Modification mechanism of caking and coking properties of Shenmu subbituminous coal by low-temperature rapid pyrolysis reatment. *Journal of Iron and Steel Research International, 26*, 1052-1060. https://doi.org/10.1007/s42243-019-00261-7.

Lotfian, S. (2018). *Alternative reducing agents in metallurgical processes: Potential of shredder residue material as a reductant in zinc fuming process.* PhD Thesis. Luleå University of Technology.

Lotfian, S., Ahmed, H., & Samuelsson, C. (2017a). Alternative reducing agents in metallurgical process: Devolatilization of shredder residue materials. *Journal of Sustainable Metallurgy, 3*, 311-321. https://doi.org/10.1007/s40831-016-0094-0.

Lotfian, S., Ahmed, H., El-Greasy, A. A., & Samuelsson, C. (2017b). Alternative reducing agent in metallurgical processes: Gasification of shredder residue material. *Journal of Sustainable Metallurgy, 3*, 336-349. https://doi.org/10.1007/s40831-016-0096-y.

Lotfian , S., Vikstrom, T., Lennartsson, A., Bijorkman, B., Ahmed, H., & Samuelsson, C. (2019). Plastic-containing materials as alternative reductant for base metal production. *Canadian Metallurgical Quarterly: The Canadian Journal of Metallurgy and Materials Science, 58*(2), 164-176. https://doi.org/10.1080/00084433.2018.1532951.

Lu, L., Devasahayam, S., & Sahajwalla, V. (2013). 14 - Evaluation of coal for metallurgical applications. *The coal handbook: Towards cleaner production, 2,* 352-386. Armsterdam: Elsevier. https://doi.org/10.1533/9781782421177.3.352.

Lundgren, M., Leimalm, U., Hyllander, G., Ökvist, L. S., & BjÖrkman, B. (2010). Off-gas dust in an experimental blast furnace Part 2: Relation to furnace conditions. *ISIJ International: Transactions of the Iron and Steel Institute of Japan, 50*(11), 1570-1580. https://doi.org/10.2355/isijinternational.50.1570.

Mahapatra, D. (2018). A review on steam coal analysis - Moisture. *American International Journal of Research in Science, Technology, Engineering and Mathematics,13(2)*, 143-152. https://doi.org/10.13140/RG.2.2.30688.38406.

Maia Star. (2020). *Direct reduced iron*. Available: http://maiastar.com/products/detail/51/DRI. [2021, May 01].

Makgato, S. S. (2013). Investigating the effect of substituting fractions of imported coals with coke oven tar on coke quality: Pilot plant study. *Journal of the Southern African Institute of Mining and Metallurgy, 113*(11), 1-7.

Makgato, S. S., & Falcon, R. M. (2013). The effect of substituting fractions of imported coking coals with coke oven tar on coal blend, carbonization, coal properties. *Journal of the Southern African Institute of Mining and Metallurgy, 113*(11), 809-815.

Makgato, S. S., Falcon, R. S., & Chirwa, E. N. (2019). Reduction in coal fines and extended coke production through the addition of carbonisation tar: Environmentally clean process. *Journal of Cleaner Production, 221*(3), 684-694.

Makukule, X, M.,Dorland, H, C., Wagner, N, N. (2016) The usefulness of petrographic information for coal industry. Available at https://www.multotech.com/public/uploads/files/media_files/file_f057decc1fc45706d269af20441ad248.pdf [26 March 2021].

Malumbazo, N., Wagner, N. J., & Bunt, J. R. (2012). The petrographic determination of reactivity differences of two South African inertinite-rich lump coals. *Journal of Analytical and Applied Pyrolysis*, *93*, 139-146. https://doi.org/10.1016/j.jaap.2011.10.008.

Mandal, G. K., Sau, D. C., Das, S. K., & Bandyopadhyay, D. (2014). A steady state thermal and material balance for an iron making blast furnace and its validation with operation data. *Transactions of the Indian Institute, 67*, 209-221. https://doi.org/10.1007/s12666-013-0338-7.

Marsh, H., & Rodriguez-Reinoso, F. (2006). Chapter 2- Activated Carbon (Origins). In *Activated Carbon.* H. Marsh, & F. Rodriguez-Reinoso, Eds. Amsterdam: Elsevier. 13-86.

Mathieson, J. G., Truelove, J. S., & Rogers, H. (2005). Toward an understanding of coal combustion in a blast furnace tuyere injection. *Fuel, 84*(10), 1229-1237. https://doi.org/ 10.1016/j.fuel.2004.06.036.

Matjie, R. H., Li, Z., Ward, C. R., Bunt, J. R., & Strydom, C. A. (2016). Determination of mineral matter and elemental composition of individual macerals in coals from Highveld mines. *The Journal of the Southern African Insitute of Mining and Metallurgy, 116*(2), 169-180.

Matsui , Y., Yamaguchi, Y., Sawayama, M., Kitano, S., Nagai, N., & Imai, T. (2005). Analyses on blast furnace raceway formation by micro wave reflection gunned through tuyere. *ISIJ International: Transactions of the Iron and Steel Institute of Japan, 45*(10), 1432-1438.

Mazumder, B. (2012). 6- Coal conversion processes. In *Coal science and engineering.* B. Mazumder, Ed. New Delhi: Woodhead Publishing. 145-451.

McKinsey & Company. (2020). *Decarbonization challenge for steel. Hydrogen as a solution in Europe*. Available: https://www.mckinsey.com/~/media/McKinsey/Industries/Metals%20and%20Mining/Our%20Insights/Decarbonization%20challenge%20for%20steel/Decarbonization-challenge-for-steel.pdf. [2021, July 30].

Merk. (2022) *Sigma-Aldrich.* [Online]. Available at: https://www.sigmaaldrich.com/IS/en/technical-documents/technical-article/analytical-chemistry/photometry-and-reflectometry/ir-spectrum-table [Accssed 25 July 2022].

MetroSteel. (2016). *The six steps to modern steel production explained*. Available: https://www.metrosteel.com.au/the-6-steps-to-modern-steel-production-explained/. [2021, February 12].

Michishita, H., & Tanaka, H. (2010). Prospects for coal-based direct reduction process. *Kobelco Technology Review, 29*, 69-76.

Mori, A., Yuniati, A., Mursito, A. T., Kudo, S., Norinaga, K., & Nonaka, M. (2013). Preparation of coke from Indonesian lignites by a sequence of hydrothermal treatment, hot briquetting, and carbonization. *Energy and Fuels, 27(11)*, 6607-6616. https://doi.org/10.1021/ef4016558.

Morley, R. J., Pisupati, S. V., & Scaroni, A. W. (2017). *Carbonisation (coke making)*. Available: https://www.britannica.com/topic/coal-utilization-122944/Carbonization-coke-making. [2021, May 19].

Moroeng, O. M. (2018). Geochemistry of South African coal: Insights into the formation of certain macerals. PhD thesis. University of Pretoria. http://hdl.handle.net/2263/70431.

Moroeng, O. N., Mhuka, V., Nindi, M. M., Roberts, R. J., & Wagner, N. J. (2019). Comparative study of a vitrinite-rich and inertinnite-rich Witbank coal (South Africa) using pyrolysis-gas chromatography. *International Journal of Coal Science & Technology, 6* (6), 621-632. https://doi.org/10.1007/s40789-019-00274-3.

Mphaphuli, M. (2017). Petrographic considertion of the impact of the Tshipise Fault on the coal quality in the Spoutpansberg coalfield, South Africa. MSc dissertation. University of Johannesburg. https://hdl.handle.net/10210/235849.

Musiiwa, A. (2018). *An investigation into the use of borates to improve coke CSR/CRI when blending metallurgical coal to make blast furnace coke*. MSc research report. University of the Witwatersrand.

Nagashanmugam, K. B., Pillai, M. S., & Ravichandar, D. (2015). 'Salem Box Test' to predict the suitability of metallurgical coke for blast furnace ironmaking. *The Journal of the Southern African Institute of Mining and Metallurgy, 115*(2), 131-136.

Nikolaeva, N. V., Aleksandrova, T. N., Chanturiya, E. L. & Afanasova, A. (2021). Mineral and Technological Features of Magnetite–Hematite Ores and Their Influence on the Choice of Processing Technology. *ACS Omega, 6*(13), p. 9077–9085.

Nonaka, M., Hirajima, T., & Sasaki, K. (2011). Upgrading of low rank coal and woody biomass mixture by hydrothermal treatment. *Fuel, 90*(8), 2578-2584. https://doi.org/10.1016/j.fuel.2011.03.028

Nourredine, M. (2007). Recycling of auto shredder residue. *Journal of Hazardous Materials, 139*(3), 481-490. https://doi.org/10.1016/j.jhazmat.2006.02.054.

Noussan, M., Raimondi, P. R., Scita, R., & Hafner, M. (2021). The role of green and blue hydrogen in the energy transition - A technological and geopolitical perspective. *Sustainability, 13*(1), 298. https://doi.org/10.3390/su13010298.

Nutting, J., Wondris, E. F., & Wente, E. F. (2019). *Steel. metallurgy*. Available: https://www.britannica.com/technology/steel. [2021, February 22].

Oboirien, B. O. (2012). Gasification of high ash coals and chars from South African coals. PhD thesis. University of the Witwatersrand. http://hdl.handle.net/10539/11625.

Ogoshi, T., Sakatsume, Y., Onishi, K., Tang, R., Takahashi, K., Nishihara, H., Nishina, Y., Campéon, B, D, L., Kakuta, T., Yamagishi, T. (2021). The carbonization of aromatic molecules with three-dimensional structures affords carbon materials with controlled pore sizes at the Ångstrom-level. *Communications Chemistry 4*(75). https://doi.org/10.1016.j.ngib.2019.01.012.

Pan, J., Zhang, Z., Li, M., Wu, Y., & Wang, K. (2019). Characteristics of multi-scale pore structure of coal and its influence on permeability. *Natural Gas Industry B, 6*(4), 357-365. https://doi.org/10.1016/j.ngib.2019.01.012.

Panic´, I., Cuculic´, A. & C'elic, J. (2022). Color-Coded Hydrogen: Production and Storage. *Journal of Marine Science and Engineering, (10),* 1-35. https://doi.org/10.3390/jmse10121995.

Pei, M. (2021). *Fossil-free steel*. Available: https://www.ssab.com/fossil-free-steel. [2021, July 27].

Pei, M., Petäjäniemi, M., & Regnell, A. (2020). Toward a fossil free future with HYBRIT: Development of iron and steelmaking technology in Sweden and Finland. *Metals, 10*(7), 972. https://doi.org/10.3390/met10070972.

Petit, S., & Madejova, J. (2013). Chapter 2.7 - Fourier transform infrared spectroscopy. *Developments in Clay Sciences, 5,* 213-231. https://doi.org/10.1016/B978-0-08-098259-5.00009-3.

POSCO. (2021). *[Exploring Hydrogen with POSCO #3]. The future of steel - Hydrogen-based steelmaking*. Available: https://newsroom.posco.com/en/exploring-hydrogen-with-posco-3-the-future-of-steel-hydrogen-based-steelmaking/. [2021, July 27].

Punathil, L., & Basak, T. (2016). Microwave processing of frozen and packaged food materials: Experimental. In *Reference module in food science.* L. Punathi, & T. Basak, Eds. Amsterdam: Elsevier. https://doi.org/10.1016/B978-0-08-100596-5.21009-3

Puyejovska, P., Jursova, S., Brozova, S., & Sousek, J. (2013). Effect of waste and alternative fuels on blast furnace operation. *Metallurgist, 56*, 908-911. https://doi.org/10.1007/s11015-013-9673-5.

Ratshomo, K.,& Nembahe, R. (2019). *South African Coal Sector Report.* Pretoria, South Africa: Department of Energy.

Raygan, S., Abdizadeh, H., & Rizi, A. E. (2010). Evaluation of four coals for blast furnace pulverised coal injection. *Journal of Iron and Steel Research International, 17*(3), 08-12. https://doi.org/10.1016/S1006-706X(10)60065-9.

Ren, S., Zhang, J. L., Liu, W. J., Su, B. X., Xing, X. D., & Bai, Y. N. (2013). An integrated evaluation system of anthracite, meager-lean coal and bituminous coal co-injection for a blast furnace. *Energy Sources, Part A: Recovery, Utilization, and Environmental Effects, 35*(22), 2123-2131. https://doi.org/10.1080/15567036.2011.645995.

Richards, J. M., Naude, G., Theron, S. J., & McCullun, M. (2013). Petrological characterisation of coal: an evolving science. T*he Journal of the Southern African Institute of Mining and Metallurgy, 113*(11), 865-875.

Rodero, J. I., Sancho-Gorostia, J., Ordiales, M., Fernández-González, D., Mochón, J., & Ruiz-Bustinza, I. (2015). Blast furnace and metallurgical coke's reactivity and its

determination by thermal gravimetric analysis. *Ironmaking and Steelmaking, 42*(8), 618-625. https://doi.org/10.1179/1743281215Y.0000000016.

Ryemshak, S. A. & Jauro, a. (2013). Proximate analysis, rheological properties and technological applications of some Nigerian coals. *International Journal of Industrial Chemistry, 4*(7).1-7.

Rzychoń, M., Żogala, A., & Róg, K. (2021). Experimental study and extreme gradient boosting (XBoost) based prediction of caking ability of coal blends. *Journal of Analytical Applied Pyrolysis, 156*, 105020. https://doi.org/10.1016/j.jaap.2021.105020

Satyendra. (2013a). *Coking coal*. Available: https://www.ispatguru.com/coking-coals/. [2020, August 13].

Satyendra. (2013b). *Fastmet and Fastmelt process of ironmaking*. Available: https://www.ispatguru.com/fastmet-and-fastmelt-processes-of-ironmaking/. [2021, February 22].

Satyendra. (2017). *Corex process for production of iron*. Available: https://www.ispatguru.com/corex-process-for-production-of-iron/. [2021, July 20].

Satyendra. (2019). *BF coke and its role in blast furnace.* Available: https//:www.ispatguru.com/bf_coke_and_its_blast_role_in_blast_furnace/. [2021, June 13]

Schwanke, A. J., Balzer, R., & Pergher, S. (2017). Microporous and mesopores materials from natural and inexpensive sources. In *Handbook of ecomaterials*. L. Martínez, O., Kharissova, & B.Kharisov. Eds. Cham: Springer. https://doi.org/10.1007/978-3-319-48281-1_43-1.

Sciazko, M., Mertas, B., & Stepien, L. (2020). Kinetic modelling of coking coal fluidity development. *Journal of the Thermal Analysis and Calorimetry, 142*, 977-990. https://doi.org/10.1007/s10973-020-09487-0.

SGS. (2021). *Rheology of coal*. Available: https://www.sgs.co.za/en/mining/analytical-services/coal-and-coke/rheology-of-coal. [2021, February 26].

SGS Minerals Services. (2013). *Analytical services for coal*. Available: https://www.sgs.com/en-ca/-/media/sgscorp/documents/corporate/brochures/sgs-min-wa073-coal-analytical-services-en-11.cdn.en-CA.pdf. [2021, July 14].

Shen, Y. S., Yu, A. B., Austin, P. R., & Zulli, P. (2012). CFD study of in-furnace phenomena of pulverised coal injection in blast furnace: Effects of operation conditions. *Powder Technology, 223*, 27-38. https://doi.org/10.1016/j.powtec.2011.07.020.

Shi, Z., Jin, L., Zhou, Y., & Hu, H. (2017). Effect of hydrothermal treatment on structure and liquefaction behavior of Baiyinhua Coal. *Fuel Processing Technology, 167*(19), 648-654.

Shui, H., Li, H., Chang, H., Wang, Z., Gao, Z., & Lei, Z.. (2011). Modification of sub-bituminous coal by steam treatment: Caking and coking properties. *Fuel Processing Technology, 92*(12), 2299-2304. https://doi.org/10.1016/j.fuproc.2011.08.001.

Shui, H., Wu, Y., Wang, Z., Lei, Z., Lin, C., & Ren, S. (2012). Hydrothermal treatment of a sub-bituminous coal and its use in coking blends. *Energy and Fuel, 27*(1), 138-144. https://doi.org/10.1021/ef301539x.

Silva, K. G., & Assis, P. S. (2019). Combustibility behavior of PCI coals, green petroleum coke and charcoal fines used as fuel for injection into blast furnace tuyeres. *International Engineering Journal, 72*(1), 125-131. https://doi.org/10.1590/0370-44672018720068.

Signh, J, K., & Rout, A. K. (2018 Advances in Green Steel Making Technology - A Review. *American Journal of Materials Engineering and Technology, 6*(1), 813. https://doi.org/10.12691/materials-6-1-2.

Speight, J. G. (2013). *The chemistry and technology of coal.* 3rd ed. Bota Raton: CRC Press. https://doi.org/10.1201/b12497.

Steel Dynamics. (2021). *Effect of chemical elements in steel.* Available: https://www.steeltank.com/Products/PressureVessels/EffectofChemicalElementsinSteel/tabid/916/Default.aspx. [2021, March 15].

Steenkamp, J. D., & Du Preez, L. (2015). Introduction to the production of clean steel. *Journal of the Institute of South African Mining and Metallurgy, 115*(6), 557-561.

Steinert. (2021). *Automotive shredder residue (ASR).* Available: https://steinertglobal.com/metal-recycling/auto-shredder-residue/. [2021, July 30].

Stepheson, M. (2013). Chapter 2 - The negative greenhouse. In *Returning Carbon to Nature: Coal, Carbon Capture and Storage.* M. Stepheson, Ed. New York: Elsevier. 23-44.

Strugala, A., Rozwadoski, A., Dziok, T. (2022). Mechanism of coking pressure generation in the light of the results of the laboratory tests. Energies, 15,2044. https://doi.org/10.3390/en15062044.

Su, B., Wang, G., Li, R., Xu, K., Wu, J., & Li, D. (2022). Co-combustion behaviour of paper sludge hydrochar and pulverised coal: Low rank coal and its product by hydrothermal carbonisation. *Energies, 15*(15), 5619. https://doi.org/10.3390/en15155619.

Sutchu, H., Toroglu, I., & Piskin, S. (2009). Prediction of metallurgical coke strength from the petrographic composition of coal blends. *Energy Sources, Part A: Recovery, Utilisation, and Environmental Effects, 31*(12), 1047-1055. https://doi.org/10.1080/15567030801909730.

Theron, J. A., & le Roux, E. (2015). Representation of coal and coal derivatives in process modelling. *The Southern African Journal of Mining and Metallurgy, 115*(5), 339-348.

Thommes, M., Kaneko, K., Neimark, A. V., Oliver, J. P., Rodriguez-Reinoso, F., & Rouquerol, J. (2015). Physisorption of gases, with special reference to the evaluation of surface area and pore size distribution (IUPAC Technical Report). *Pure and Applied Chemistry, 87*(9-10), 1051-1069. https://doi.org/10.1515/pac-2014-1117.

Todoshuk, T. W., Price, J. T., & Grandsen, J. F. (2004). Development of coke strength after reaction (CSR) at Dofasco. *Iron and Steel Technology*, *1*, 73-84. Ontario: Dofasco Inc.

Tollip, H. (2021). *Green iron in South Africa.* Available: https://ddpinitiative.org/wp-content/pdf/Green_Iron_production_SA_18052021.pdf. [2021, July 26].

Tsutsumi, H., Yoshida, S., & Tetsumo, M. (2010). Features of FASTMET process. *Kobelco Technology Review, 12*, 85-92. Available: https://www.kobelco.co.jp/english/ktr/pdf/ktr_29/whole.pdf. [2023, April 03].

UNT Digital Library. (2021). *Coal composition, coal plasticity, and coke strength.* Avaialable: https://digital.library.unt.edu/ark:/67531/metadc12806/m1/25/. [2023, April 02].

U.S Department of Energy. (2020). *Hydrogen production and distribution.* Available: https://afdc.energy.gov/fuels/hydrogen_production.html. [2021, July 26].

Viljoen, J., Campbell, Q. P., le Roux, M., & Hoffman, J. (2015). The qualification of coal degradation with the aid of micro-focus computed tomography. *South African Journal of Science, 111*(9/10), 1-10. https://doi.org/10.17159/sajs.2015/20140025.

Wagner , N. (2021). Geology of Coal. In: Alderton, D., & Elias, S, A, *eds. Encyclopedia of Geology (Second Edition).* Academic Press.

Wagner , N., Malumbazo, N., & Falcon, R. (2018). *Southern African coals and carbons.* Cape Town: Struik Nature.

Wang, Q., Zhang, T, K., Yu, Zhao, Y, Q., He, S, H., Zhang, Y, F. (2019). Structural evolution and formation mechanisms of caking components of modified lignite in subcritical H2O-CO systems. Energy & Fuels. 33. 12073-12082. https:// 10.1021/asc.energyfuels.9b02784

Wang, Z., Shui, H., Pei, Z., & Gao, J. (2008). Study on hydrothermal treatment of Shenhua coal. *Fuel, 87*(4-5), 527-533. https://doi.org/10.1016/j.fuel.2007.03.017.

Ward, C. R., & Suárez-Ruiz, I. (2008). Introduction to applied coal petrology. In *Applied coal petrology: The role of petrology in coal utilization.* I. Suárez-Ruiz, & J. C. Crelling, Eds. Amsterdam: Elsevier. 1-18.

Wei, Q., & Tang, Y. (2018). ^{13}C-NMR study on structure evolution characteristics of high organic sulphur coals from typical Chinese areas. *Minerals, 8*(2), 49. https://doi.org/10.3390/min8020049.

Williams, O., Ure, A., Stevens, L., Binner, E., Dodds, C., & Kingman, S. (2019). Formation of metallurgical coke within minutes through coal densification and microwave energy. *Energy & Fuels, 33*(7), 6817-6828. https://doi.org/10.1021/acs.energyfuels.9b00511.

Wood, J. (2020). *What are the three colours of hydrogen*. Available: https://spectra.mhi.com/what-are-the-three-colors-of-hydrogen. [2021, July 24].

World Steel Association. (2018). *World steel in figures 2018.* Available: https://worldsteel.org/wp-content/uploads/2018-World-Steel-in-Figures.pdf. [2020, June 30].

World Steel Association. (2019). *Fact sheets: Steel and raw materials.* Available: https://worldsteel.org/publications/fact-sheets/. [2023, April 03].

Xinglong, Z., Dazhen , T., Hao, X., Shu, T., & Shen, Z. (2010). Effect of coal metamorphic process on pore system of coal reserves. *Journal of China Coal Society, 35*(9), 1506-151

Yao, S., Zhang, K., Jiao, K., Hu, W. (2011). Evolution of coal structures:FTIR analysis of experimental simulations and naturally matured coals in the Ordos Basin, China. *Energy expliration &exploitation.* 1-19.

Yan, M., Song, X., Tian, J., Lv, X., Zhang, Z.,Yu, X., Zhang, X. (2020). Construction of a new type of coal moisture control device based on the characteristics of indirect drying process of coking coal. *Energies (13)*16. https://doi.ord/10.3390/en13164162

Yu, J., Jiang, C., Guan, Q., Gu, J., Ning, P., Miao, R., Chen, Q., Zhang, J. (2018). Conversion of low-grade coals in sub-and critical water: A review. *Fuel. 217*. 275-284. https://doi.org/10.1016/j.fuel.2017.12.113

Yustanti, E., Wardhono, E. Y., Mursito, A. T., & Alhamidi, A. (2021). Types and compositions of biomass in biocoke synthesis with the coal-blending method. *Energies, 14*(20), 6570. https://doi.org/10.3390/en14206570.

Zhang, D., Liu, P., Wang, L., & Pan, T. (2016). Upgrading of low rank coal by hydrothermal treatment: Coal tar yield during pyrolysis. *Fuel Processing Technology, 141*(1), 117-122. https://doi.org/10.1016/j.fuproc.2015.06.037.

Zhao, Y., Zhang, M., Ciu, X., Dong, D., Wang, Q., Zhang, Y. (2016). Converting lignite to caking coal via hydro-modification in a subcritical water-CO system. Fuel 167.1-8.

Zhixiu, H., Lijuan, J., Ying, D., Ruan, R., Srinivasakannan, C., & Chenhui, L. (2019). Upgradation of Zhaotong drying ignite through microwave drying. *Materials Research Express, 6*(4), 6 045515. https://doi.org/10.1088/2053-1591/aafdeb.

Zhou, X., Shi, Z., Zhang, G., Ding, Y., & Yang, X. (2015). Operating line for Corex smelting reduction ironmaking process. *Materials Research Innovations, 19*(S8), 99-101. https://doi.org/10.1179/1432891715Z.0000000001630.

Zuo, H., Long, S., Wang, C., & Zhang, P. (2016). A review of microwave treatment on coal. In 1*7th International Symposium on High Temperature Metallurgical Processing*. Y. Hwang, T. Jiang, P. C. Pistorius, G. R. Alvear, O. Yücel, & L. Cai, Eds. Hoboken, NJ, USA: John Wiley & Sons, Inc. 617-624. https://doi.org/10.1002/9781119274643.ch76.

APPENDIX A

Table A1: Grootegeluk sample nomenclature

Samples	Reaction conditions		
	Time (min)	Temperature (°C)	Mass (g)
GG-HTC-300A	30	100	300
GG-HTC-450A	30	100	450
GG-HTC-600A	30	100	600
GG-HTC-300-A1	30	150	300
GG-HTC-450-A1	30	150	450
GG-HTC-600-A1	30	150	600
GG-HTC-300-A2	30	200	300
GG-HTC-450-A2	30	200	450
GG-HTC-600-A2	30	200	600
GG-HTC-300B	90	100	300
GG-HTC-450B	90	100	450
GG-HTC-600B	90	100	600
GG-HTC-300-B1	90	150	300
GG-HTC-450-B1	90	150	450
GG-HTC-600-B1	90	150	600
GG-HTC-300-B2	90	200	300
GG-HTC-450-B2	90	200	450
GG-HTC-600-B2	90	200	600
GG-HTC-600C	180	280	600

Table A2: Moatize sample nomenclature

Samples	Reaction conditions		
	Time (min)	Temperature (°C)	Mass (g)
M-HTC-300A	30	100	300
M-HTC-450A	30	100	450
M-HTC-600A	30	100	600
M-HTC-300-A1	30	150	300
M-HTC-450-A1	30	150	450
M-HTC-600-A1	30	150	600
M-HTC-300-A2	30	200	300
M-HTC-450-A2	30	200	450
M-HTC-600-A2	30	200	600
M-HTC-300B	90	100	300
M-HTC-450B	90	100	450
M-HTC-600B	90	100	600
M-HTC-300-B1	90	150	300
M-HTC-450-B1	90	150	450
M-HTC-600-B1	90	150	600
M-HTC-300-B2	90	200	300
M-HTC-450-B2	90	200	450
M-HTC-600-B2	90	200	600
M-HTC-600C	180	280	600

Table A3: Maceral group analysis

Sample identification:		Moatize		Grootegeluk	
		inc. mm	mmf	inc. mm	mmf
MACERAL GROUP	MACERAL (vol%)	vol%	vol%	vol%	vol%
Vitrinite	telinite	0,0	0,0	1,2	1,4
	collotelinite	59,3	67,0	48,4	57,8
	vitrodetrinite	0,0	0,0	0,0	0,0
	collodetrinite	15,7	17,7	15,9	19,0
	corpogelinite	0,0	0,0	2,2	2,6
	gelinite	0,0	0,0	0,0	0,0
	pseudovitrinite	0,0	0,0	4,9	5,9
Inertinite	fusinite	3,1	3,5	3,5	4,2
	reactive semifusinite	1,2	1,3	0,2	0,2
	inert semifusinite	7,4	8,3	3,7	4,4
	micrinite	0,0	0,0	0,0	0,0
	macrinite	0,0	0,0	0,0	0,0
	secretinite	0,0	0,0	0,0	0,0
	funginite	0,0	0,0	0,0	0,0
	inertodetrinite R	0,0	0,0	0,2	0,2
	inertodetrinite I	1,9	2,2	1,6	1,9
Liptinite	sporinite	0,0	0,0	1,8	2,1
	cutinite	0,0	0,0	0,2	0,2
	resinite	0,0	0,0	0,0	0,0
	alginite	0,0	0,0	0,0	0,0
	liptodetrinite	0,0	0,0	0,0	0,0
	suberinite	0,0	0,0	0,0	0,0
	exsudatinite	0,0	0,0	0,0	0,0
Mineral matter	clay	4,8		7,3	
	quartz	4,3		8,0	
	pyrite	0,4		0,4	
	carbonate	0,8		0,6	
	other	1,2		0,0	
SUMMARY TABLE					
MACERAL GROUP TOTALS (vol%)	**VITRINITE**	**75,0**	**84,7**	**72,5**	**86,7**
	INERTINITE	**13,6**	**15,3**	**9,2**	**11,0**
	LIPTINITE	**0,0**	**0,0**	**2,0**	**2,3**
	MINERAL MATTER	**11,4**		**16,3**	
	TOTAL INERTINITE	**13,6**	**15,3**	**9,2**	**11,0**
	TOTAL REACTIVE MACERALS	**76,2**	**86,0**	**74,9**	**89,5**

Table A4: Vitrinite reflectance analysis

Sample no:		2139		2140	
Sample identification:		**Moatize**		**Grootegeluk**	
Vitrinite reflectance (RoV%)	R_{max}				
	st. dev.				
	R_{random}	**1,28**		**0,72**	
	st. dev.	0,095		0,169	
	maximum reading	1,554		1,364	
	minimum reading	1,034		0,515	
	number of points	152		181	
	RANK CATEGORY	Med Rank B bit		Med Rank C bit	

Table A5 Microlithitype

Sample no:		**2139**	**2140**
Sample identification:		**Moatise**	**Grootegeluk**
Group	MICROLITHOTYPE (vol%)		
MONOMACERAL	vitrite	68,6	66,6
	semifusite	6	2,8
	fusite / secretinite	4.8*	1,4
	inertodetrite	0	0
	Inertite sf+int	0	0
	liptite	0	0
	TOTAL	**74,6**	**70,8**
BIMACERAL	Vitrinertite vit+sf/f	4,6	2,8
	Vitrinertite vit+int	6	1
	Clarite vit+lipt	0	3,6
	Durite int+lipt	0	0
	TOTAL	**10,6**	**7,4**
TRIMACERAL	Duroclarite (V>I, L)	0	3,4
	Clarodurite (I>V, L)	0	0
	Vitrinertoliptite (L>I, V)	0	0
	TOTAL	**0**	**3,4**
CARBOMINERITE	cbm argillite	2,8	6
	cbm silicate (quartz)	1,8	1,2
	cbm pyrite	0,6	0,6
	cbm ank/carb	0,4	0,4
	cbm poly	0,4	0,2
	TOTAL	6	**8,4**
ROCK	rock	4	10

Table A6: The Grootegeluk/Moatize coal bend nomenclature

Sample	Composition (wt%)	Residence time
R-(15%GG+85%M)	15% GG, 85% Moatize	Raw Coal (0 minutes)
R-(30%GG+70%M)	30% GG, 70% Moatize	Raw Coal (0 minutes)
R-(50%GG+50%M)	50% GG, 50% Moatize	Raw Coal (0 minutes)
90-(15%GG+85%M)	15% GG, 85% Moatize	90 minutes
90-(30%GG+70%M)	30% GG, 70% Moatize	90 minutes
90-(50%GG+50%M)	50% GG, 50% Moatize	90 minutes